MODELLING OF DOWNSLOPE DISPLACEMENT OF FAILED SOIL BLOCKS ORIGINATING FROM SUBMARINE LANDSLIDES

by

© BINOY DEBNATH

A thesis submitted to the

School of Graduate Studies

in partial fulfilment of the requirements for the degree of

Master of Engineering (Civil Engineering)

Faculty of Engineering and Applied Science

Memorial University of Newfoundland

October, 2018

St. John's Newfoundland Canada

ABSTRACT

Submarine landslides are regarded as one of the major offshore geohazards that might affect offshore structures and associated facilities. The failed soil mass or debris that originate from a submarine landslide might travel hundreds of kilometres at a high speed and could affect offshore infrastructures. In the present study, numerical simulations are performed to investigate the velocity and run-out distance of the failed soil mass. The computational fluid dynamics (CFD) approach in ANSYS CFX is used for numerical simulation of the process, where the soft clay-rich sediments/debris are modelled as a non-Newtonian fluid. Large-deformation finite element (FE) simulations are also performed using the coupled Eulerian-Lagrangian (CEL) approach in Abaqus FE software. Similar to other large deformation FE analysis, Abaqus CEL and ANSYS CFX are computationally expensive. In offshore environments, the debris flows through water. The drag force resulting from water has a significant influence on the velocity of the debris and run-out distance. Modelling the downslope movement of an idealized soil block, it is shown that the pressure drag resulting from the pressure in front of the sliding block is the main source of the drag force. Progressive formation of additional shear planes, through localized plastic shear strain, might occur in the soil block during downslope displacements. A parametric study shows that the seabed slope angle and shear strength degradation due to undrained remoulding and/or water entrainment influence the failure patterns. For the cases analyzed, “flowslide” and “spread” type failures are obtained when the shear strength degradation of soil is considered. In terms of practical implications, the run-out distance will provide the information on whether an offshore structure will be affected by a failed soil mass resulting from a landslide. If so, the velocity will help to estimate the exerted force because it depends on the velocity of the moving soil block.

ACKNOWLEDGEMENTS

First of all, I am grateful to God Almighty for the good health and well-being that were necessary to complete this thesis.

The research work was carried out under the supervision of Dr. Bipul Hawlader, Professor, Memorial University of Newfoundland, Canada. I wish to express my sincere gratitude to him for providing me continuous support with all the necessary facilities, valuable suggestions and encouragement throughout the research work. His guidance helped me throughout my research and the writing of this thesis. I could not have imagined having a better supervisor for my Master's study.

I would like to thank the School of Graduate Studies, Natural Sciences and Engineering Research Council of Canada (NSERC), Mitacs and Statoil Canada for their financial support to conduct the research presented in this thesis.

My sincerest thanks go to Dr. Sujan Dutta for his invaluable suggestions and help to do the initial numerical modelling. Thanks to Dr. Tarun Kumar Sheel for his kind advice and comments. I would also like to thank Dr. Kshama Roy, Mr. Chen Wang and Mr. Shubhagata Roy for their kind words and helpful suggestions. Thanks to all my friends and colleagues at Memorial University for their tremendous help and advice throughout this work. Also, my sincerest thanks go to all the faculty and staff of the Faculty of Engineering and Applied Science who helped me directly or indirectly in my research work.

Last but not least, I would like to thank my parents and my younger brother for their endless love, encouragement and spiritual support throughout this study.

Table of Contents

List of Figures

List of Tables

List of Symbols

L	length of the soil bock/ debris slurry
L_R	length of the rigid soil bock
H	height of the soil block/ debris slurry
H_R	height of the rigid soil block
D	thickness at the middle of the parabolic slurry
D_{in}	initial thickness of the slurry
α	side slope of soil block
β	seabed slope angle
γ'	submerged unit weight of soil
s_u	undrained shear strength of soil
s_{up}	peak undrained shear strength of soil
s_{uR}	remoulded undrained shear strength of soil
s_{u95}	s_u mobilized at ξ_{95}
$s_{u(weak)}$	undrained shear strength at weak layer
$\tau_{y(ld)}$	large displacement shear strength with shear wetting
E_u	undrained Young's modulus
ν_u	undrained Poisson's ratio
$\dot{\gamma}$	shear strain rate
μ_d	dynamic viscosity
S_t	soil sensitivity
ξ	accumulated plastic shear strain

ξ_{95} value of accumulated shear strain where 95% of soil strength is reduced

ξ_{ld} shear wetting parameter

t time

v velocity

τ_y yield stress

$\tau_{y,\infty}$ remoulded yield stress

Y undrained yield strength

Y_∞ residual remoulded strength

γ total shear deformation

Γ dimensionless remoulding efficiency

x coordinate parallel to the seabed

y thickness of the debris slurry or soil block at any distance x

C coefficient

n coefficient

F force

m mass of the sliding block

a acceleration of the sliding block

g gravitational acceleration

F_g driving force/force due to gravity

F_d drag force

F_f frictional force

ρ_s density of soil/debris slurry

ρ_w	density of water
A	area of the sliding block/ debris slurry
A_{front}	frontal area of the sliding block
A_{top}	area of the top surface of the sliding block
V	volume of the sliding block/ debris slurry
W	weight of the sliding lock/debris slurry
C_d	drag coefficient
C_{front}	pressure drag coefficient in the front
C_{top}	friction drag coefficient at the top

CHAPTER 1

Introduction

1.1 General

Submarine landslides are major subsea geological events. The occurrence of many small- to large-scale submarine landslides has been reported in the literature (Hampton et al. 1996; Shanmugam and Wang 2015). Some of these landslides could be two to three orders of magnitude larger than subaerial landslides, and these landslides result in transport of a huge volume of sediment in the downslope direction (Hampton et al. 1996; De Blasio et al. 2004a).

The development of oil and gas fields in the offshore is growing day by day and is moving from shallow to deep water. Offshore sediments in deep water are typically soft fine-grained sediments which can be either clay or in some regions muds and silts (Randolph et al. 2011). The clay-rich debris formed by a submarine landslide might affect offshore structures, including as-laid offshore pipelines.

The progression of a submarine landslide consists of the following phases: (i) initiation of failure of the slope, (ii) run-out of the sliding soil blocks, (iii) transformation to the debris flowing as a viscoplastic fluid and then to the turbidity current as heavy fluid (Hampton et al. 1996; Boukpeti et al. 2012). The failure of a submarine slope can be triggered by various factors, such as an earthquake, pore pressure generation, gas hydrate dissociation, rapid sedimentation and weakening of a soil layer. After the failure of a slope, blocks of soil might be displaced downslope at a different velocity, depending upon their size, shearing resistance between the soil block and seabed,

inclination of the seabed slope, and soil–water interaction. Interacting with water, the soil block might be transformed into debris flows and turbidity currents due to significant loss of shear strength, remoulding and mixing of soil with water (Taylor et al. 2008). The failed soil mass or debris might travel hundreds of kilometres at a high speed and could pose a significant threat to offshore infrastructures such as deep water as-laid suspended pipelines on the seabed. The present study focuses on the second stage—the downslope movement of the soil block. While some shear strength degradation of the soil block is considered, the transformation to turbidity current is not modelled in this study.

Based on post-slide investigations, it has been inferred that submarine debris might travel at a very high speed, in the range of 7–30 m/s, to a maximum run-out distance of more than 100 km, even on very gentle slopes (Hampton et al. 1996; Locat and Lee 2000; De Blasio et al. 2004a; Elverhøi et al. 2010; Sahdi et al. 2014) . The 1929 Grand Banks landslide of offshore Newfoundland, which was triggered by an earthquake, involved transportation of 100–150 km^3 of sediments and damaged several transatlantic telegraph cables that were located hundreds of kilometers downslope from the place where the failure was initiated (Piper et al. 1999; Fine et al. 2005). The velocity of the debris reached 28 m /s (Elverhøi et al. 2010). Compared to subaerial landslides, fewer detailed case studies on submarine landslides are available in the literature. The development of modern sea floor mapping techniques provides information on the occurrence of historic submarine landslides and provides post-failure features. It has been reported that in many cases, the debris was deposited hundreds of kilometres from the place of origin. Therefore, for offshore development activities, only the geotechnical issues around the area of the infrastructure is not sufficient; instead, the impacts of submarine slide block run-out need to be integrated for safe design.

1.2 Scope and objectives of the study

The run-out of a submarine slide is a large deformation problem. As the failed soil blocks transform to different phases, from the parent soil behaviour to the turbidity current, two approaches are commonly used to model the run-out: (i) geotechnical approach and (ii) fluid mechanics approach. In the former one, the soil is modelled using typical geotechnical properties, and the analysis is performed using a large deformation FE modelling technique. The latter one is based on rheological properties of the fluid/slurry, and analysis is performed using a computational fluid dynamics (CFD) approach. Each of these approaches has some advantages and limitations. Therefore, it is essential to compare the performance of these approaches for modelling submarine landslides. Moreover, as the failed soil mass moves through water, it is necessary to investigate the effect of water.

The objective of the present study is to develop numerical modelling techniques for a submarine slide run-out. The following steps are taken to achieve this objective:

i. Develop a large deformation finite element model based on geotechnical properties to simulate the run-out of a slide block;
ii. Develop a computational fluid dynamics modelling technique to simulate the same problem and compare its performance with FE modelling;
iii. Analyse the effect of water on the velocity of the slide block and run-out distance; and
iv. Identify the effect of shear strength degradation during downslope movement of the soil block on the failure pattern of the block and run-out.

1.3 Outline of thesis

This thesis contains five chapters. The outline is as follows:

Chapter 1 contains the background, scope and objectives of the study.

Chapter 2 presents a literature review related to submarine slope failure and run-out of the failed soil mass.

Chapter 3 presents the performance of a large deformation finite element modelling and a computational fluid dynamics approach to simulate the run-out of a slide block.

Chapter 4 investigates the effect of water on run-out. The influence of shear strength degradation on the failure of the slide block and run-out is also investigated in this chapter.

Chapter 5 presents the conclusions of the study and some recommendations for future studies.

CHAPTER 2

Literature Review

2.1 Introduction

Submarine landslides are common offshore natural phenomena that occur when the failure of a seabed slope causes the movement of a huge amount of sediment. This event represents the most effective process of the movement of an enormous deposit from the shallow continental shore to the deeper parts of the ocean (Marr et al. 2002; De Blasio et al. 2004a). The sliding deposits often show very long run-out, more than 100 km in many cases, even on very gentle slopes of less than 2° (Hampton 1972; Hampton et al. 1996; Vorren et al. 1998). Compared to subaerial landslides, submarine landslides have some different features, such as long run-out distances and sliding of a large volume of sediment over a very gentle slope (Hampton et al. 1996; Harbitz et al. 2003; De Blasio et al. 2004a). For example, the Storegga landslide in the Norwegian Sea, which occurred ~8,200 years ago, represents one of the major well-documented landslides where the failed soil travelled more than 400 km (Elverhøi et al. 2010). Figure 2.1 shows the major worldwide incidence of submarine landslides. Almost half of these landslides involved the volume of failed sediment of more than 100 km^3 and among them the Storegga slide was the largest one that involved the transportation of ~ 3,500 km^3 of sediment (Gauer et al. 2005). In addition, the occurrence of many small- to medium-scale landslides have also been reported in the literature (Hampton et al. 1996).

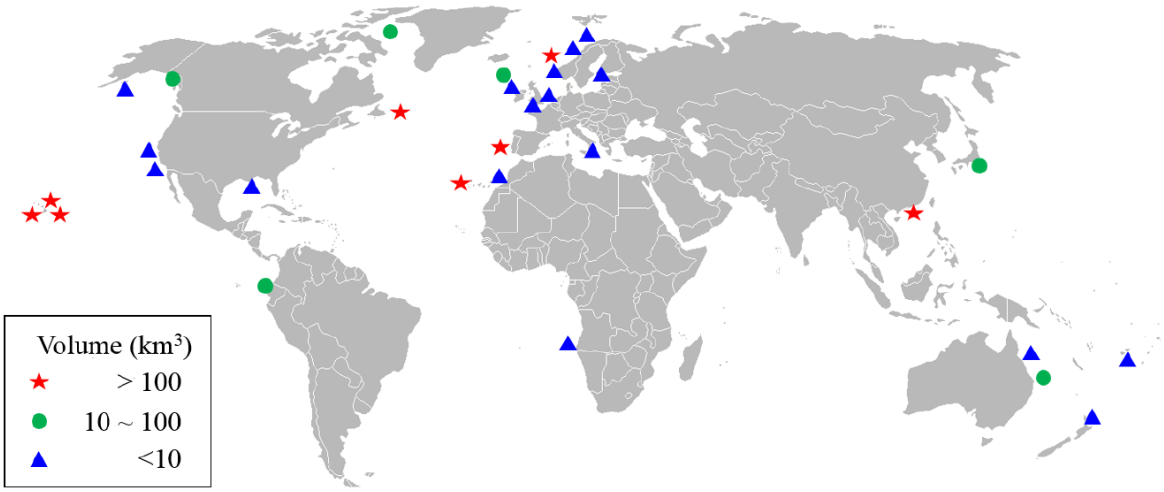

Fig. 2.1 Incidence of major submarine landslides (after Dong 2017)

While most of the large-scale submarine landslides are prehistoric, there are also some events that occurred in recent years. Shanmugam and Wang (2015) compiled some of the major submarine mass-transport phenomena of varying sizes (volume), triggering mechanisms and landslide associated damages that occurred in the 20th and 21st centuries. For example, the landslide in Prince William Sound in Southeastern Alaska in 1964, which occurred due to an earthquake, had a volume of failed material of ~211,000,000 m^3 that killed 122 people (Shanmugam and Wang 2015).

2.2 Phases of submarine mass movements

A submarine landslide and associated mass movements involve a complex process. The entire process of submarine mass movements can be divided into various phases, including the initiation of slope failure, downslope displacement of the failed soil mass, breakdown into smaller pieces, and transformation into viscous fluid and turbidity current (Locat and Lee 2002, 2005; Boukpeti et al. 2012; Shanmugam and Wang 2015). Figure 2.2 shows the typical values of shear strength and unit weight of the sliding sediment with downslope displacements. After the failure of the

slope, the displaced intact soil carries the parent soil properties of high shear strength and bulk unit weight. The sliding soil may lose shear strength due to interaction with seabed and water (remoulding and water entrainment). The water content in the debris increases with further displacements, and finally it transforms into a turbidity current, behaving like a fluid. The run-out distance could be more than 100 km.

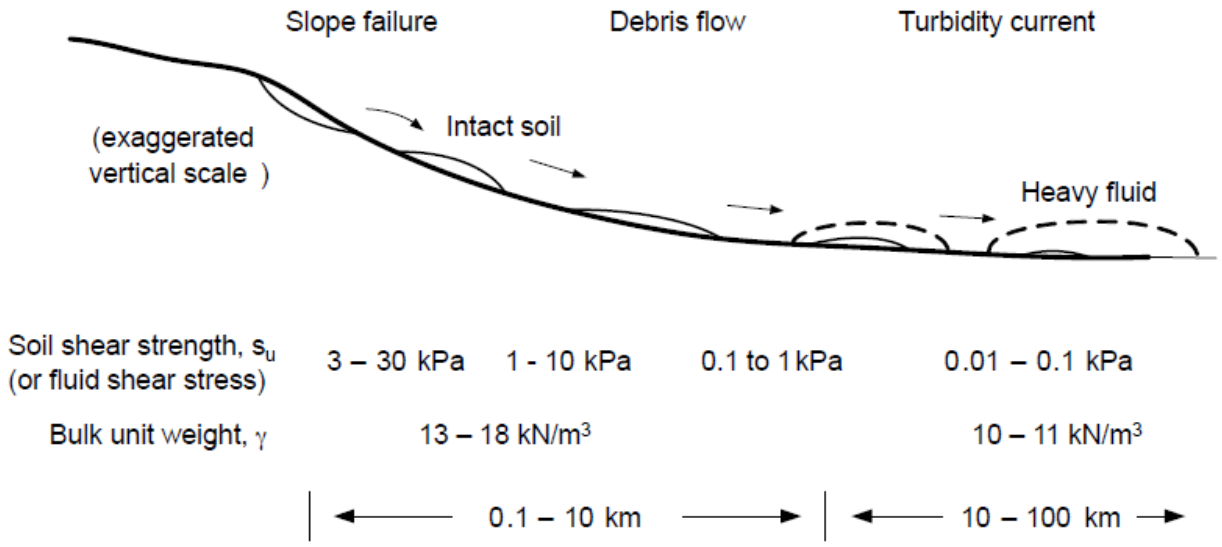

Fig. 2.2 Phases of submarine mass movements (after Randolph et al. 2011)

The Palos Verdes slide in offshore Los Angeles is a good example of the submarine mass transport process. The slide occurred ~7500 years ago and generated a tsunami wave with an amplitude of 8–12 m in the San Pedro Basin (Locat and Lee 2002; Bohannon and Gardner 2004). The debris travelled 8–10 km downslope and created a 10–15 m thick deposit (Locat et al. 2004) (Fig. 2.3).

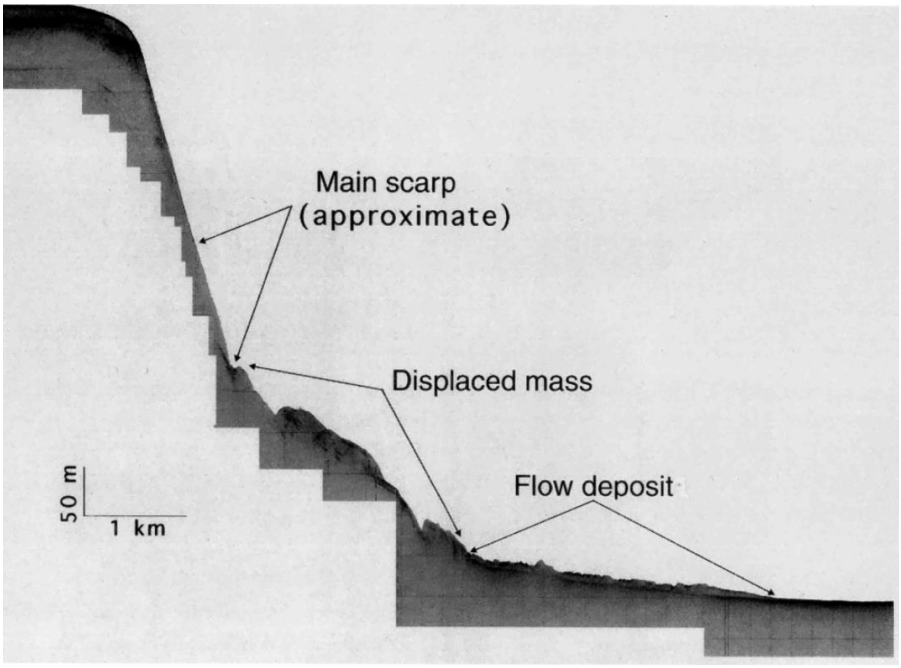

Fig. 2.3 Depositional pattern of the San Pedro Basin, Los Angeles, California, USA (after Hampton et al. 1996)

2.3 Terminologies in submarine landslides and debris flow

The sediment transport process in submarine landslides plays an important role in the construction of deep sea fans and channels. There are different terms available to describe each phase in the entire process of sediment transport (Zakeri and Hawlader 2013). These are described below.

(a) Glide block: The glide block is an intact clay-rich block during the early stages of sediment transport, carries the strength of the parent soil mass. The block has not been remoulded during the movement.

(b) Out-runner block: The out-runner block is an intact block of cohesive sediment that detaches from the parent density flow due to the effect of hydroplaning during the movement of flow. The block has not been remoulded and still carries the strength of the parent soil.

(c) Debris flow: Debris flow represents the flow of high-density cohesive materials, generally the combinations of solids and fluids with a minimum sediment concentration of 50% by volume. The material behaviour of debris flow can be characterized by rheological models for non-Newtonian fluids.

(d) Turbidity current: Turbidity current represents the flow of sandy or clayey materials with the material concentration of less than 50% by volume. The flow behaviour of the turbidity current can be characterized as a Newtonian fluid with a density of lower or higher than the density of seawater.

2.4 Velocity and run-out of the sliding mass

The velocity of the submarine sliding mass or debris is an important parameter in the field of the submarine landslide and its impact analysis. The calculated velocities can be useful in many aspects. For example, the velocity can be used for the approximations of the tsunami produced by the failed soil mass of any previous landslides (De Blasio et al. 2004b). The estimated velocities can also be used to predict the potential risk from the impact of a future sliding mass on offshore structures (De Blasio et al. 2004b; Zakeri and Hawlader 2013). Generally, the velocity of sliding mass or debris can be in the range of 7–30 m/s or higher (De Blasio et al. 2004a; Sahdi et al. 2014).

The run-out of the sliding mass is another important parameter in the post-failure analysis of submarine landslides. The sliding material that originates from the shelf-break after the initial failure will tend to flow down the continental slope. The distance between the initial slope failure and the final position of the deposit of sliding soil is known as run-out distance. The shear strength and water content of the sliding material show a gradual transition during the process of run-out. For the safe design of offshore structures, run-out distance is important, because it gives the general

idea of what distance the slides can travell and also, within this travelling zone, where a structure (pipe/cable) can be installed.

2.5 Previous studies on modeling of submarine slides and run-out

2.5.1 General

A large number of studies are available in the literature on post-failure analysis of submarine landslides. Based on the back-analysis of post-failure deposits identified from geophysical surveys, these analyses focused on the mobility (run-out distance and velocity) and dynamics of the sliding mass and associated hazards. Small-scale laboratory experiments were conducted to understand the characteristics of debris flows or sliding masses. In addition, analytical and theoretical solutions, as well as numerical techniques, have been developed to model this process.

2.5.2 Experimental studies

Wright and Krone (1987) carried out laboratory tests to simulate dam break phenomena. A bentonite slurry was released in an inclined flume from an upstream reservoir. The flow of slurry remained laminar throughout the process of run-out.

Several other experimental studies are available in the literature, which were carried out in the laboratory in a 1g test environment, to examine the flow mechanisms (Mohrig et al. 1998, 1999; Marr et al. 2001; Mohrig and Marr 2003; Ilstad et al. 2004a, 2004b, 2004c). These experimental studies provided insights into the process of dynamics of non-Newtonian fluid flows and the behaviour of fluid during the downslope movement.

Mohrig et al. (1998) carried out experiments on debris flows at the St. Anthony Falls Laboratory at the University of Minnesota. In the experiments, debris flows through a 10-m long and 0.2-m wide channel with smooth wall. Formation of hydroplaning (a layer of slurry with a high water

content) was observed at the front of the debris in subaqueous (i.e., channel filled with water) cases. Mohrig and Marr (2003) conducted an experimental study using the same facility, where a slurry or debris was released in the channel. The generation of the turbidity current was captured by several cameras at different locations. A typical test result is shown in Fig. 2.4.

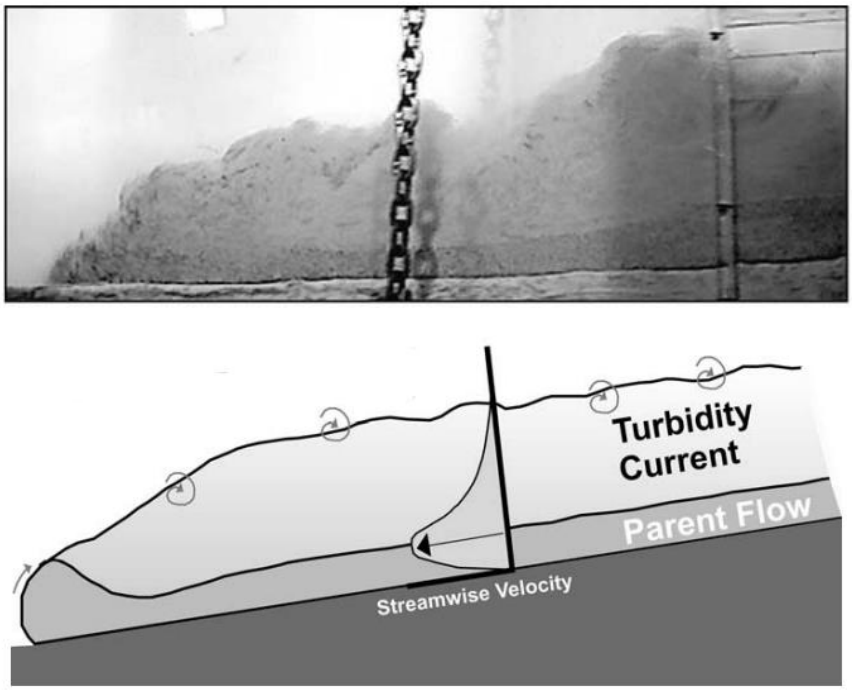

Fig. 2.4 Generation of turbidity in an experiment (after Mohrig and Marr 2003)

Ilstad et al. (2004a) also performed a set of similar experiments to investigate the frontal dynamics and morphology of submarine debris flows. The experiments were conducted to study the depositional patterns of post-failure submarine deposits.

In the experimental studies, the sliding soil mass was typically a fluidized material having the shear strength of less than 0.1 kPa, which could be two orders of magnitude lower than the shear strength of an actual slide in its intact state.

2.5.3 Theoretical studies

Theoretical studies are available in the literature that describe the dynamics and force balance equilibrium of the soil block and debris when it moves in the downslope direction (Cannon and Savage 1988; Huang and Garcia 1997; Harbitz et al. 2003). These studies modelled the flow behaviour analytically and provide theoretical solutions for the dynamics of the flow. Cannon and Savage (1988) used a mathematical model based on the momentum conservation principle to analyze the run-out of the debris flow.

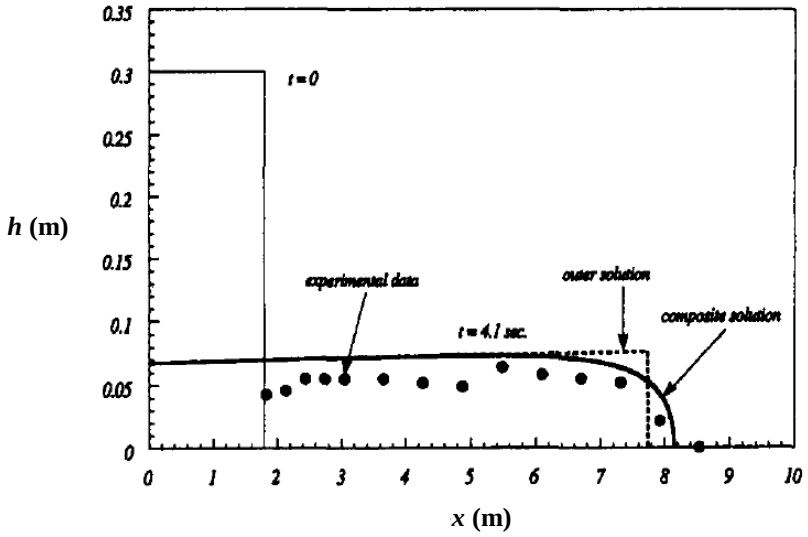

Fig. 2.5 Analytical and experimental results comparison (after Huang and Garcia 1997)

Huang and Garcia (1997) presented an analytical solution for laminar mudflows and debris flows that can be modeled as Bingham material. They verified the solution for muddy debris flow of a dam-break case considered in a flume test (Wright and Krone 1987). The results of the analytical solution compared with the experimental one are shown in Fig. 2.5.

Harbitz et al. (2003) proposed an equilibrium solution for the steady motion of a glide block, based on the lubrication theory. This solution describes the effects of hydroplaning on a moving glide block as well as its frontal dynamics.

2.5.4 Numerical studies

Even though various theoretical models have been proposed to analyze the frontal dynamics of slurry and run-out mechanisms, studies on the hydrodynamics of soil–water interaction and evolution of morphologies are limited (Harbitz et al. 2003; De Blasio et al. 2004a, 2006). Numerical studies have been performed to overcome these issues. Different numerical techniques have been used to predict the run-out behaviour, including the finite element (FE) method, material point method (MPM), finite difference method and finite volume method. The sliding behaviour is commonly modelled using two approaches: geotechnical approach and fluid mechanics approach. As discussed above, the shear strength of the sliding materials decreases with its downslope displacement. Therefore, both approaches are needed for successful modelling of submarine landslides.

In finite-element and material point method (MPM) analysis, modelling techniques are typically based on the geotechnical approach, where the soil is modelled using the geotechnical properties. For example, large deformation finite-element analyses are performed using the geotechnical approach that describes large-scale submarine landslides (Zhang et al. 2015; Dey et al. 2016b). Wang et al. (2013) used Abaqus-based dynamic RITSS (Remeshing and Interpolation Technique with Small Strain) to determine the velocity and run-out of a hypothetical sliding block. Their numerical model also captured the process of out-runner block formation due to the strain-softening effect on the soil shear strength, as shown in Fig. 2.6.

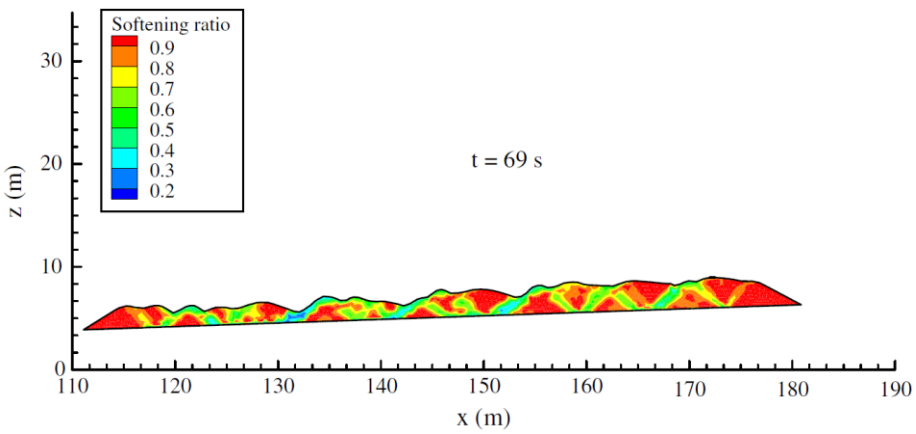

Fig. 2.6 Formation of the shear band in a typical sliding block (after Wang et al. 2013)

The run-out of slides on a rigid base is also modelled using MPM, which is a combination of finite-element and mesh-free methods, originating from the particle-in-cell method in CFD (Ma 2015; Dong et al. 2017). These numerical models consider the strain-rate and strain-softening effects on shear strength of the sliding materials. Both in the large deformation finite element method and material point method, the submerged unit weight is used to adjust the effect of underwater offshore environments, and the rest of the domain is taken as a void.

For the post-failure analysis, the behaviour of the sliding soil mostly relies on fluid mechanics principles (Locat and Lee 2002). Thus, the modelling of the submarine debris soil using the fluid mechanics approach has gained interest. In this case, the soil is modelled as a fluid by defining it as viscous behaviour (e.g., Jiang and Le Blond 1993). Jiang and Le Blond (1993) have presented a numerical model of an underwater landslide on a gentle uniform slope with the generation of water waves where the soil is modelled as a Bingham fluid. Based on the numerical model of Jiang and Le Blond (1993), Imran et al. (2001) presented a numerical model, known as the BING model, which was developed using a finite difference method, to simulate the muddy debris flow in an ambient quiescent fluid. They incorporated both the Herschel–Bulkley model and the bilinear

rheologies of viscoplastic fluid, and the program has been used later in a number of studies (Marr et al. 2002; De Blasio et al. 2004a, 2004b, 2005; Locat et al. 2004; Elverhøi et al. 2010). As the BING model is based on a fluid mechanics approach; the dynamic viscosity and yield strength are needed as inputs.

The BING code developed by Imran et al. (2001) can incorporate only a constant dynamic viscosity and a constant yield strength. However, in real cases, when a sliding soil block moves through the water, the reduction of shear strength occurs due to various factors, such as remoulding, water entrainment and soil–water interaction. Some studies considered the degradation of shear strength in numerical analysis (De Blasio et al. 2003, 2005).

As discussed, laboratory tests were conducted to understand the frontal dynamics of debris slurry and effects of hydroplaning. However, the first version of BING code cannot simulate hydroplaning. De Blasio et al. (2004a) advanced it by developing the W-BING code to model hydroplaning. Elverhøi et al. (2010) used both the BING and W-BING to model debris flow and back-calculated the run-out. There are more uncertainties in modelling using W-BING than with BING because modelling of the thin water layer is difficult (Elverhøi et al. 2010).

The Computational Fluid Dynamics (CFD) technique, which has been developed based on fluid mechanics principles has been well adapted recently in the Finite Volume Method (FVM) for the post-failure analysis of submarine landslides. Here the dynamic viscosity is required to define the rheological behaviour of soil. Gauer et al. (2005) used a CFD technique in ANSYS CFX4.0 and simulated the last phase of the Storegga slide. The simulated retrogressive failure is similar to the morphology observed in the upper part of the slide scar, as shown in Fig. 2.7.

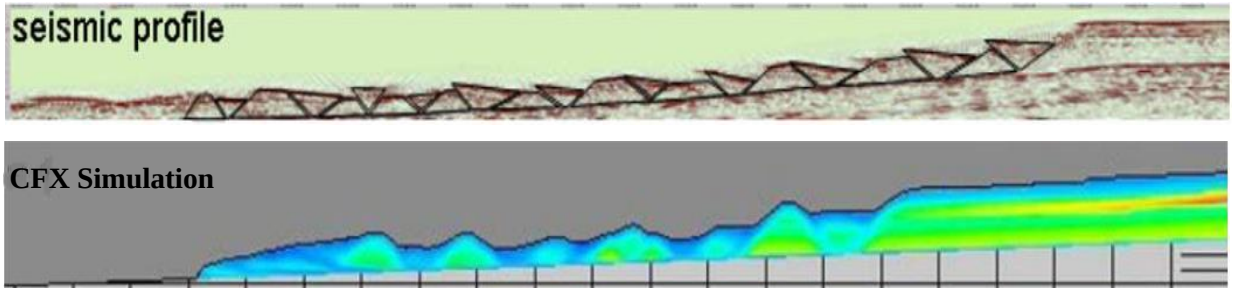

Fig. 2.7 Final deposition pattern from CFX compared with the seismic profile (after Gauer et al. 2005)

The CFX code has also been used to back-calculate laboratory test results (Gauer et al. 2006). The hydroplaning phenomenon has been captured and the formation of out-runner blocks has been modelled.

The progressive development of numerical tools for modelling submarine landslides, debris flow and run-out are summarized in Table 2.1.

Table 2.1 Numerical tools for modelling of submarine landslides

Reference	**Modelling technique**	**Comments**
Norem et al. (1990)	Two-dimensional model, finite-difference	Modelled flowslides with viscoplastic (Bingham) fluid.
Jiang and Le Blond (1993)	Finite-difference	Modelled the dynamics of underwater landslides; mud from the landslide is modelled as Bingham plastic flow.
Locat et al. (1996)	Bingham flow model: VIFLOW 2D visco-plastic model: SKRED	Mobility analysis of the debris flows on the Mississippi Fan.

Imran et al. (2001)	BING, depth-averaged method	1D numerical simulation of run-out of muddy debris flows; incorporated the Herschel–Bulkley model and a bilinear viscoplastic fluid.
Marr et al. (2002)	BING	Bingham rheology is considered to model run-out of mud-rich debris flow.
De Blasio et al. (2003)	BING	Incorporated remoulding effects on soil shear strength and progressive decrease of the yield strength.
Locat et al. (2004)	BING	Bi-linear rheology is incorporated to model the post-failure analysis of the submarine failed mass from Palos Verdes debris avalanche.
De Blasio et al. (2004a)	BING, W-BING	Modelled the effect of hydroplaning in the run-out analysis.
De Blasio et al. (2005)	W-BING	Modeled the dynamics of clay-rich debris flow from the Storegga landslide; a finite thickness of water layer is considered at the bottom of the debris to model hydroplaning effect
Gauer et al. (2005)	Computational fluid dynamics approach in ANSYS CFX code	Back-calculated the sliding behaviour of the last phase of the Storegga landslide;

		strength degradation is included in the rheological model of the soil.
Gauer et al. (2006)	ANSYS CFX	Back-calculated the laboratory test; observed hydroplaning and formation of out-runner blocks.
Zakeri et al. (2009)	ANSYS CFX	Simulated debris flows and their impact on pipelines.
Wang et al. (2013)	RITSS	Simulated sliding of out-runner blocks; incorporated strain-softening in soil model.
Ma (2015)	MPM	Simulated run-out; considered shear strength degradation.
Xiu et al. (2015)	FLUENT two-phase flow model	Simulated run-out; compared FLUENT and BING.
Dey et al. (2016b)	CEL, finite element	Simulated submarine landslides with sensitive clay layers.
Dong et al. (2017)	MPM	Simulated run-out and impact on offshore structures.

2.6 Resistance of water

During the process of run-out, the sliding block gets resistance from the surrounding water. The interaction between the sliding soil block and water starts with the initiation of the landslide. The resistance increases with an increase in velocity of the soil block.

2.6.1 Previous studies

The hydrodynamics of soil–water interaction has been discussed in many studies. The motion of a moving block can be described by Newton's Second Law using the force balance theorem (Cannon and Savage 1988; Pelinovsky and Poplavsky 1996; Ilstad et al. 2004a; Abadie et al. 2010). The following forces act on the block during its movement: driving force (gravitational force), and resisting forces (drag and frictional forces). The drag force is dependent on velocity. The frictional force is also dependent on velocity because the increase in velocity will increase the shear strain rate and thereby shear strength and interface frictional resistance. The surrounding water around the moving block is the main source of these resisting forces, which can play a major role in the movement of the soil block, as discussed in many relevant works. For example, Legros (2002) discussed the role of water on frictional resistance and mobility of the soil block. Pudasaini (2012, 2014) also showed the influence of water drag force on the motion of the slide. Yang et al. (2014) conducted laboratory experiments of slide block movement in a water tank. A different size of blocks was used for the experiments that moved at a varying speed in the water tank. They also showed that the maximum velocity considering the hydraulic resistance was 18.6% smaller than that without hydraulic resistance. The plot of the velocities with the travel distance of one real event with and without hydraulic resistance from the Yang et al. (2014) analysis is shown in the following Fig. 2.8.

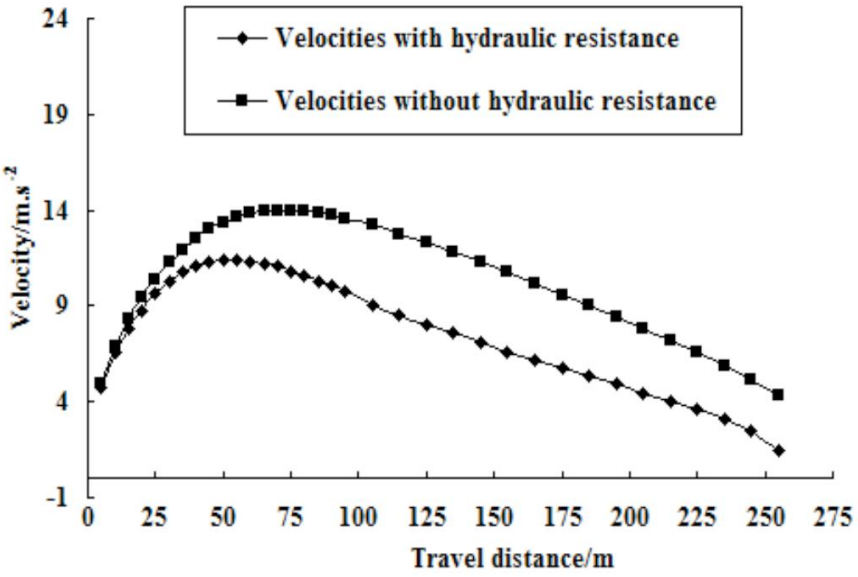

Fig. 2.8 Velocities of the Dayantang landslide (after Yang et al. 2014)

Xiu et al. (2015) conducted numerical simulations of run-out using the two-phase flow model (ANSYS FLUENT) and compared the results with the BING simulation. The evolution of the front velocity and run-out distance are shown in Fig. 2.9 and Fig. 2.10, respectively, where the BING model represents the in-air and the two-phase flow model represents the in-water simulations. From the analysis, they found the peak velocity of the slide front is lower in the water model (two-phase flow model) than in air (BING). However, the run-out distance is higher in the in-water than the in-air cases. They suggested it is due to the occurrence of hydroplaning in water that causes a longer movement time and thereby a larger run-out distance.

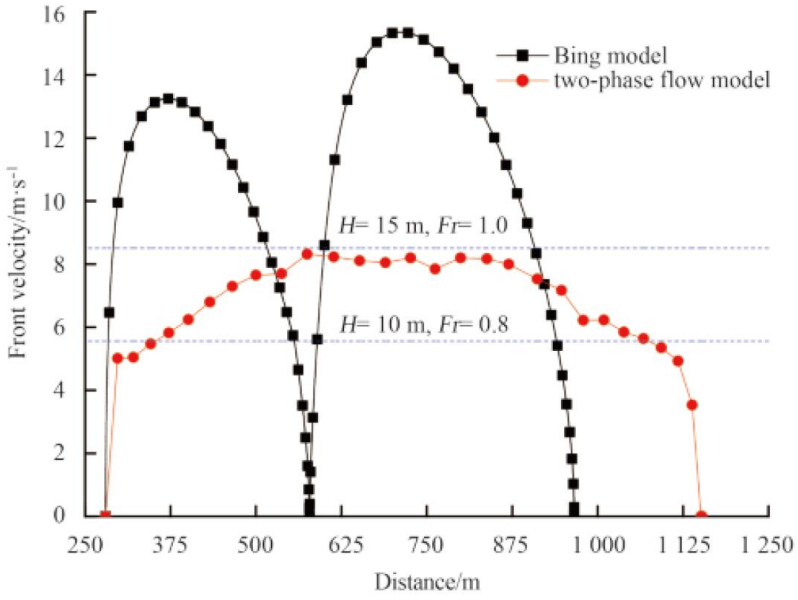

Fig. 2.9 Front velocity of the two models (after Xiu et al. 2015)

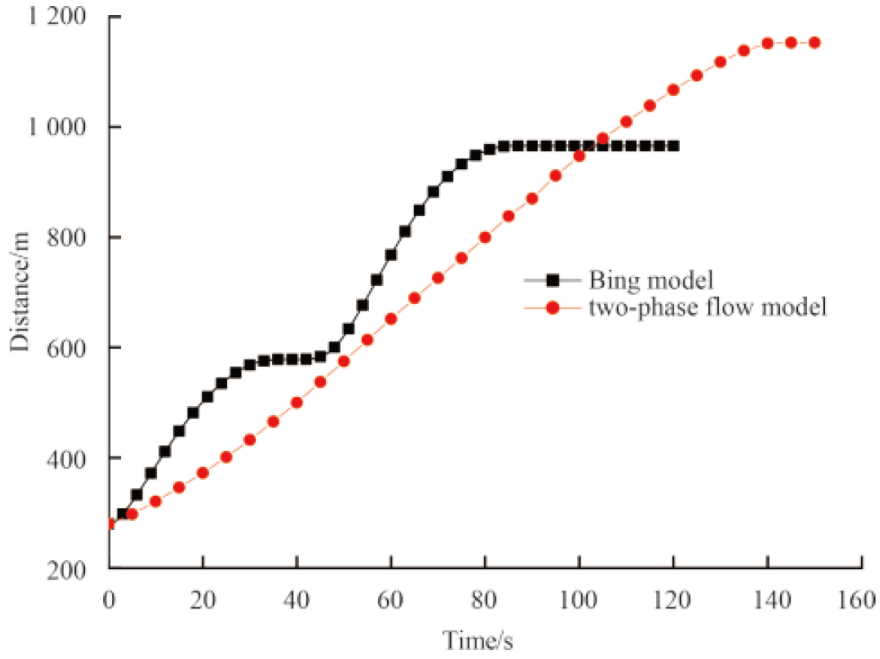

Fig. 2.10 Front toe run-out distance of the two models (after Xiu et al. 2015)

From the preceding discussion, it can be concluded that the water or hydraulic resistance is one of the most important factors that affects the mobility (velocity and run-out distance) of the sliding soil block.

2.7 Strain-softening behaviour of sliding soil

During the progress of run-out, the shear strength of the sliding mass might be affected by remoulding and water entrainment. Remoulding is the degradation of the shear strength with development of plastic shear strain. Due to remoulding, the strength of the slide can be reduced gradually to several times smaller than its intact value (Ma 2015; Dong 2017). The water entrainment can further reduce the shear strength together with an increase in water content.

The BING model developed by Imran et al. (2001) cannot model the shear strength degradation. To accommodate this, De Blasio et al. (2003) combined the effects of particle rearrangement (remoulding) and shear wetting and provided the following empirical equation, which has also been implemented in the BING code.

$$\tau_y(\gamma) = \tau_{y,\infty} + \left[\tau_{y,0} - \tau_{y,\infty}\right] \exp[-\Gamma\gamma] \qquad (2.1)$$

where $\tau_{y,0}$ and $\tau_{y,\infty}$ are the initial and final yield stresses, γ is the total shear deformation, and Γ is a dimensionless remoulding efficiency. The reduction of shear strength at high strains, presumably due to water entrainment, has been referred to as “shear wetting.”

To model the transition from an initially intact soil with high shear strength to a mobile slide with a considerably low strength, Gauer et al. (2005) modified the rheological description of the Bingham model by considering a strain-dependent yield stress. The evolution of the yield strength was expressed by the following equation.

$$\frac{DY}{Dt} = C\ \min(Y_\infty - Y, 0)\left(2\sqrt{-\Pi_D}\right)^n \quad (2.2)$$

Here, Y is the undrained yield strength, Y_∞ denotes the residual remoulded strength, C and n are coefficients, Π_D is the second invariant of the strain rate tensor, and D/Dt is the material differentiation in time. In their analysis, n = 1 and C = 1–3 were used.

Einav and Randolph (2005) proposed the following simple exponential decay function to model the strain-softening behaviour of offshore soft sediments.

$$s_u = \left[\frac{1}{S_t} + \left(1 - \frac{1}{S_t}\right) e^{-3\xi/\xi_{95}}\right] s_{up} \quad (2.3)$$

where remoulded sensitivity, $S_t = s_{up}/s_{uR}$, s_{up} is the peak undrained shear strength, s_{uR} is the remoulded shear strength, ξ is the accumulated plastic shear strain, and ξ_{95} is the value of ξ required to cause the 95% reduction of the peak shear strength.

The strain-softening equation given by Einav and Randolph (2005) is quite similar to the strength degradation equation used by previous researchers. The equation (Eq. 2.3) has been used by a number of researchers for the analysis of the effect of strain-softening (Wang et al. 2013; Ma 2015; White et al. 2016; Dey et al. 2016b; Dong et al. 2017; Dutta and Hawlader 2018).

2.8 Impact on offshore structures

The sliding soil mass or debris flows that originate from submarine landslides have significant impacts on coastal communities and offshore infrastructures. As an example, the 1929 Grand Banks Landslide of Newfoundland, which produced debris flow and turbidity current of a possible maximum velocity of up to 28 m/s, destroyed a number of telecommunication cables located more than 300 km in the downslope area (Elverhøi et al. 2010) and generated a tsunami wave that reached the southern coast of Newfoundland and caused damage to a small village, killing 33 people (Piper and Aksu 1987; Locat and Lee 2002). The force exerted by the impact of a slide is

a key parameter for the safe design of infrastructures in offshore environments. The velocity of the sliding mass remains relatively low at the early stages of a submarine landslide. Thus, at these stages, the exerted force on the structure is governed by the shear strength of the sliding mass rather than the inertial force (Dong 2017). The impact force becomes a function of the velocity and shear rate dependent undrained shear strength with the increase of velocity (De Blasio et al. 2004b; Dong 2017). In fact, the calculation of impact forces on specific offshore structures is still very difficult, as the shear strain rate dependent properties of the flowing material can play an important role (De Blasio et al. 2004b). If a sliding block or debris hits an offshore infrastructure, the resulting damage depends on both the peak pressure during the instant of impact and the continued hydrodynamic pressure. These pressures can be estimated from the velocity, density and strength of the sliding soil.

2.9 Summary

This chapter presents a literature review on submarine landslides and run-out of sliding mass. The existing research includes field investigations, experimental, theoretical and numerical studies. The effect of water pressure on the dynamics of the sliding block and the strain-softening effect on the shear strength of soil are two issues which need to be investigated further. As the failed soil mass displaces over a very large distance (order of kilometres), numerical modelling would be a better choice. However, such a large-scale modelling is computationally challenging. In the present study, the run-out of a sliding block or debris is simulated using two types of numerical modelling technique. Analyses are performed mainly for downslope displacement of soft clay blocks, although some analyses are conducted for slurries having a very low shear resistance (<100 Pa). To investigate the effect of water as the ambient fluid, a computational fluid dynamics approach is used in numerical modelling.

CHAPTER 3

Modelling of Run-out of a Soil Block using Finite Element and Computational Fluid Dynamics Approach

3.1 General

Submarine landslides are considered one of the major geohazards in offshore oil and gas development activities. After the failure of a slope, the failed soil mass may travel over a large distance during which it disintegrates into smaller pieces and might be fluidized due to interaction with surrounding water. For modelling a submarine landslide and its impact on offshore structures, two approaches are commonly used, geotechnical and fluid mechanics. Comparison between these two approaches for modelling run-out of a failed soil mass is presented in this chapter. Large deformation finite-element analyses are performed using the Coupled Eulerian–Lagrangian (CEL) approach in Abaqus FE software. The computational fluid dynamics approach in ANSYS CFX is used to model the same process where the shear resistance of soft clay sediment is defined as a non-Newtonian fluid using the dynamic viscosity. The similarities and differences between the simulation results using these two approaches are discussed.

3.2 Introduction

Many small to large-scale landslides occur in offshore environments that displace large amount of soil mass. The run-out distance and the velocity of the failed soil mass are important in the design of offshore structures and the evaluation of potential risks associated with submarine landslides.

The run-out of the sliding mass on a rigid seabed is analysed in this chapter using two different numerical approaches.

After the failure of a slope, the failed soil mass is transferred into different phases, during the process of run-out, due to the effects of various factors, including the change in shear strength, remoulding and fluidization. In the initial stages, the failed sediment blocks carry the parent soil property and do not experience a significant loss of shear strength. These blocks are generally called “glide blocks” and “out-runner blocks.” However, after travelling a large distance, the cohesive sediment becomes a slurry of high clay concentration and is called “debris flow” and “turbidity current.”

Two approaches are commonly used to model submarine landslides and their impact. In the geotechnical approach, the soil is modelled using the undrained shear strength. As the failed soil mass travels a large distance, large deformation finite-element modelling techniques are used to simulate this process. For example, Dey et al. (2016b) used the Coupled Eulerian–Lagrangian (CEL) approach in Abaqus FE software to model the failure initiated through a thin weak layer and subsequent propagation in the upper clay layers. The large deformation finite-element (LDFE) approach based on the “remeshing and interpolation technique by small strain (RITSS)” has been used by other researchers (Zhu and Randolph 2010; Liu et al. 2011; Wang et al. 2013). Other approaches, such as material point methods, have also been used in some studies to simulate the run-out process (Ma 2015; Dong et al. 2017).

In the fluid mechanics approach, the debris is typically modelled as non-Newtonian viscous fluids; the shear resistance is defined using the dynamic viscosity of the fluid (soft clay or clay slurry) as a function of shear strain rate. Imran et al. (2001) conducted numerical modelling by developing the finite-difference program BING to simulate the debris flow using the Herschel–Bulkley model

and a bilinear rheology for viscoplastic fluid. This program and its modified form have been used by a number of researchers for modelling debris flow (Marr et al. 2002; De Blasio et al. 2003, 2004a, 2004b, 2005; Locat et al. 2004; Elverhøi et al. 2010). The BING code developed by Imran et al. (2001) is based on constant dynamic viscosity as well as constant yield strength. De Blasio et al. (2003) developed an approach to model the decrease in shear stress due to shear wetting to incorporate the enhanced softening due to water entrainment. Gauer et al. (2005) showed that a computational fluid dynamics approach can be used to simulate the initiation and progressive failure of large-scale submarine landslides.

The aim of this research is to develop appropriate numerical modelling tools to simulate the run-out of submarine landslides. A comparison of run-out simulations using a large deformation finite element program and a computational fluid dynamics approach is presented in this chapter.

3.3 Numerical modelling tools

The following two numerical approaches are used to model large deformation of the failed soil mass.

3.3.1 Finite-element analysis

Abaqus Version 6.14.2 software is used for FE analyses. The soil is modelled as a Eulerian material to simulate the large deformation of the failed soil. Note that, unlike the approaches used for modelling Eulerian materials in typical computational fluid dynamics (CFD) programs, such as the one discussed in the following sections, the Eulerian time integration in Abaqus FE program is performed in the computational solid mechanics framework. The benchmark studies of CEL analysis and its applications to large-scale landslide modelling could be found in previous studies (Dutta and Hawlader 2016; Dey et al. 2016b). Unlike typical Lagrangian FE formulations, where

the material time derivatives are used, the Eulerian formulation is based on spatial time derivatives. Abaqus CEL uses operator splitting to solve the governing equations. Each time step has two phases of calculations: a conventional Lagrangian phase followed by a Eulerian phase. In the Eulerian phase, the solution obtained from the Lagrangian phase is mapped back to the spatially fixed Eulerian mesh.

3.3.2 Computational fluid dynamics analysis

The computational fluid dynamics (CFD) approach available in ANSYS CFX Version 16.2 is used to model run-out of the failed soil mass. Unlike Abaqus CEL, a finite-volume technique is used in CFX for modelling Eulerian material flow. The momentum and mass transfer processes are modelled using the Navier–Stokes equations, which have been developed applying Newton's second law of motion to fluid elements (soft clay sediment in the present study).

Both of these numerical tools allow only three-dimensional modelling. In addition, in both cases, Eulerian materials flow through the fixed mesh and therefore numerical issues related to mesh distortion are not encountered. Note that mesh distortion is one of the main limitations of typical Lagrangian-based FE programs and therefore cannot be used for this type of large-deformation run-out modelling. Table 3.1 shows a brief summary of the key features of these two numerical tools.

Table 3.1 Key features of Abaqus CEL and ANSYS CFX

	CEL	CFX
Modelling framework	Solid mechanics	Fluid mechanics
Method	Finite-element	Finite-volume
Integration scheme	Explicit	Implicit
Element type	Linear	Linear
Implementation	Three-dimensional	Three-dimensional
Mesh	Fixed in space	Fixed in space or deformable

Both CEL and CFD approaches can be used for modelling large deformation geotechnical problems. In recent years, Abaqus CEL has been used for modelling different large deformation problems, such as pipe–soil interaction (Dutta et al. 2015), large-scale landslides (Dey et al. 2015) and offshore foundations (Tho et al. 2010; Qiu and Henke 2011; Hu et al. 2014). Further details on mathematical formulation and comparison between implicit and explicit solution schemes are available in Benson and Okazawa (2004) and Dutta and Hawlader (2016). Compared to CEL, there is less use of ANSYS CFX for geotechnical problems (Zakeri and Hawlader 2013). A brief overview of the mathematical formulation of CFX and its application to submarine landslide impacts on pipelines is available in (Zakeri et al. 2009; Dutta and Hawlader 2018).

3.4 Problem statement

A hypothetical clay block of trapezoidal shape on a mild inclined seabed, having a slope angle (β) of 5°, as shown in Figure 3.1, is modelled. In offshore environments, the failed soil mass might accumulate due to a submarine landslide in the downslope areas when the propagation of failure is arrested by strong soil or reduction in slope angle (Trapper et al. 2015; Dey et al. 2016b). In a favourable condition—higher downslope angle and sufficient height of the accumulated soil—this clay block could travel over the seabed and affect offshore facilities.

Although the shape of the accumulated soil on the seabed that results from submarine landslides varies widely, as observed in post-slide investigation (Prior et al. 1982; Van Weering et al. 1998) and numerical simulations (Trapper et al. 2015; Dey et al. 2016b), a trapezoidal shape of soil block is assumed in this study for simplicity to show the performance of these two numerical approaches for modeling run-out (Fig. 3.1).

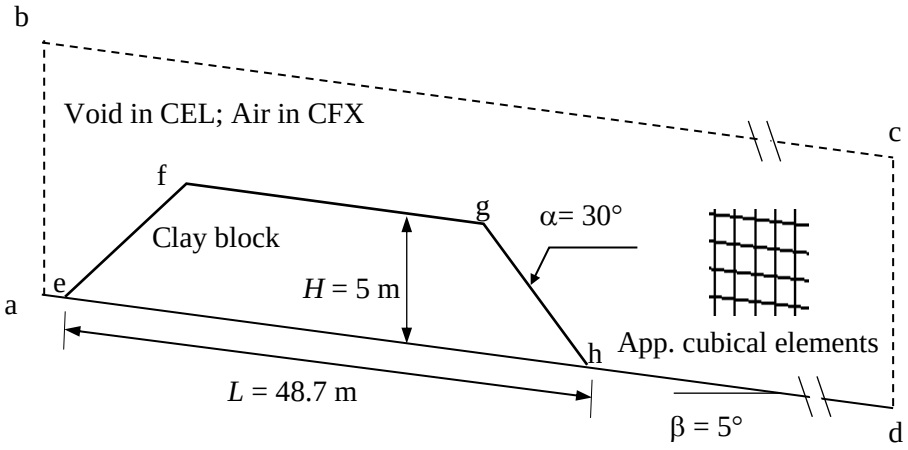

Fig. 3.1 Problem statement

3.5 Model setup

3.5.1 CEL model setup

As the CEL allows only three-dimensional modelling, in order to simulate the plane strain condition, FE analysis is performed with only one element length in the out-of-plane direction. Eight-node Eulerian brick elements (EC3D8R in Abaqus) of 0.25-m length are used to discretize the domain, except for the mesh sensitivity analyses. The FE domain has three parts: (i) a clay block (e.g. 'efgh' in Fig. 3.1 for the initial condition), (ii) a void space outside the soil block (abcdhgfe) to accommodate the displace soil and (iii) a rigid Lagrangian body below the line 'ad' in Fig. 3.1.

The initial condition is defined using the Eulerian Volume Fraction (EVF) available in Abaqus CEL. For an element, EVF = 1 means that the element is filled with soil and EVF = 0 means the element is void. A fractional value of EVF means that the element is partially filled with soil. The density of submerged soil is assigned to all the soil elements.

Zero velocity boundary conditions are applied normal to all the vertical faces of the domain shown in Fig. 3.1. No boundary conditions are applied along the clay–void interface, which allows the displacement of clay in the void space when needed. A rough condition is used to define the interface behaviour between the clay and rigid body.

FE analysis consists of two loading steps. Firstly, in the gravitational step, the gravitational acceleration is applied quickly to create geostatic stresses in the soil elements while maintaining the ratio between horizontal and vertical stresses equal to 1.0. In the next step, no external load is applied and the analysis is continued over a period of time until the instantaneous velocity of the soil elements becomes negligible.

3.5.2 CFX model setup

Similar to CEL, the three-dimensional CFX model is developed with one element length in the out-of-plane direction, in order to simulate the plane strain condition. The domain is discretized into approximately cubical shape elements of 0.25 m length. A submerged unit weight of 5.9 kN/m^3 is assigned to the clay elements.

Two types of materials are considered: soft clay in the clay block (efgh) and air outside the block. Both clay and air are modelled as homogeneous multiphase Eulerian materials.

A symmetry plane boundary condition is applied to the vertical faces. The interface behaviour between the bottom boundary and clay is defined using a no-slip boundary condition.

3.6 Modelling of soil

Deep water offshore sediments are typically soft clays. The behaviour of soft clay sediment is modelled using a uniform undrained shear strength (s_u) of 2.1 kPa. In Abaqus CEL, it is defined using the yield strength (= $2s_u$), adopting the von Mises yield criterion in total stress analysis.

In CFX, there is no direct option to define the undrained shear strength of clay. Therefore, it is defined using the dynamic viscosity of non-Newtonian fluid (μ_d), which is related to s_u as $s_u/\dot{\gamma}$, where $\dot{\gamma}$ is the shear strain rate. Further details on the implementation of soft clay sediment behaviour in CFX are available in Dutta and Hawlader (2018). The built-in dynamic viscosity of air of 1.831×10^{-5} Pa.s in CFX is used, which does not have significant effects on run-out. Table 3.2 shows the geometry and geotechnical parameters used in numerical analyses. These parameters have been selected from a review of geotechnical properties of offshore clay sediments reported in the literature (Kvalstad et al. 2005; Wang et al. 2013).

Table 3.2 Geometry and soil parameters used in analysis

Parameter	Value
Initial base length of clay block, L (m)	48.7
Initial height of clay block, H (m)	5.0
Side slope of clay block, α (°)	30
Seabed slope angle, β (°)	5
Submerged unit weight of clay, γ' (kN/m^3)	5.9
Undrained shear strength of clay, s_u (kPa)	2.1
Undrained Young's modulus, E_u (kPa)*	$500s_u$
Undrained Poisson's ratio, ν_u*	0.495

*E_u and ν_u are needed only for CEL analysis

3.7 Verification of numerical techniques

Wright and Krone (1987) conducted a laboratory experiment of slurry flow with a reservoir of 1.8 m length in the upstream and a 7.3 m long channel in the downstream. The experimental results of the "Run 15" of their study are simulated here to verify the present numerical techniques. In this experiment, the reservoir was filled with a bentonite slurry. A vertical sliding gate was used at the downstream end of the reservoir to simulate an instantaneous dam break, by sudden releasing the bentonite slurry from the reservoir into the rectangular glass flume. The reservoir was filled with a 1.8 m × 0.3 m × 0.6 m (length × height × width) slurry having the shear strength of 42.5 Pa and density of 1,073 kg/m^3. The flume bed had a constant inclination of 3.43° to the horizontal. The flow of a slurry of high bentonite concentration can be considered as a non-Newtonian fluid flow.

This experiment is simulated in CFX by developing a three-dimensional model with one element thickness in the out-of-plane direction. The bottom of the Eulerian domain is inclined at 3.43° to the horizontal. The domain is discretized by 0.015 m of approximately cubical shape elements. Similar to the experiment, a 1.8 m × 0.3 m section in the upstream (reservoir in the experiment) is filled with slurry using the volume fraction tool. Outside the slurry, the domain is filled with air; that is, the flow will occur through the air as the ambient fluid, as used in the experiment. The built-in air density of 1.185 kg/m^3 and dynamic viscosity of 1.831×10^{-5} Pa.s are used. The dynamic viscosity of the slurry is defined using the undrained shear strength, as discussed in Section 3.6. The bottom boundary of the domain is defined as a no-slip wall, while the top one is kept open. The vertical faces are defined as a symmetry plane boundary condition.

Similar to CFX modelling, the three-dimensional CEL simulation is performed with only one element length in the out-of-plane direction. In this case, the domain outside the slurry is defined as a void, to accommodate the displaced slurry. A Lagrangian rigid body is considered at the bottom of the domain to define the flume bed surface. Zero velocity boundary conditions are applied normal to all the vertical faces of the domain and no boundary condition is applied along the slurry–void interface. The interface behaviour between the slurry and rigid body is defined as a rough condition.

After the development of the model, the slurry is allowed to flow under gravity. The analysis is continued for 10 s, without application of any external load. Figure 3.2 shows the profiles of the slurry, obtained from CEL and CFX simulations, at t = 4.1 s, which match well with the experimental results of Wright and Krone (1987). For comparison, the results of the analytical solution developed by Huang and Garcia (1997) and numerical simulation using the BING (Imran

et al. 2001) are also shown in Fig. 3.2. As shown, all these solutions provide the slurry profile and run-out distance comparable to the experimental results.

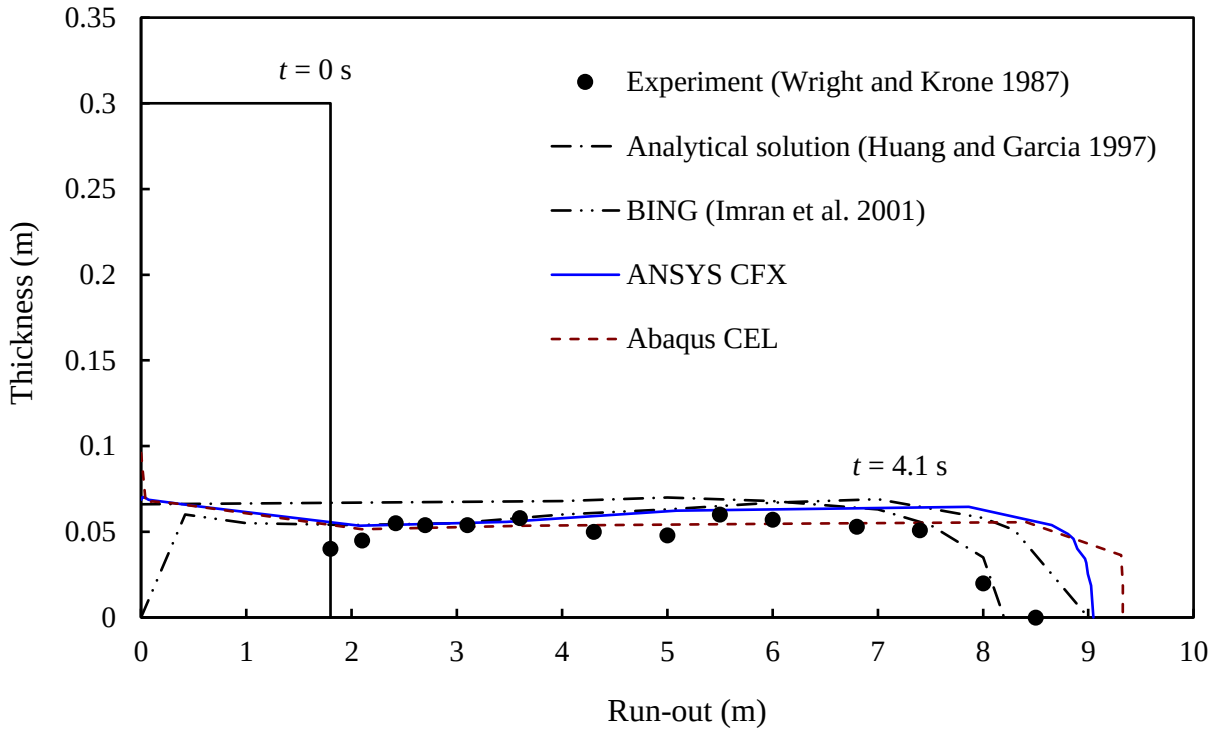

Fig. 3.2 Comparison of numerical simulations and experimental results at t = 4.1 s

3.8 Results of soil block modelling

In the assessment of geohazard risks associated with submarine landslides, two key parameters need to be considered: (i) run-out distance and (ii) velocity of the failed soil mass. The former item provides information on whether a submarine landslide could affect an offshore structure in the downslope area. If a structure is located in the run-out zone, the drag force resulting from the failed soil mass depends on impact velocity (Zakeri and Hawlader 2013; Dutta and Hawlader 2018).

3.8.1 Frontal velocity and run-out distance

Figure 3.3 shows the calculated run-out distances using CFX and CEL. In both analyses, the Eulerian material (soil) flows through the fixed mesh. Therefore, the deformed positon of the soil block cannot be obtained directly from nodal displacements, as in typical Lagrangian-based FE analysis. Based on simulation results, the coordinates of the front of the failed soil mass with time are obtained, and the horizontal distance from the initial positon of the clay block is calculated to obtain the run-out distance. The solid line in Fig. 3.3(a) for 0.25-m mesh shows that the frontal velocity starts to increase immediately after the start of calculation because of plastic deformation and failure of slope in the downslope side (right side of the clay block in Fig. 3.1). The maximum frontal velocity of ~ 4 m/s is calculated at t ~ 3 s. Thereafter, the velocity decreases and at t ~ 10 s, the velocity becomes almost zero. In other words, the downslope movement of the failed soil mass stops at this time.

The solid line in Fig. 3.3(a) also shows that the run-out distance increases with time and at t ~ 10 s, the maximum run-out of ~ 18 m is obtained. At this time, the soil mass spreads horizontally over a large distance of ~ 68 m (originally 48.7 m), which increases the shear resistance at the bottom of the failed soil mass. Moreover, as it spreads over a large distance, the height of the soil mass decreases. Therefore, the downslope movement of the soil block stops.

Figure 3.3(b) shows a similar calculation using Abaqus CEL. This analysis also shows that the velocity increases with time for $t \leq 3$ s and then reduces to zero at t ~ 10 s. A comparison between the results obtained from these two methods shows that both numerical techniques can simulate the large deformation of the failed soil mass.

3.8.2 Velocity of soil elements

In addition to frontal velocity, as presented in Fig. 3.3, the velocity of soil elements during the process of run-out is also compared. Figure 3.4(a) shows that, at t ~ 2.8 s, a maximum velocity of ~ 4 m/s occurs in a small zone near the front of the failed soil mass. The magnitude of velocity gradually decreases with distance. On the upslope side (left side of the clay block in Fig. 3.1), the velocity is almost zero, which indicates that this side of the soil block does not fail. Figure 3.4(d) shows a similar instantaneous velocity contour obtained from Abaqus CEL. At t = 6 s; the velocity of the soil elements decreases, compared to those at t = 2.8 s (Figs. 3.4(b) & 3.4(e)). Finally, at t = 9 s, the velocity is very small, indicating the completion of run-out.

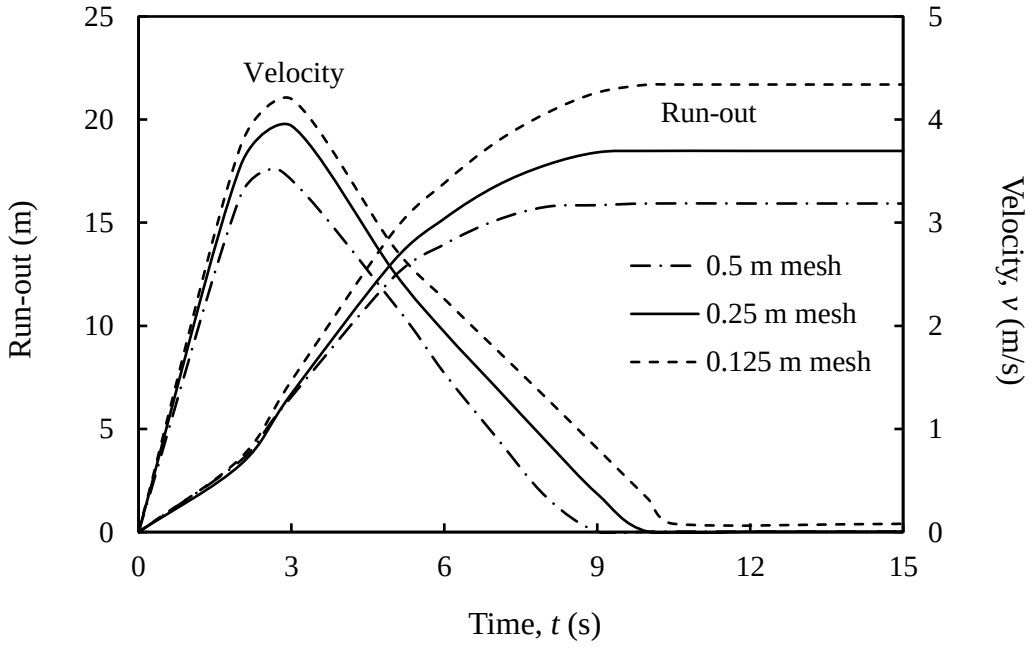

(a)

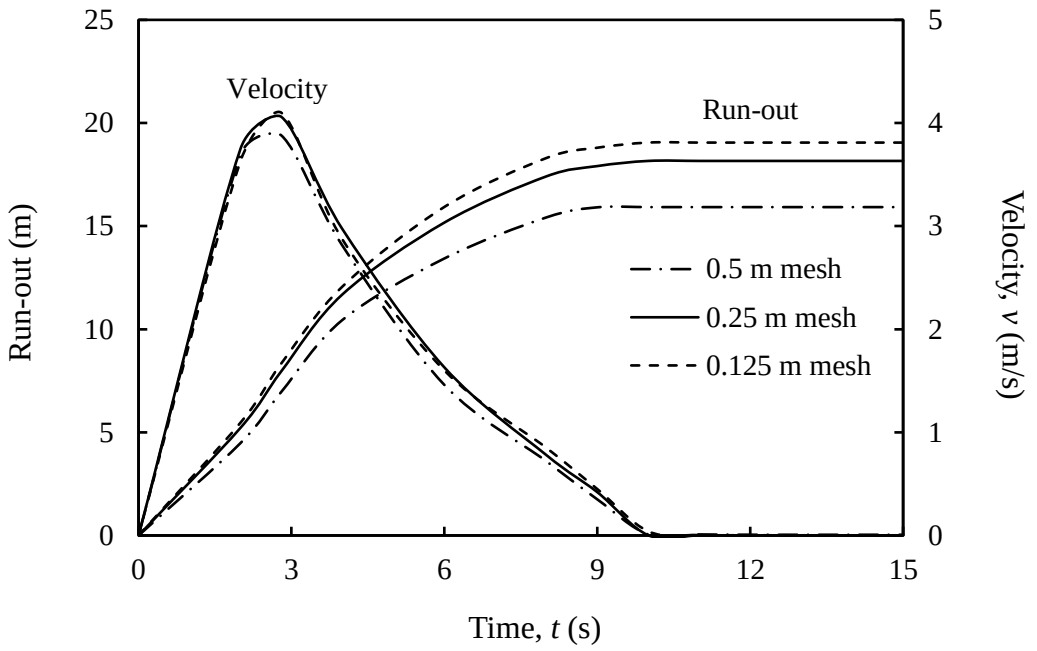

(b)

Fig. 3.3 Frontal velocity and run-out: (a) using CFX, (b) using CEL

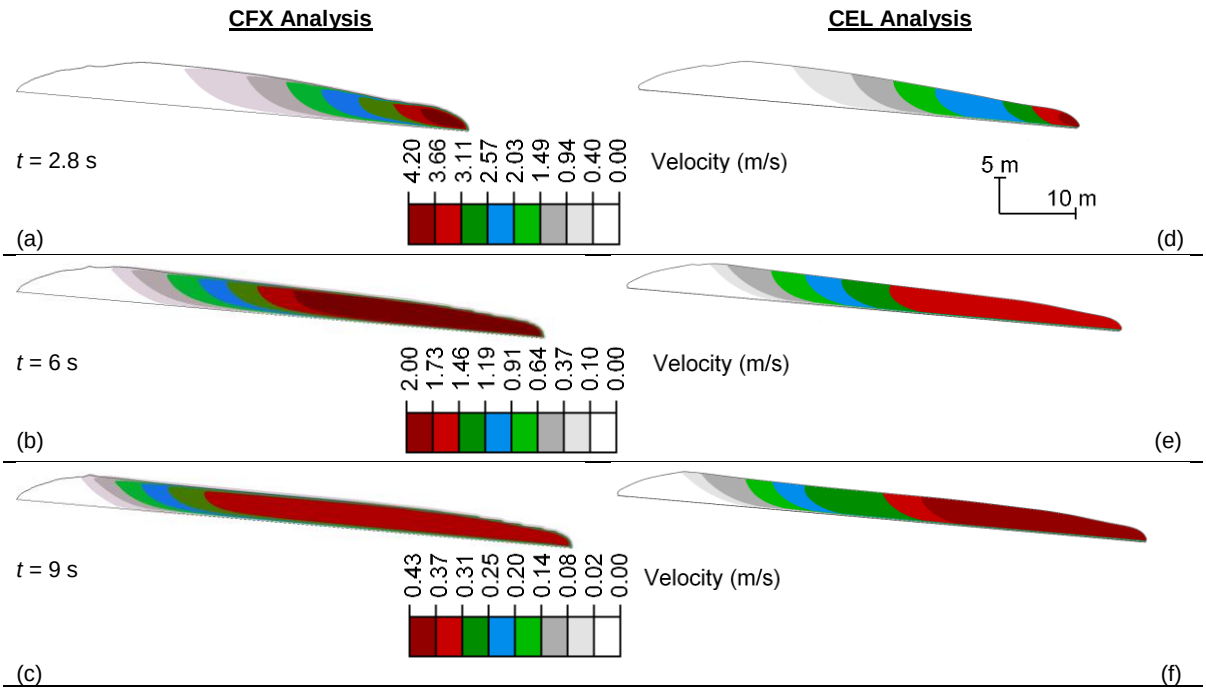

Fig. 3.4 Comparison of soil element velocities in CFX and CEL analysis

3.8.3 Mesh sensitivity

Analyses are also performed for two more mesh sizes (approximately cubical elements of 0.125 m and 0.5 m). Figure 3.3(a) shows that velocity and run-out distance increase with a decrease in mesh size. This is because of failure of the soil through a thinner zone in a finer mesh. A mesh sensitivity analysis is also performed with Abaqus CEL for similar mesh sizes. Compared to CFX, frontal velocity and run-out distance are less sensitive to mesh size in Abaqus CEL for the mesh sizes considered. This difference might result from differences in solution techniques used in these two computational tools. Note that mesh sensitivity has also been observed in run-out simulations with the material point method (Dong et al. 2017). Further studies are required to resolve this issue.

3.8.4 Comparison with other numerical solutions

The numerical simulations conducted in the present study using CFX and CEL are also compared with the other simulation techniques (RITSS and MPM) used in previous studies (Wang et al. 2013; Ma 2017). As the RITSS and MPM simulations were conducted using small size elements, the analyses results for the fine mesh size (0.125 m) of CFX and CEL simulations are used for the purpose of comparison. The run-out of the frontal toe and toe velocity are plotted in Fig. 3.5. As shown, the results from all four numerical techniques are comparable; however, Abaqus CEL gives slightly lower velocity and run-out distance than do other methods.

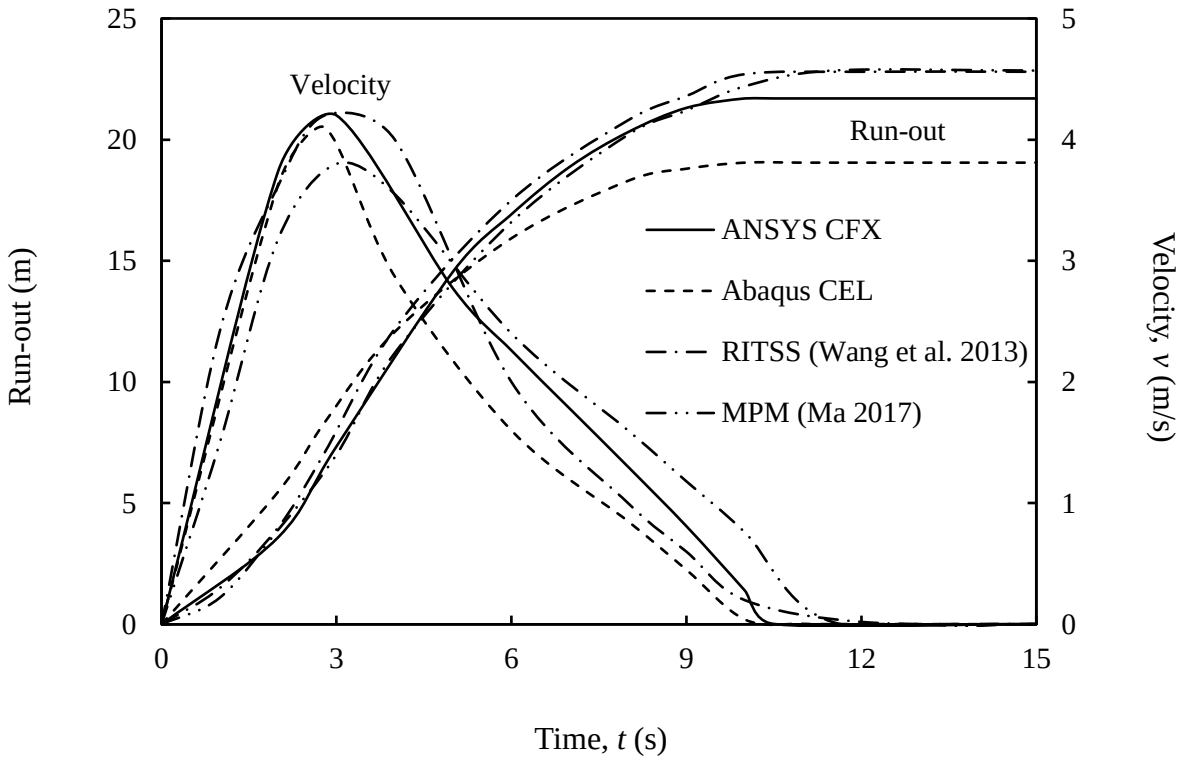

Fig. 3.5 Comparison of run-out and velocity of front toe

3.9 Summary

The run-out of a failed soil mass resulting from a submarine landslide can pose a significant threat to offshore structures. Numerical simulation of run-out of a soil block is performed using a large-deformation finite-element modelling technique and a computational fluid dynamics approach. The analyses are performed for air as the ambient fluid in CFX and a void in FE simulations. The velocity of soil elements and run-out distance obtained from the numerical simulations are comparable to that of in laboratory test and other numerical simulations available in the literature. The comparison of simulations for the present idealized cases using CFX and CEL shows similar results.

In offshore environments, the debris moves through water, during which shear failures of the soil block might occur. Moreover, the interaction between soil and water, especially at a high velocity, could change its velocity and run-out. These issues are investigated in Chapter 4.

CHAPTER 4

Effects of Water Resistance and Shear Strength Degradation on Debris Flow

4.1 General

The sliding soil blocks that are generated from a submarine landslide tend to move in the downslope direction. The total distance travelled by the sliding soil mass, from the initiation of failure to the final position, is called the run-out distance. During travel, depending on the shape of the block and its speed, the surrounding water provides resistance to the movement of the sliding block, in addition to the basal geotechnical resistance between the sea floor and soil block. The effect of water resistance on the velocity and run-out distance is analysed in this chapter. The process is further complicated by the reduction of shear strength during the movement, due to the influence of a number of factors, including strain-softening of the soil, water entrainment, potential hydroplaning and even the change of the soil block to a turbidity current. In the present study, the reduction of soil shear strength is empirically modelled as a function of accumulated plastic shear strain, instead of simulating each process (e.g. water entrainment) separately. The computational fluid dynamics approach in ANSYS CFX is used for numerical analysis.

4.2 Introduction

In many offshore landslides, the failed soil mass is displaced over a large distance through water. In case of a subaerial landslide, a sliding mass experiences negligible air resistance in the front when it travels through the air. However, a failed soil mass in offshore can experience a

considerable drag force from water, which can affect the velocity and run-out of the sliding mass. De Blasio et al. (2004a) conducted numerical simulations with the BING computer program for both air and water as the ambient fluid and found that the sliding sediment has a longer run-out distance in the air than in water, which is because of the larger drag force in water. Xiu et al. (2015) showed that the water resistance in the subaqueous case gives a lower peak velocity than that in the subaerial case; however, the travel time and run-out distance are more in the former one. Yang et al. (2014) conducted laboratory tests to understand the dynamics of partially submerged submarine landslides and calculated the velocity of the sliding soil with and without considering the water resistance. They found a larger velocity in the models without water resistance than that in water. These studies highlighted the importance of water resistance in modelling run-out/mobility of debris.

The degradation of the shear strength of the debris during downslope movement is another important aspect that might affect the mobility. Generally, offshore sediments in deep water are soft and sensitive. Compared to typical highly sensitive or quick clays in onshore environments, offshore sediments are less sensitive—typically sensitivity, S_t = 2–6, but can be as high as 10 (Zhang et al. 2015; Dey et al. 2016a; Dey et al. 2016b). The shear strength of soil is reduced due to remoulding of soil and accumulation of shear strain along the failure planes. The degradation of shear strength is further enhanced by the water entrainment (De Blasio et al. 2005; Dong 2017). The water entrainment could reduce the shear strength to a significantly low value (<1.0 kPa) (Boukpeti et al. 2009). With movement, the sliding blocks might break down into smaller pieces due to the formation of shear bands and may generate smaller out-runner blocks or turbidity current. The debris can travel a large distance and affect underwater infrastructures. The overall

process of a submarine landslide and its possible impact on offshore structures is illustrated in Fig. 4.1.

The failure of a submarine slope and run-out generally occur in a short period. Therefore, the shearing behaviour of the sliding material can be modelled as an undrained condition. However, when water entrainment occurs, the process is no longer undrained, and the shearing resistance should not be defined as the undrained shear strength. The shear strength magnitude and its degradation influence the velocity and run-out of the failed soil mass and failure patterns.

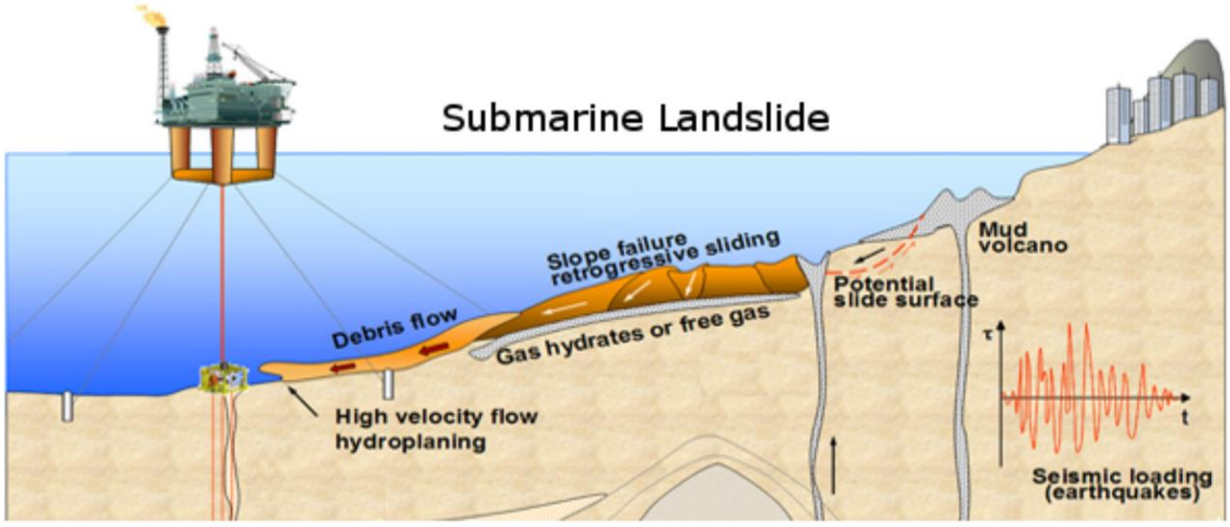

Fig. 4.1 Development of submarine landslide and its impact (after Ma 2015)

4.3 Dynamics of a sliding mass

Figure 4.2 shows the sliding of an idealized soil mass on an inclined seabed. The force acting on the sliding block (F) has three components.

$$F = F_g + F_d + F_f \tag{4.1}$$

The first one is the gravitational component, $F_g = V\gamma'\sin\beta$, where γ' is the submerged unit weight, V is the volume of the sliding block and β is the slope angle. The second component of the force

(F_d) in Eq. (4.1) results from the interaction between the sliding block and ambient fluid (water/air). Finally, F_f in Eq. (4.1) represents the frictional resistance between the seabed and sliding block.

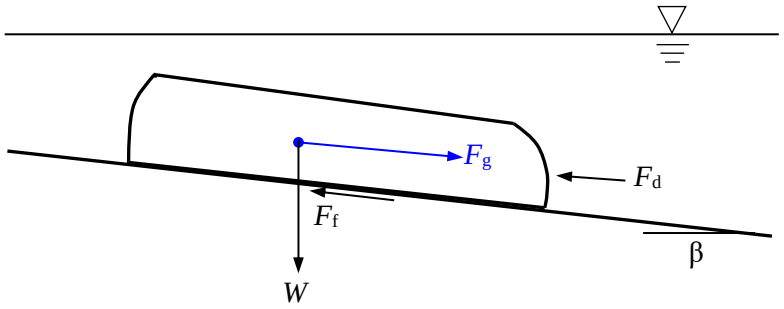

Fig. 4.2 Forces acting on the sliding block

4.4 Numerical modelling technique

Similar to the analyses presented in Chapter 3, the computational fluid dynamics approach in ANSYS CFX is used for modelling the effects of water resistance and shear strength degradation on downward displacement of the failed soil blocks.

4.5 Verification of numerical technique with BING (subaqueous) model

To simulate the muddy debris flow in an ambient quiescent fluid (water or air), Imran et al. (2001) developed a computer program known as BING, which is a one-dimensional finite-difference program. They also showed the effects of initial shape of the debris, rheological modelling of the debris and ambient fluid.

To examine the effects of ambient fluid, Imran et al. (2001) used water and air in separate programs named BING (subaqueous) and BING (subaerial), respectively. In this section, the performance of the present numerical model using CFX, with water as the ambient fluid, is examined by

comparing the results with a BING (subaqueous) analysis. Using BING (subaqueous), Imran et al. (2001) modelled the run-out characteristics of a debris that was initially in a parabolic shape (Run-AQ in their analysis), which was defined using Eq. 4.2.

$$\frac{D_{in}}{D_0} = 1 - 4\left[\left(\frac{x - L_0/2}{L_0}\right)^2\right] \tag{4.2}$$

where D_{in} is the initial thickness of the slurry at any distance x measured from point O in Fig. 4.3, D_0 is the maximum thickness of the debris at the middle, and L_0 is the initial length of the debris profile. They presented a simulation for L_0 = 600 m and D_0 = 24 m for debris having the density of 1,500 kg/m^3 that travels over a seabed that is inclined at 2.87° to the horizontal (i.e. 20:1 slope). The slurry was modelled using the Herschel-Bulkley model, with a yield stress of 1,000 Pa and dynamic viscosity of 400 Pa-s.

This problem is simulated using CFX to show the performance of the present CFX modelling. In CFX, the dynamic viscosity of soil slurry is calculated using the same yield stress as did Imran et al. (2001) (=1,000 pa). A no-slip interface condition between the debris and seabed is used.

Figure 4.3 shows the shape of the debris at the end of run-out. In the vertical axis, *y* represents the current height of the debris. Figure 4.4 shows the maximum and frontal velocities with downslope displacement of the debris.

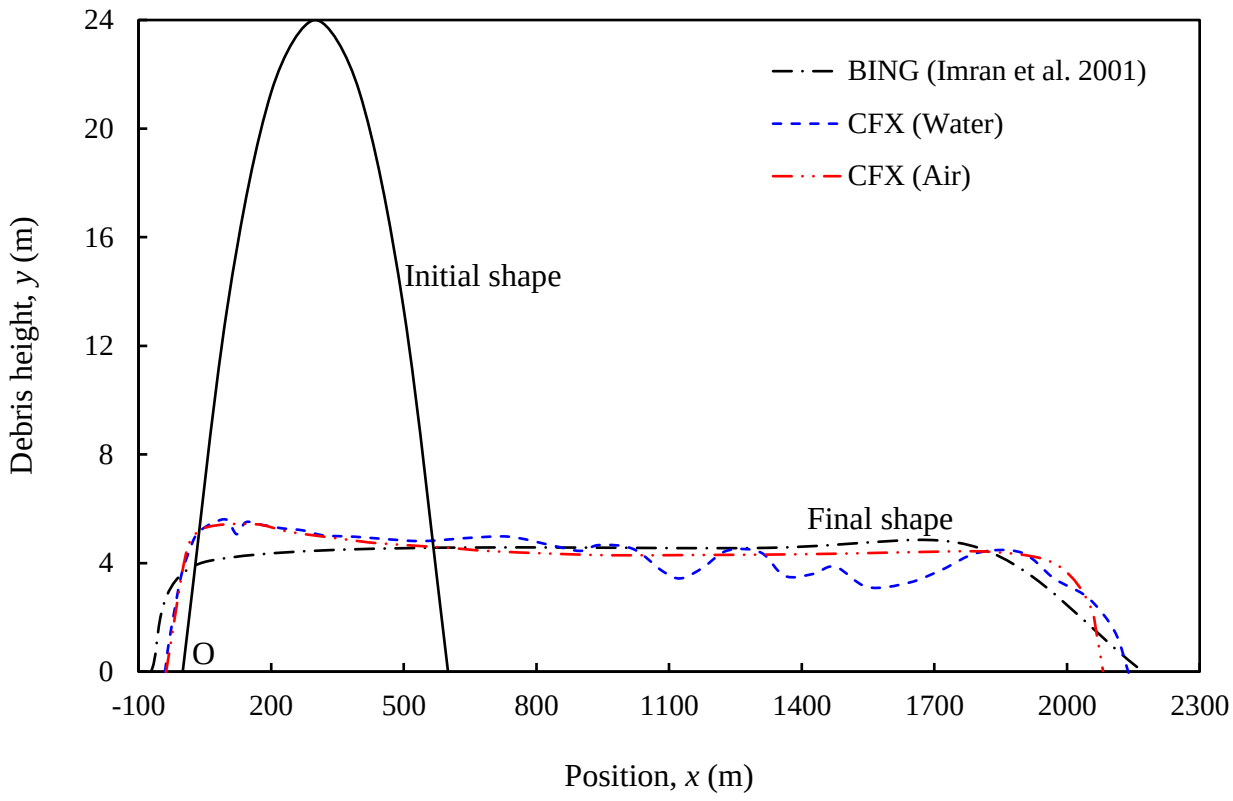

Fig. 4.3 Initial and final shapes of the debris

Figure 4.3 shows that, at the end of run-out, the debris spreads over ~3.7 times of its initial width (L_0 = 600 m). The front of the debris displaces downslope ~1536 m laterally (i.e. from $x = L_0$ = 600 m to x = 2,140 m). The back of the debris also moves slightly upslope by ~78 m laterally (i.e. from x = 0 to x = -78 m) because the slope of the seabed is very mild (20:1). The maximum depth of the debris is reduced to ~22% of its original depth (i.e., from $y = D_0$ = 24 m to y = 5.6 m). The profile of the debris obtained from the present CFX simulation is comparable to the simulation with BING (Imran et al. 2001). The slight difference might result from the difference between the rheological models of debris used in the simulations. A close examination of the velocity of soil elements in the debris show that the instantaneous velocity of the soil element during its downslope movement causes a slightly uneven profile, especially in the front part of the debris, as shown in

Fig. 4.3. In addition, the water pressure in the front also influences the instantaneous velocity. This has been confirmed by conducting another analysis with air as the ambient fluid, together with the submerged unit weight of soil, which gives a smoother surface of the debris, as shown in Fig. 4.3.

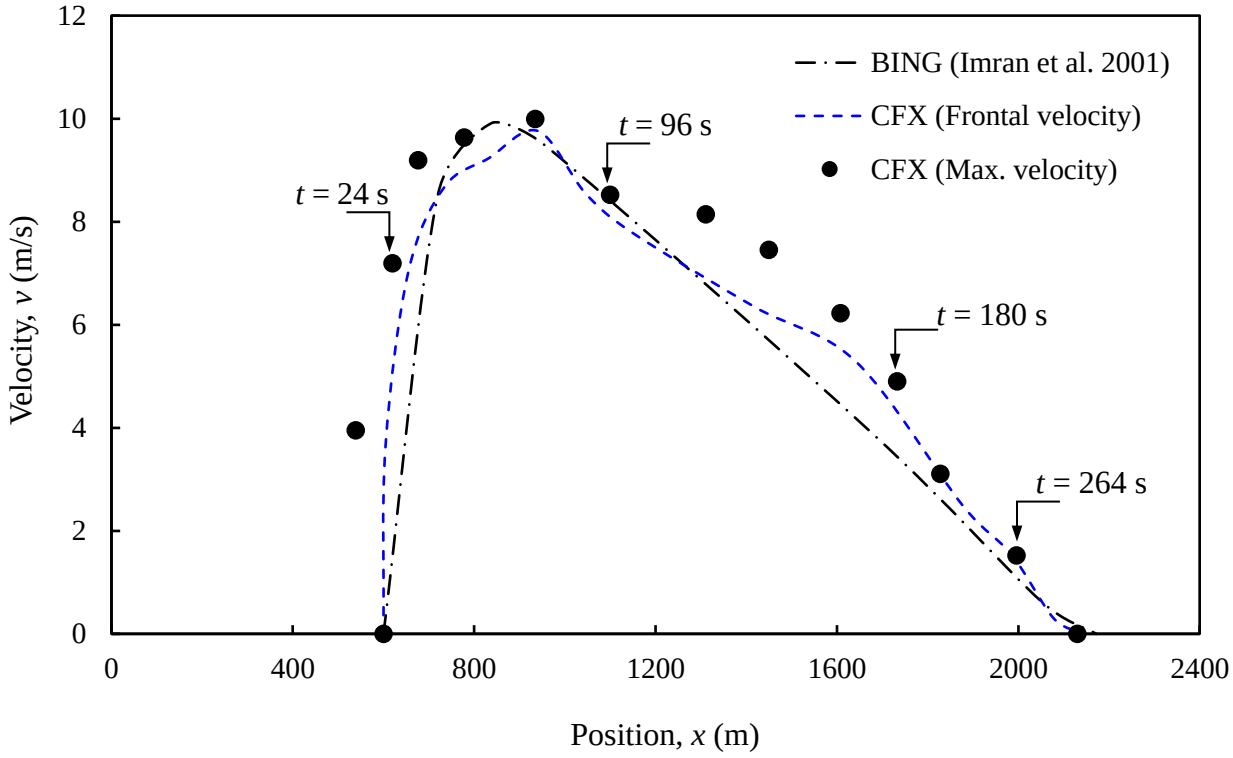

Fig. 4.4 Maximum and frontal velocities with downslope displacements

For a number of given time intervals, the maximum velocity (v_{max}) of the soil elements in the debris and its location (x-coordinate) are obtained. Figure 4.4 shows the variation v_{max} with x, which represents the maximum velocity that a soil element will experience during its flow through that particular section. For example, the maximum velocity of a soil element is ~8.5 m/s among the soil elements that pass through a vertical section at x = 1,100 m. The time required for the soil element of maximum velocity to reach this point is 96 s. The velocity of the soil element has a significant influence on the calculation of drag force on a suspended pipeline in deep water environments.

The same approach, discussed above, is used to obtain the frontal velocity of the debris during downslope movement, which is also plotted in Fig. 4.4. The frontal velocity is very comparable to v_{max}, which indicates that the maximum velocity mainly occurs in the front part of the debris, except for the early stage of displacement, where the maximum velocity is higher than the frontal velocity.

4.6 Frontal flow dynamics of the submerged sliding block

The dynamics of a submarine debris flow is a complex process. The resisting forces arise from different sources. The water pressure around the sliding body could significantly influence the velocity and run-out of the sliding mass. The total water pressure in front of the moving soil block consists of the hydrostatic pressure and hydrodynamic pressure. The hydrostatic pressure is due to the weight of the water column above it and the hydrodynamic pressure comes from the flow velocity during the movement of the soil block through the water.

The role of water is investigated in this section by simulating downslope displacement of a very strong sliding mass of $L_R \times H_R$ through water on a frictionless seabed of 2° inclination (Fig. 4.5). The unit weight (total) of the sliding block is 15.81 kN/m^3 and is allowed to move under gravitational force from an initial at-rest position. Although the debris in offshore environments is generally soft, as modelled in the following sections, a high undrained shear strength of 50 kPa is considered in this section; the sliding block does not fail by shear during downslope movement, because the shear failure could change the shape of the debris block and thereby hydrodynamic behaviour.

As the block moves through the water over a large distance, a large domain (abcd) of 2,000 m × 20 m is considered, which has been discretized into 1.0-m cubical elements. Analyses are

performed for one-element length in the out-of-plane direction in order to simulate the plane strain condition. All other boundary conditions are the same as the conditions described in Chapter 3 (Section 3.5.2). Analyses are performed for L_R = 10–170 m and H_R = 5 m.

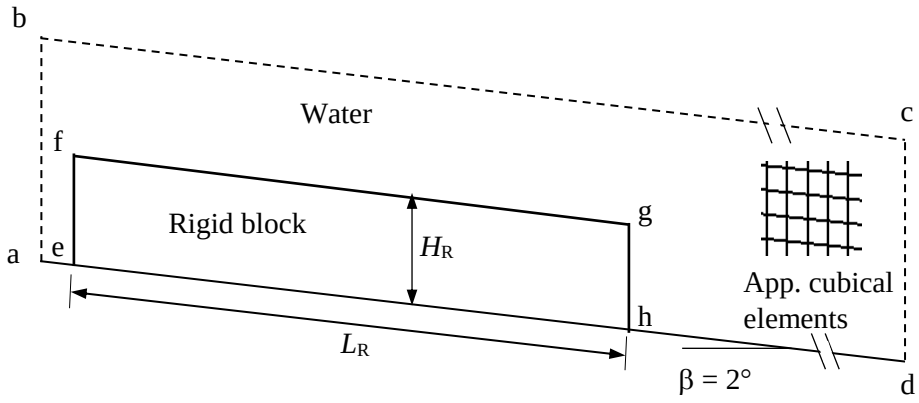

Fig. 4.5 Problem geometry for flow dynamics of the sliding block

4.6.1 Results

Figure 4.6 shows the velocity (v) of the block with time (t). The velocity increases with time and with an increase in the length of the sliding block. The velocity becomes constant after $t \sim 200$ s.

Based on Newton's second law, $F = ma$, the effect of water resistance is investigated. Differentiating v with respect to time, the acceleration of the sliding block (a) is calculated. F is calculated using Eq. (4.1), where $V = L_R H_R$ for the unit thickness of the sliding block and $F_f = 0$ (frictionless between the seabed and sliding block). Inserting the preceding information in $F = ma$, the drag force (F_d) is calculated, which is shown in Figure 4.7. Similar to velocity (Fig. 4.6), the drag force increases with time and also with an increase in length of the sliding block.

Figure 4.8 shows the variation of F_d/v^2 with time for the cases analyzed. As shown, F_d/v^2 decreases with time and remains almost constant after ~75 s. For a given time, the value of F_d/v^2 is higher for a longer block, especially at low t (< 100 s).

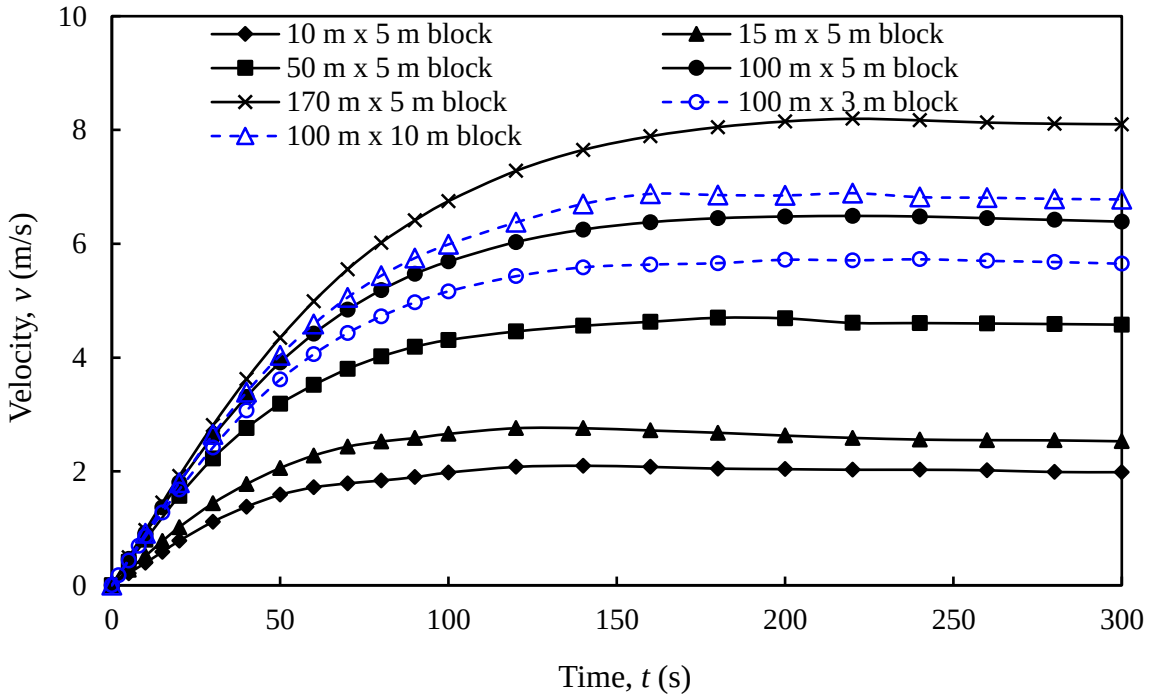

Fig. 4.6 Velocity of the block with time

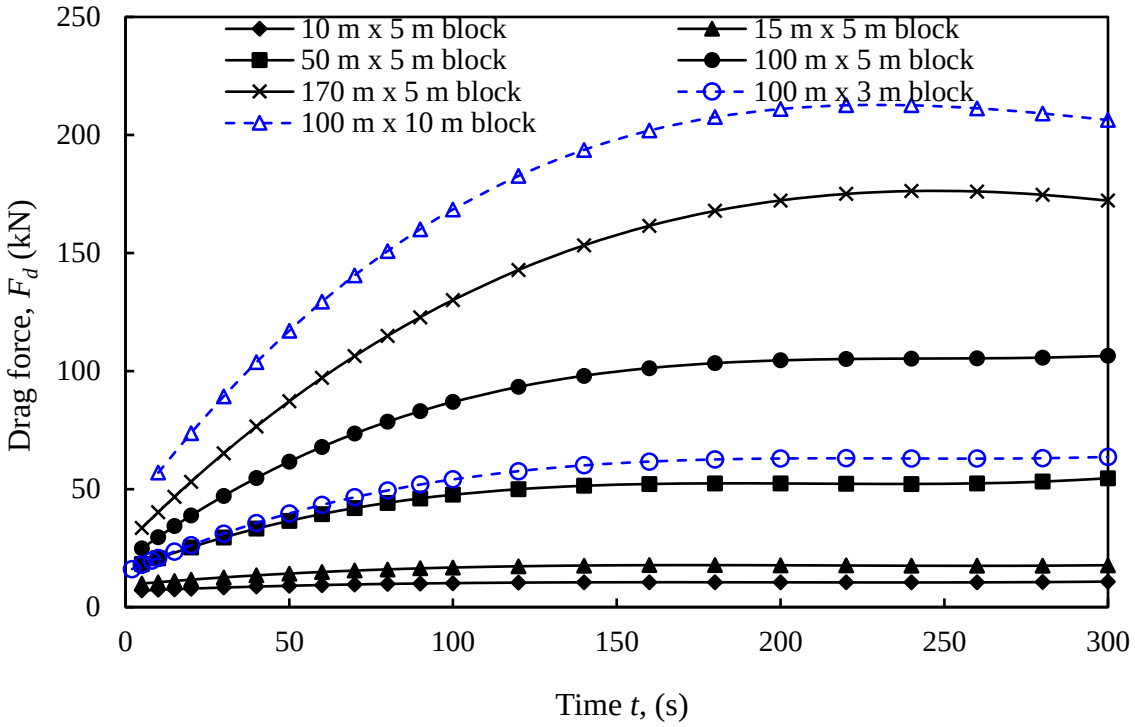

Fig. 4.7 Variation of drag force with time

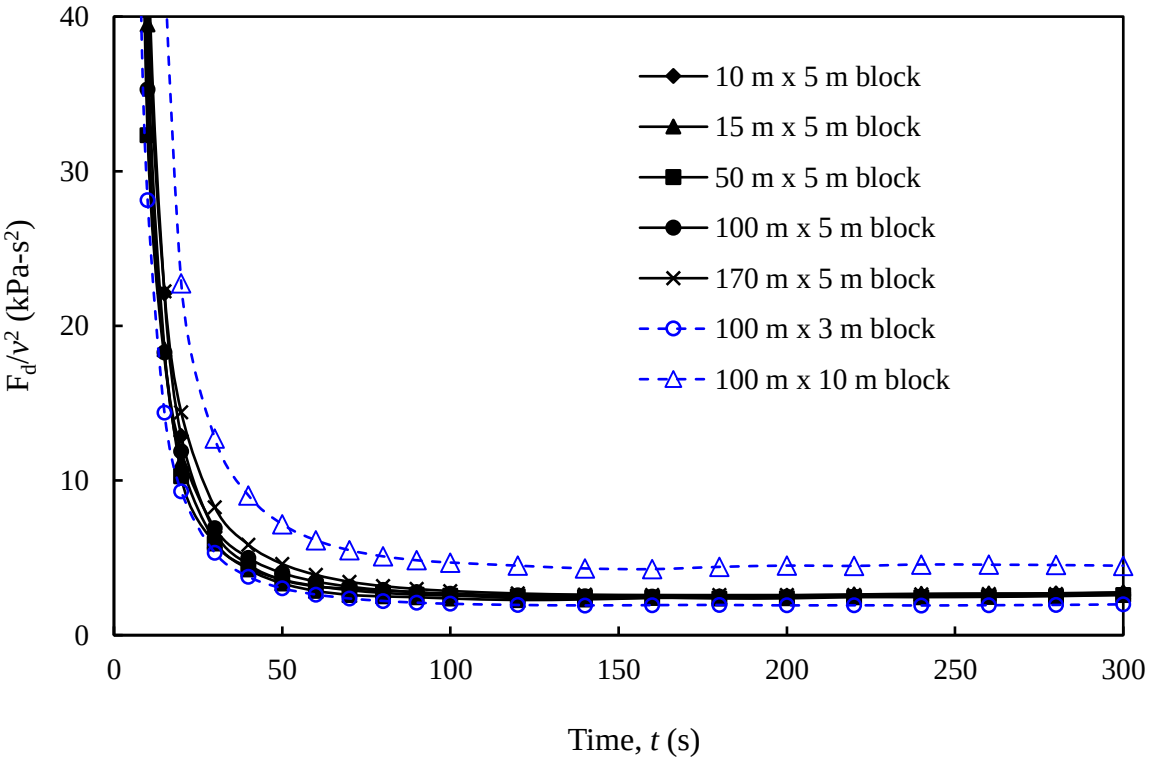

Fig. 4.8 Variation of F_d/v^2 with time

To calculate the drag force resulting from fluid-structure interactions, the contributions from different locations are not separated. For example, the drag force exerted by a debris flow on a pipeline is calculated using the drag coefficient (C_d) (Zakeri et al. 2009). However, in some studies, the total drag force has been divided into two components: (i) the pressure drag at the front of the block and (ii) the frictional drag that arises from the top of the soil block (Hoerner 1965; Newman 1977; Ilstad et al. 2004a). The pressure drag depends on the frontal area (A_{front}) of the sliding block (i.e., H_R in this case), whereas the frictional drag mainly depends on the area of the top surface (A_{top}) (i.e., the length of the sliding soil block, L_R). Ilstad et al. (2004a) suggested calculating the total drag force using the following equation:

$$F_d = 0.5\rho_w v^2 \left(C_{front}A_{front} + C_{top}A_{top}\right) \quad (4.3)$$

where ρ_w is the density of water; and C_{front} and C_{top} are the pressure drag coefficient in the front and friction drag coefficient at the top, respectively. Proper estimation of C_{front} and C_{top} separately is difficult. In their analyses, Ilstad et al. (2004a) used C_{front} = 0.4 and C_{top} = 0.005 for laboratory experiments and C_{front} = 0.25 and C_{top} = 0.0025 for the Finneidfjord field in northern Norway. If these values are used for the cases simulated in this study (H_R = 5 m and L_R = 10–170 m), the second component in the parenthesis of Eq. (4.3) (i.e., $C_{top}A_{top}$) is ~2% and ~25%–30% of the total (i.e., $C_{front}A_{front} + C_{top}A_{top}$) for L_R = 10 m and L_R = 170 m, respectively.

In the following sections, instead of separating the pressure and friction drags, a single value of drag coefficient (C_d) is used to calculate the drag force as:

$$F_d = 0.5\rho_w v^2 C_d A_{front} \quad (4.4)$$

C_d is calculated using this equation. The variation of C_d is plotted against time in Fig. 4.9, for A_{front} = 5 × 1 = 5 m^2. As shown, C_d decreases with time and at large values of time, the difference is not significant. The calculated C_d is higher for lower t, where the velocity is smaller (see Fig. 4.6). An

increase in C_d with a decrease in velocity (or Reynolds number, which is proportional to the velocity of Newtonian fluid) has also been reported in previous studies (Newman 1977; Yoon et al. 2010).

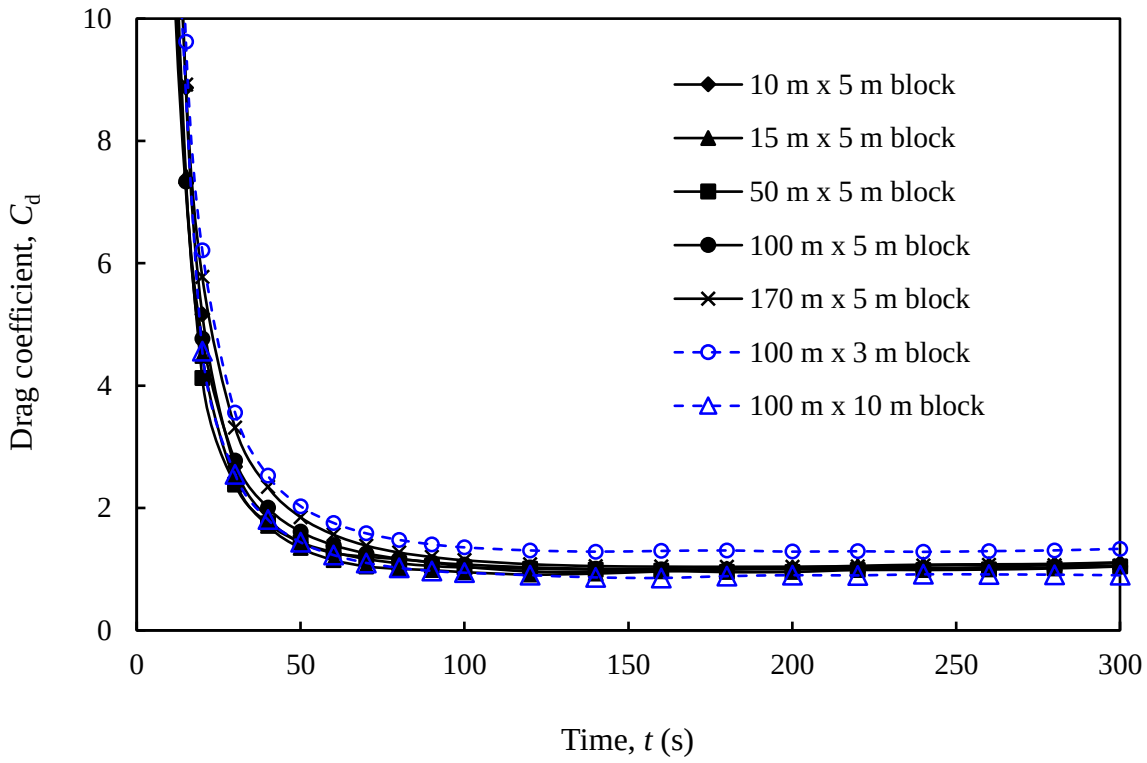

Fig. 4.9 Variation of drag coefficient with time

Note that during the downslope movement of the soil block, some soil particles might be eroded from the surface and mix with the surrounding water. Therefore, the fluid surrounding the sliding body might behave as a non-Newtonian fluid. A typical variation of the drag coefficient of slurries of varying soil contents is shown in Fig. 4.10.

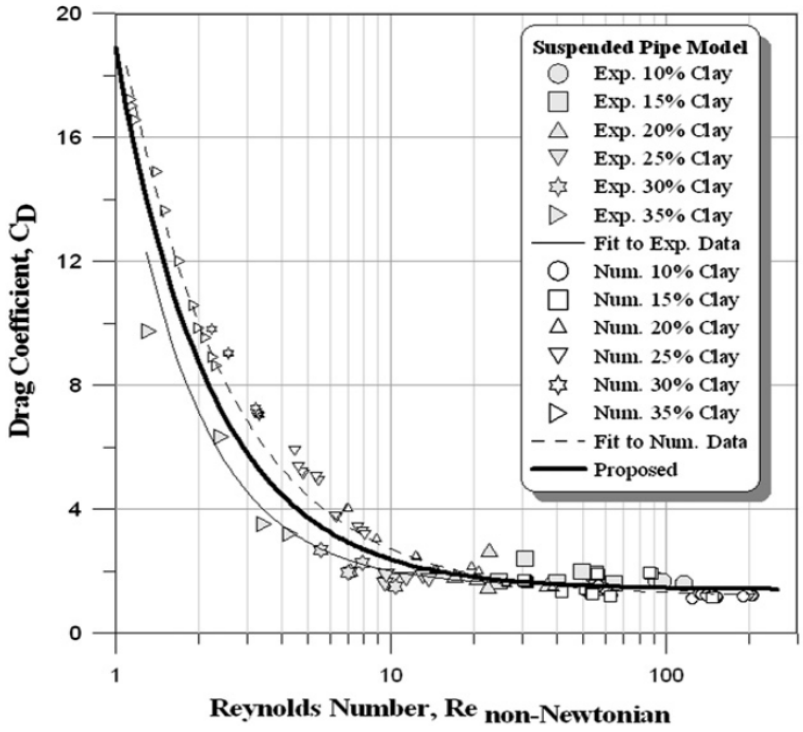

Fig. 4.10 Variation of drag coefficient with Reynolds Number (after Zakeri et al. 2009)

Effects of height of the soil block

In the previous section, analyses are performed for a 5-m height of the soil blocks. Analyses are also performed varying the height of the block (H_R = 3–10 m) for L_R = 100 m. The other parameters are the same as those above. The dashed lines with open symbols show the results for varying heights. Again, the trends of v, F_d, F_d/v^2 and C_d for varying heights are similar (Figs. 4. 6–4.9).

4.7 Effect of soil failure and ambient fluid

In Section 4.6, the shear failure of the sliding block is avoided by assigning a high undrained shear strength. In this section, the shear failure of the soil block during downslope movement occurs because of relatively low shear strength. Similar to previous cases (Section 4.6), the soil block is displaced through the water.

The geometry shown in Fig. 3.1 is used here. A trapezoidal debris block is displaced over a mildly-inclined seabed ($\beta = 5°$); however, in this case, the ambient fluid is water. The built-in dynamic viscosity of water of 8.899×10^{-4} Pa-s is used. For debris, the dynamic viscosity is defined as $s_u/\dot{\gamma}$, where $\dot{\gamma}$ is the shear strain rate. In this simulation, $s_u = 2.1$ kPa is used. Further discussion of numerical implementation is provided in the previous chapter (Section 3.5.2). The standard k–Omega model is used to represent the turbulence generated in the fluid. The geometry and geotechnical properties of the debris are the same as in Table 3.2 (Chapter 3).

4.7.1 Results

Figure 4.11 shows the velocity and the run-out distance. For comparison, the results for the air as the ambient fluid, as presented in Chapter 3, are also plotted in Fig. 4.11. As shown, the peak velocity for the in-water condition is lower than in the in-air case. The time required to attain the peak velocity in the water domain is almost double that for the in-air condition. In the air domain, the soil block attains the maximum velocity of ~ 4 m/s after ~ 3 s, while it takes ~ 6 s in the water domain to reach the maximum velocity of ~ 2 m/s.

The lower velocity of the sliding block in the water domain is due to considerable drag force resulting from water, as discussed in Section 4.6. When the block moves in the in-air condition, the drag forces are negligible compared to in-water drag force.

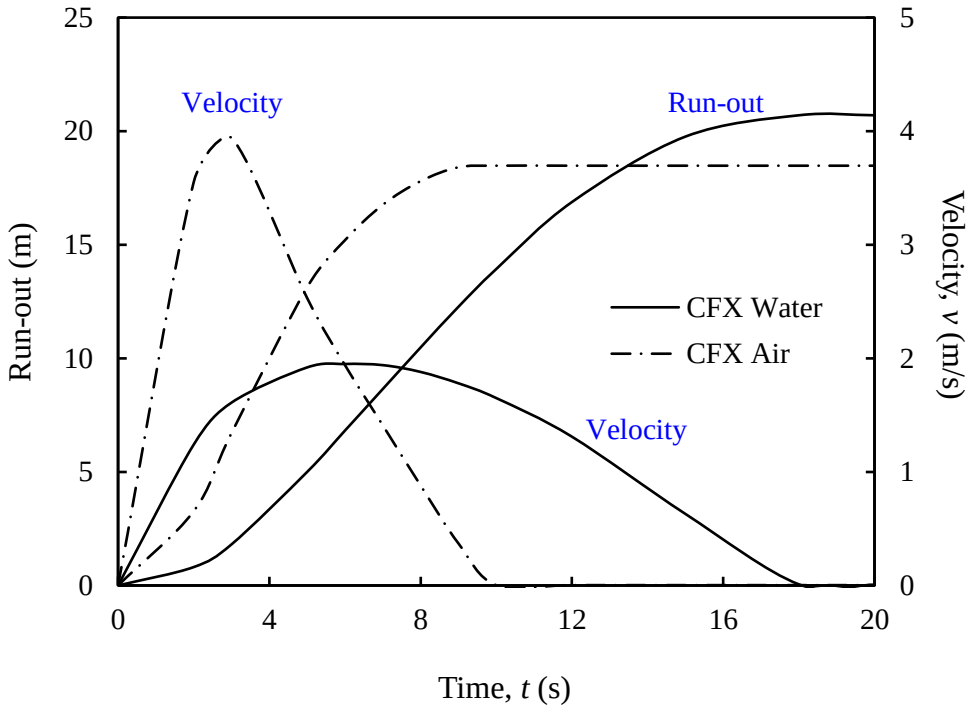

Fig. 4.11 Run-out distance and velocity of the front toe in the two-phase flow model

As discussed in Section 4.6, the pressure drag resulting from the pressure in the front of the soil block is the primary source of drag force. Figure 4.12 shows the frontal pressure for both domains when the maximum velocity is attained (i.e. t = 3 s and t = 6 s for the in-air and in-water cases, respectively, as shown in Fig. 4.11). Note that the frontal pressure is velocity dependent. Figure 4.12 shows that, although the maximum velocity for the in-air case is almost double that of the in-water case, the frontal pressure is low for the in-air simulations (< 8 pa). However, a significantly large pressure develops (maximum of 2,000 pa) when it slides through a water domain.

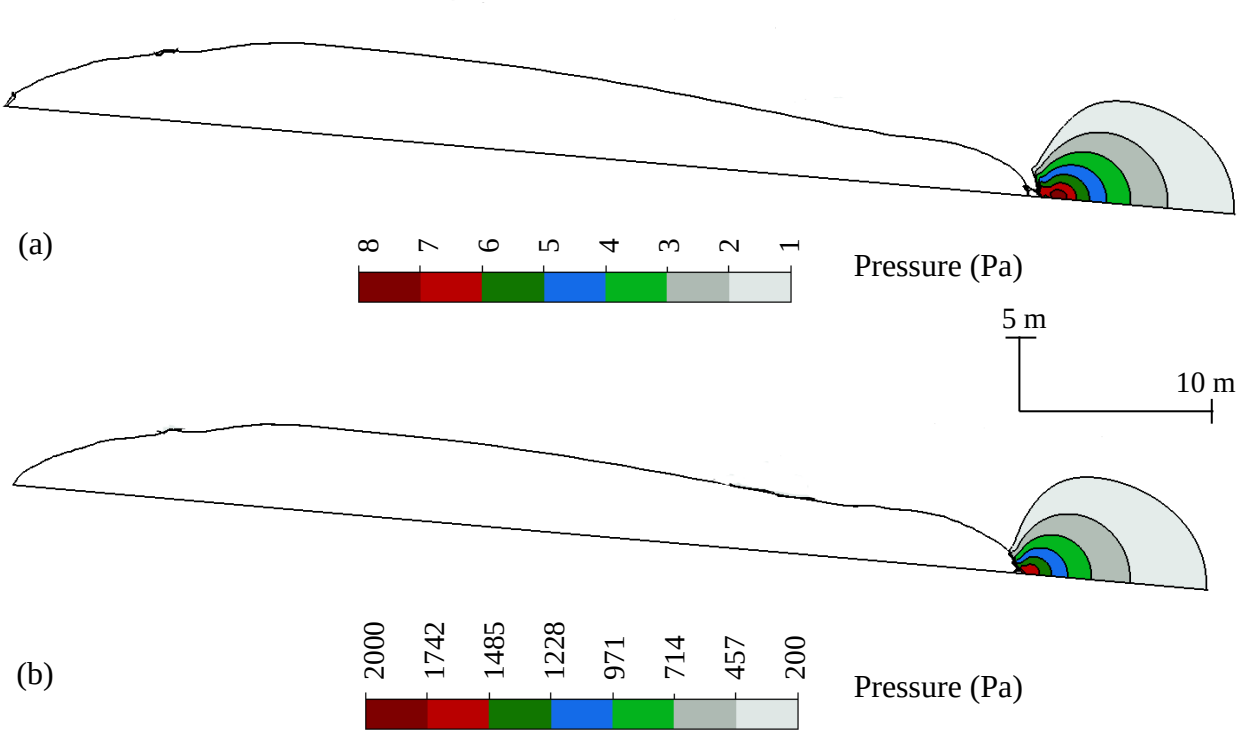

Fig. 4.12 Frontal pressure at the maximum velocity (a) in-air (b) in-water

Figure 4.11 also shows that the run-out occurs faster in the air domain than in the water domain. The run-out is completed in ~10 s in the air while it takes ~18 s in the water. This difference is primarily due to the drag force resulting from the ambient fluid, which is higher in the water than in the air domain. The sliding block stretches due to plastic deformation and shear failure of the soil. The development of plastic shear strain at an early stage and also at the end of run-out is shown in Fig. 4.13. Figures 4.13(a) and 4.13(c) show that the failure of slopes at both ends occurs at the early stage. With a displacement of the failed soil mass, additional failure planes form and plastic shear strains are generated in most of the whole sliding body, as shown in Figs. 4.13(b) and 4.13(d). The deformed shape of the sliding block, with respect to the initial one, at t = 6 s and at the end of run-out, is shown in Figs. 4. 14(a) and 4.14(b) for the in-air and in-water conditions, respectively.

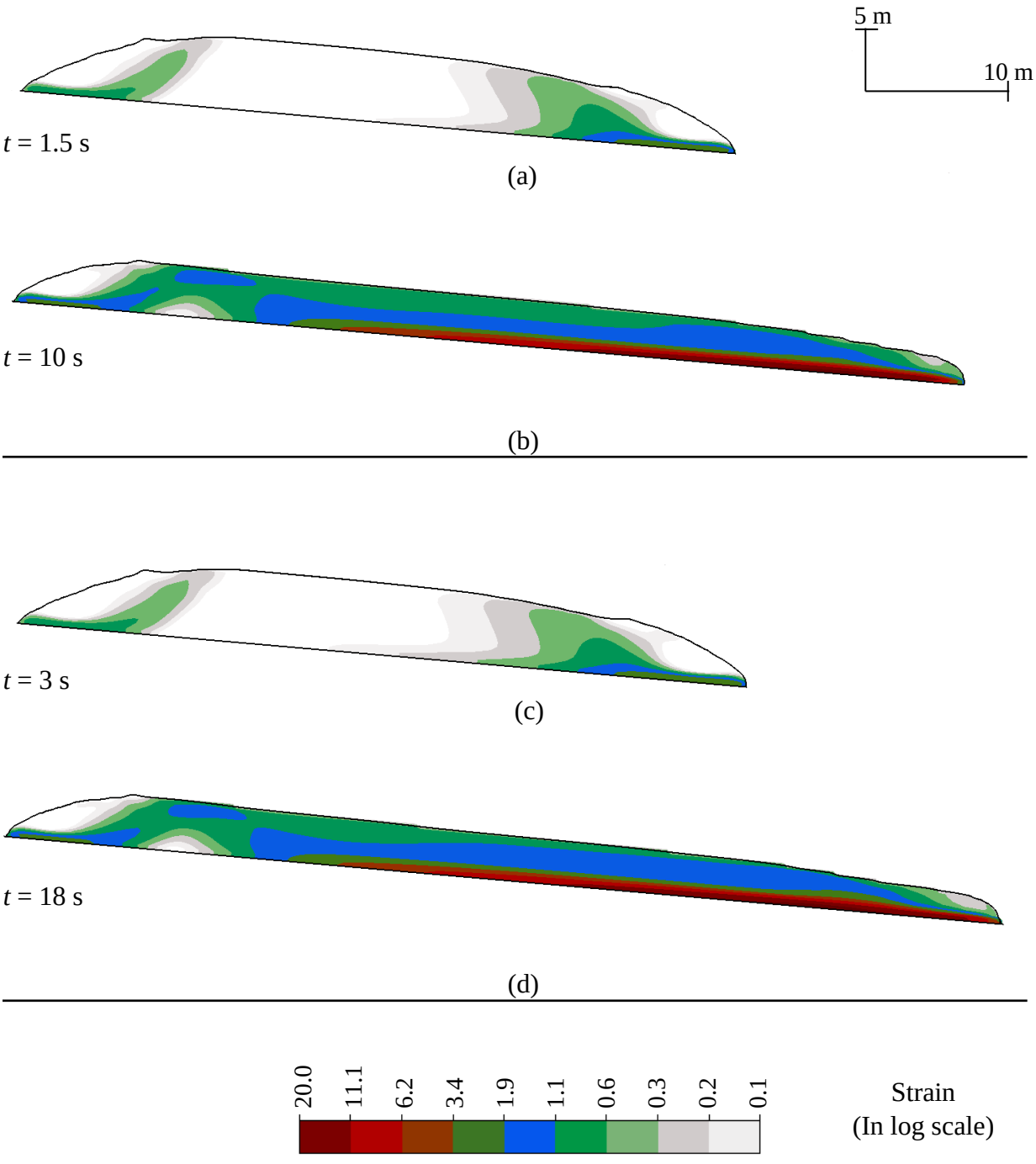

Fig. 4.13 Development of plastic shear strains: (a & b) in-air (c & d) in-water

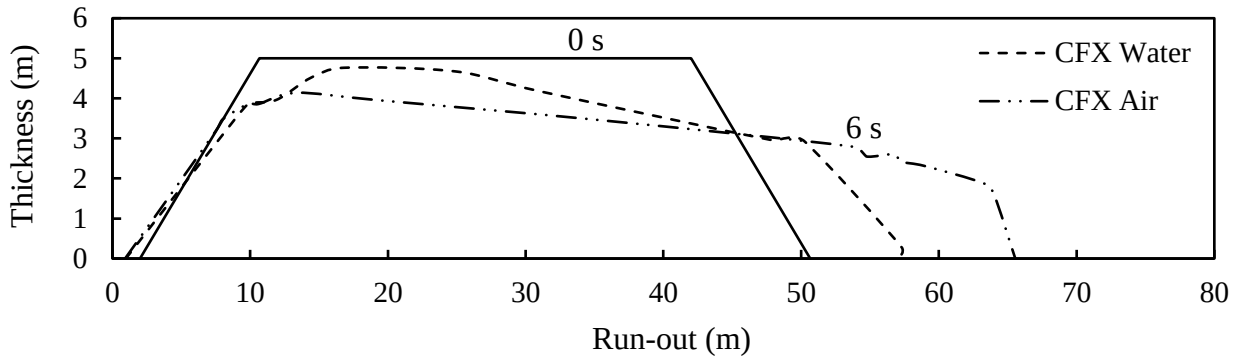

(a)

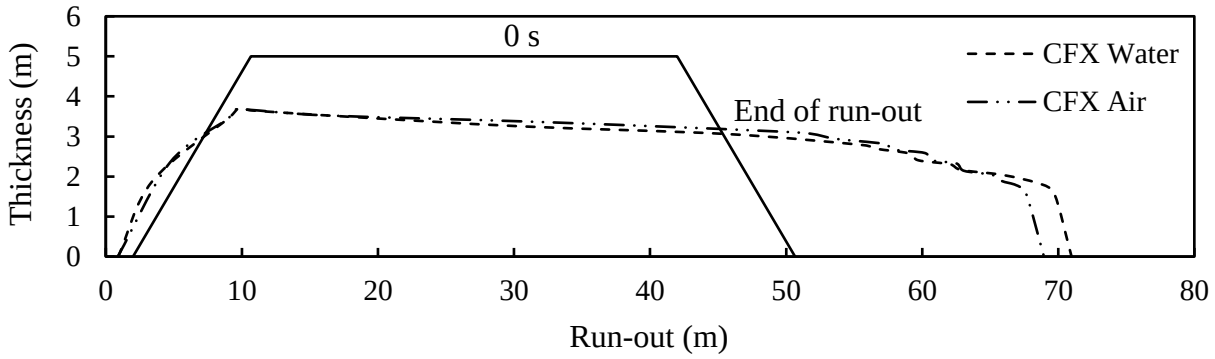

(b)

Fig. 4.14 Shape of the sliding block: (a) at 6 s (b) end of run-out

4.8 Effects of shear strength degradation

A constant undrained shear strength is used for debris in the previous simulations. As shown above, significantly large shear strains are generated due to the large displacement of the debris block or failure of the soil mass (e.g. see Fig. 4.13). Previous studies showed that the undrained shear strength of offshore sediments degrades with an accumulation of plastic shear strain (Ma 2015; Dong 2017). In this section, analyses are performed considering shear strength degradation of the sediment.

The simulation is performed using a similar trapezoidal soil block, as is considered in Section 4.7 and Chapter 3; however, a thin weak layer of 0.25 m just above the seabed is considered in some cases (Fig. 4.15). In the field, this weak layer represents the existence of very soft soil near the seabed surface. All the simulations are performed with water as the ambient fluid.

The CFX model is developed with one-element length in the out-of-plane direction, in order to simulate the plane strain condition. The domain is discretized into approximately cubical shape elements of 0.25-m length. The seabed–soil interface is defined as a no-slip boundary condition. The modelling technique and all other boundary conditions are the same as those above (e.g. see Section 4.7).

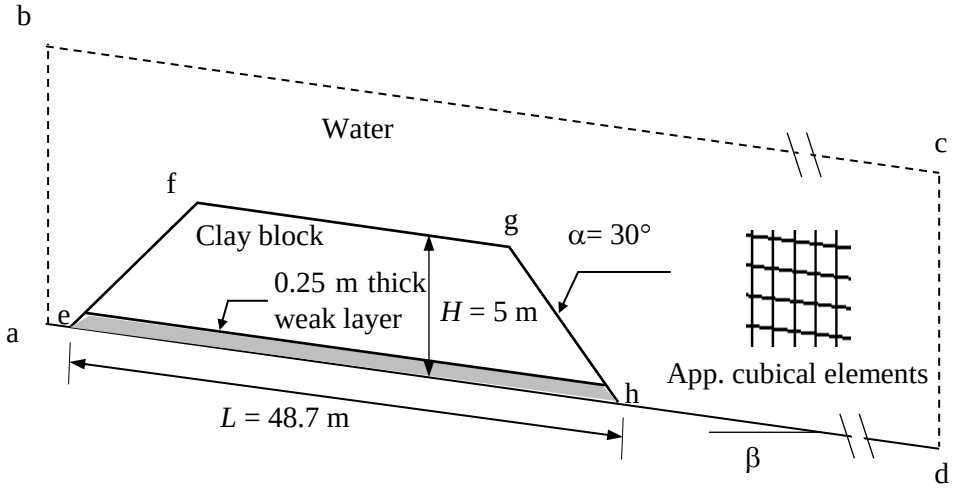

Fig. 4.15 Problem statement for simulations with strain-softening behaviour of soil (not in scale)

4.8.1 Shear strength degradation of soft clay

The shear strength degradation of soft offshore clay sediments in submarine landslides and subsequent run-out occurs primarily for two reasons: (i) undrained remoulding and (ii) shear wetting due to water entrainment (De Blasio et al. 2005; Dutta et al. 2018). The undrained remoulding occurs because of the accumulation of plastic shear strain (ξ), without any change in water content. This process causes the breakdown of soil microstructure and rearrangement of soil

particles. The second component, due to water entrainment, occurs in the highly sheared zone near the soil–water interface where there is an availability of "free water." When water entrainment occurs, the behaviour of soil cannot be considered as undrained any longer. Therefore, in the following section, the symbol τ_y is used for the mobilized shear strength.

The process of shear strength degradation due to undrained remoulding is modelled using a simple exponential decay function given by Einav and Randolph (2005):

$$s_u = \left[\frac{1}{S_t} + \left(1 - \frac{1}{S_t}\right) e^{-3\xi/\xi_{95}}\right] s_{up} \tag{4.5}$$

where sensitivity, $S_t = s_{up}/s_{uR}$, s_{up} is the peak undrained shear strength, s_{uR} is the remoulded shear strength and ξ_{95} is the value of accumulated shear strain required to cause a 95% reduction of the peak undrained shear strength.

Shear wetting due to water entrainment is a complex process which is difficult to model. In the present study, following the work of Dutta et al. (2018), a linear degradation of shear strength with accumulated plastic shear strain (line *bc* in Fig. 4. 16) is used to model water entrainment effects. Note that De Blasio et al. (2005) also used a similar model for water entrainment. Further discussions on this modelling approach are available in those studies (De Blasio et al. 2005; Dutta et al. 2018).

Figure 4.16 shows the shear strength degradation curve (*abcd*) used in the present study. Here the lines *ab* and *bc* represent the undrained remoulding (Eq. 4.5) and shear wetting due to water entrainment, respectively. Mathematically, the segments of the shear strength degradation curve can be expressed as:

$$\tau_y = \begin{cases} \left[\frac{1}{S_t} + \left(1 - \frac{1}{S_t}\right) e^{-3\xi/\xi_{95}}\right] s_{up} & \text{if } \xi \le \xi_{95} \\ \left[s_{u95} - \left(s_{u95} - \tau_{y(ld)}\right)\left(\xi - \xi_{95}\right)/\left(\xi_{ld} - \xi_{95}\right)\right] & \text{if } \xi_{95} < \xi \le \xi_{ld} \\ \tau_{y(ld)} & \text{if } \xi > \xi_{ld} \end{cases} \tag{4.6}$$

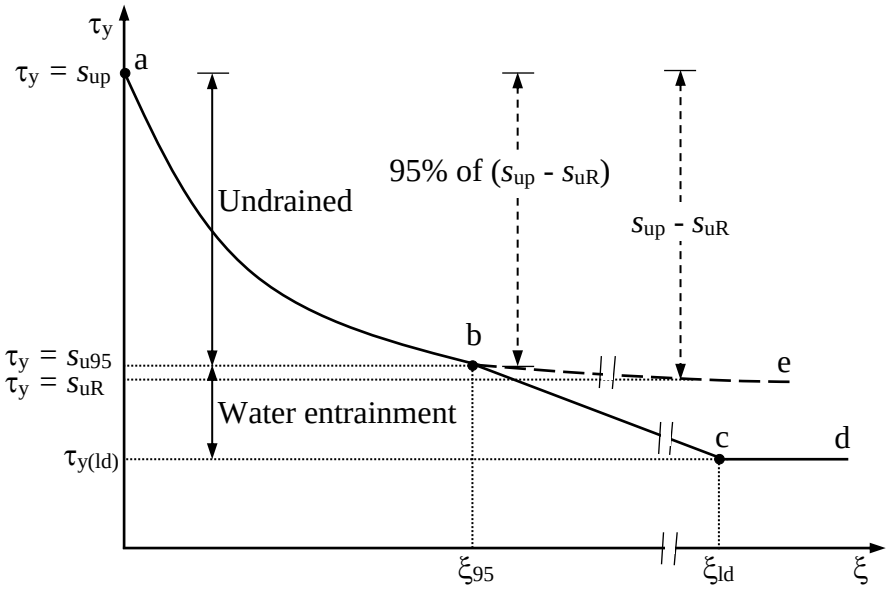

Fig. 4.16 Shear strength degradation model (after Dutta et al. 2018)

4.8.2 Geotechnical parameters and slope angle

The typical range of S_t of offshore sediment is 2–5 (Kvalstad et al. 2001). The value of ξ_{95} can vary from 10 to 50, as found from the analyses of T-Bar test results on soft clays (Einav and Randolph 2005). As sensitive soil is considered in these simulations, where a higher structural breakdown is expected, a value of $\xi_{95} = 2.0$ is used to model a faster reduction of shear strength with plastic shear strain. Table 4.1 shows the slope angle and geotechnical parameters used in the present study. Post-failure investigations show that a submarine landslide and subsequent run-out could cause varying soil failure patterns. The effects of geotechnical properties and slope angle on failure patterns are investigated through simulation of six cases, as listed in Table 4.1.

Table 4.1 Slope angle and soil properties used in simulations

Case	β (°)	γ (kN/m^3)	s_{up} (kPa)	$s_{u(weak)}$* (kPa)	$\tau_{y(ld)}$ (kPa)	S_t	ξ_{95}	ξ_{ld}	Failure shape
1	5	15.7	4	1	-	-	-	-	Elongation
2	5	15.7	4	-	-	5	2	-	Flowslide
3	5	15.7	4	-	$0.1s_{up}$	5	2	10	Flowslide
4	4	15.7	4	-	$0.1s_{up}$	5	2	10	Flowslide
5	4	15.7	5	1	$0.1s_{up}$	5	2	10	Spreading
6	2	15.7	4	1	$0.1s_{up}$	8	2	10	Spreading

*$s_{u(weak)}$ represents a constant undrained shear strength of the weak layer

4.8.3 Results

4.8.3.1 Simulation results for Case-1

Figure 4.17 shows the velocity of the soil elements at different times. The failure is initiated from the right toe by the formation of a failure plane through the weak layer. As it propagates, plastic shear strains are generated in the soil above the weak layer, which cause downslope movement of the failed soil. The right side of the debris block moves downslope, which causes lateral stretching of the block with a gradual reduction in height (Fig. 4. 17 and 4.18).

Case - 1

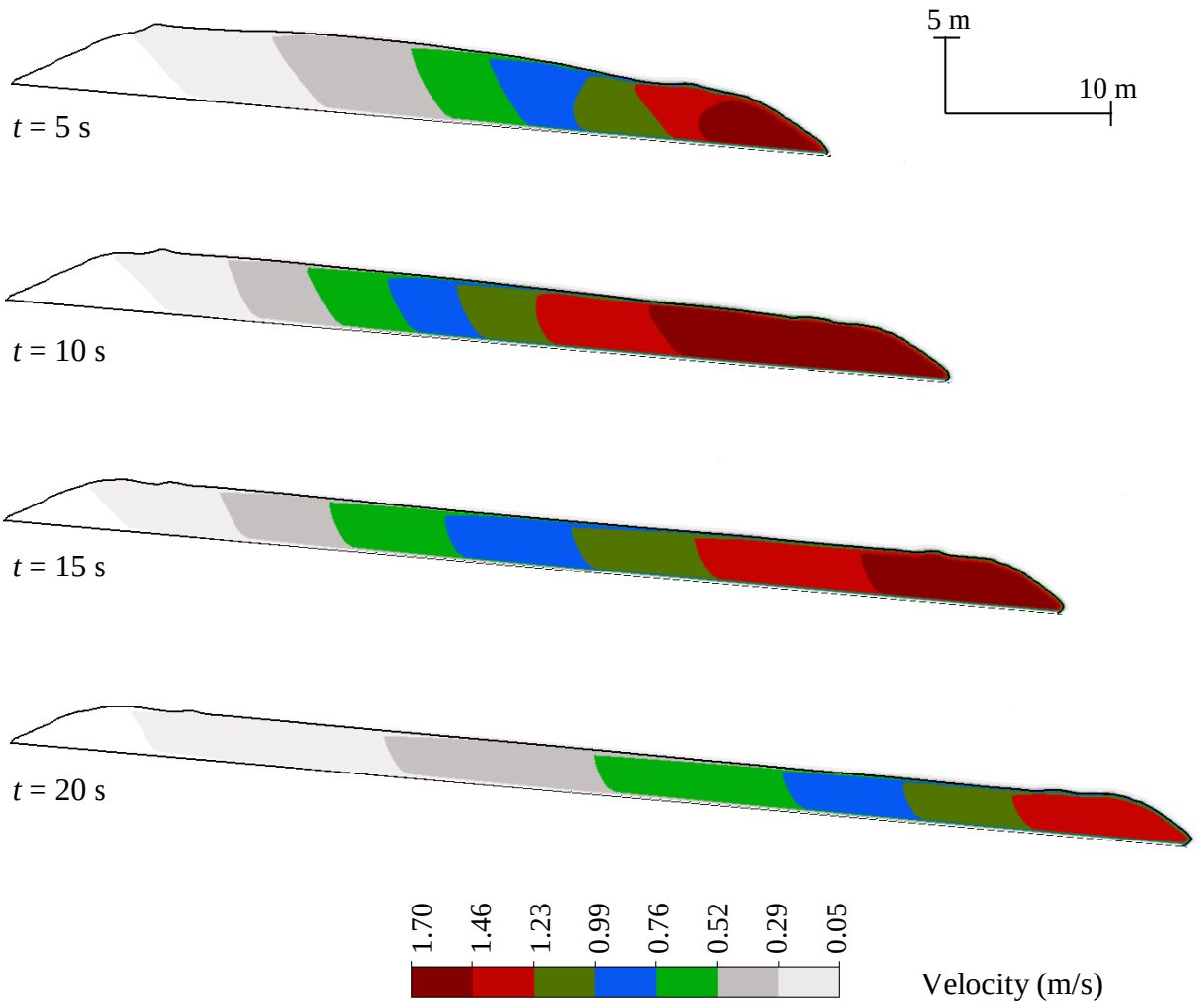

Fig. 4.17 Velocity contours at different times for Case-1

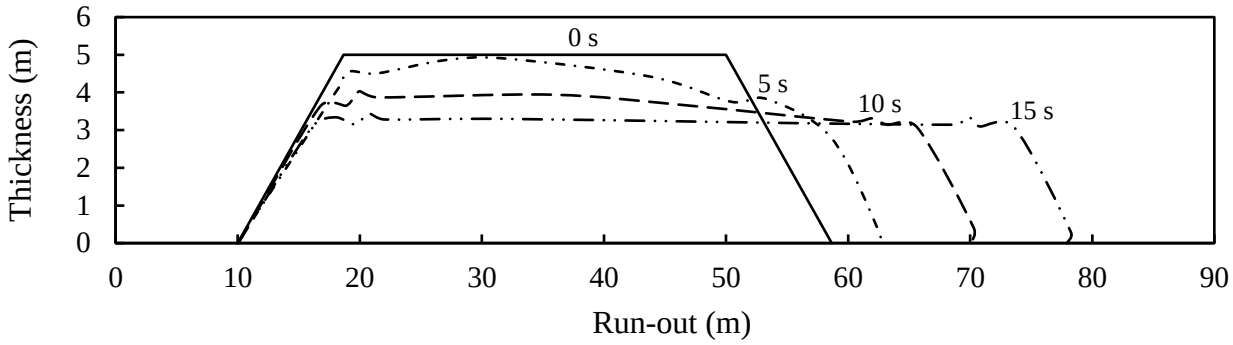

Fig. 4.18 Progression of run-out for Case-1

The velocity and acceleration of the front toe and mid-point of the stretched soil block are also plotted as a function of time (Figs. 4.19 & 4.20). Note that the toe and mid-point shift due to stretching with time. As high strains generate in the front part of the block, a large shear strength degradation occurs in this part. As a result, the front part moves faster than the middle part. During the downslope movement, the maximum velocity of the soil elements is found near the right side, and it gradually decreases to the left. Once the sliding block elongates, the total frictional resistance from the bottom increases due to the increase in interface length of the block. Therefore, deceleration occurs in the movement of the soil elements after $t \sim 12$ s, as shown in Fig. 4.20.

The downslope displacement of the front toe with time is shown in Fig. 4.21. The run-out increases with time, and at $t \sim 32$ s the run-out is completed. The maximum run-out distance is ~ 37 m.

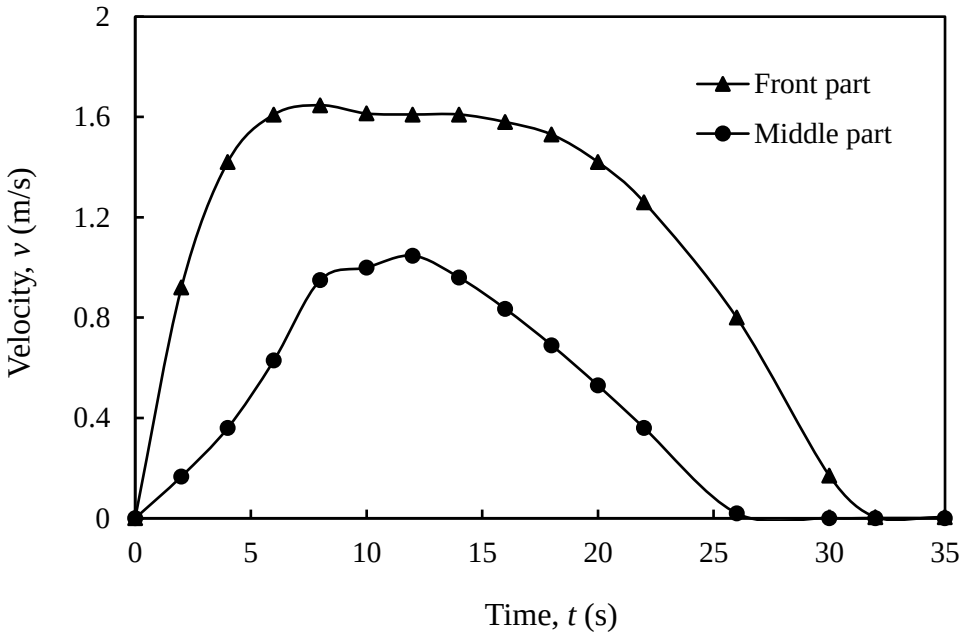

Fig. 4.19 Velocity of the front and middle part of the soil block (Case-1)

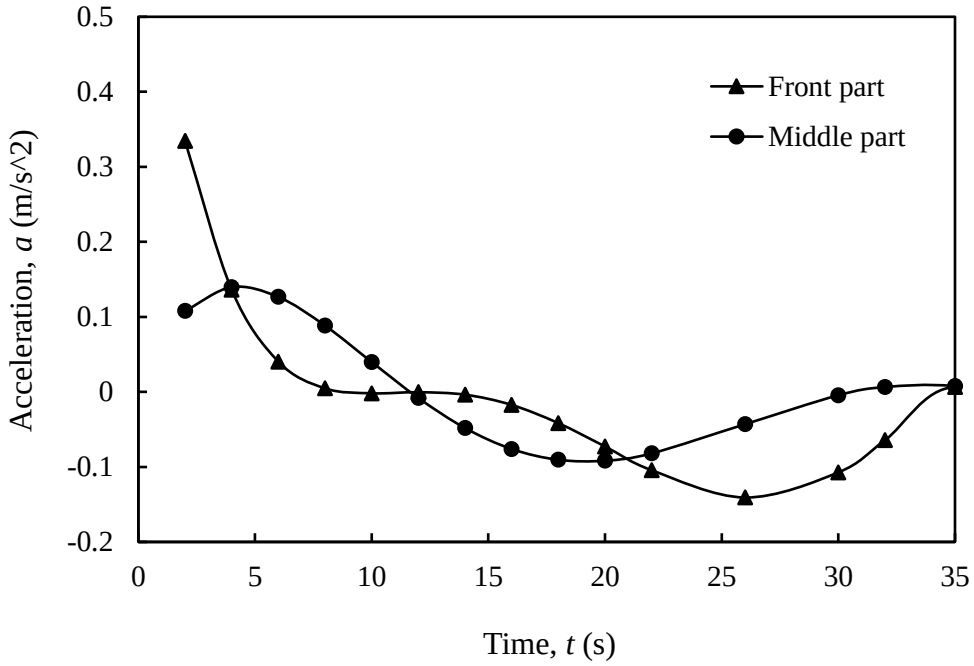

Fig. 4.20 Acceleration of the front and middle part of the soil block (Case-1)

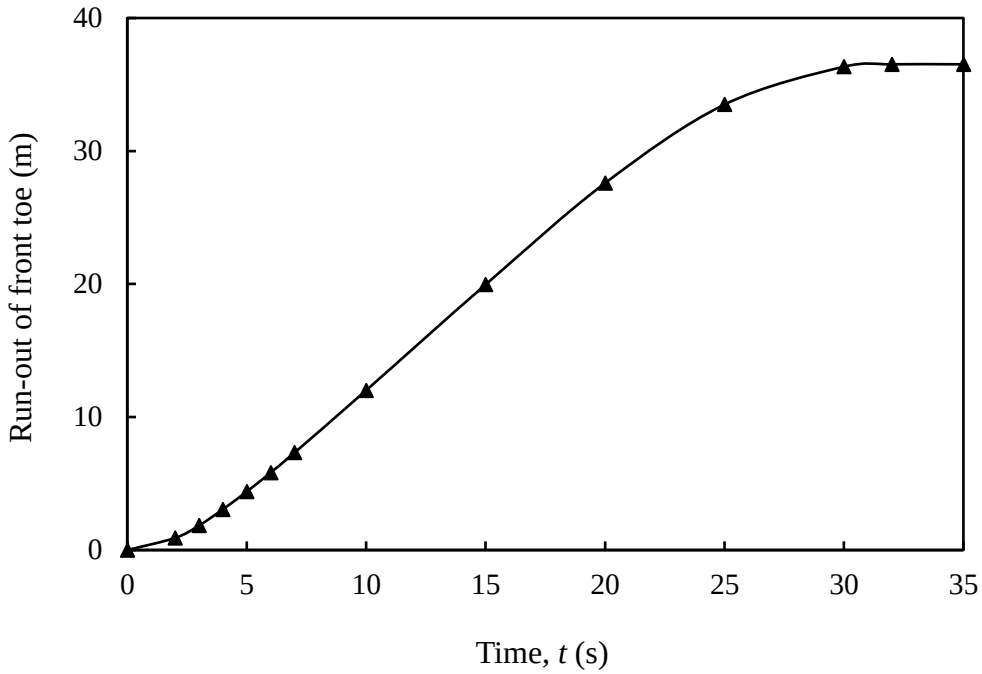

Fig. 4.21 Front toe run-out plot for Case 1

4.8.3.2 Simulation results for Cases 2–4

Figures 4.22–4.30 show the simulation results for Cases 2–4. As shown in Table 1, unlike Case-1, the shear strength degradation due to undrained remoulding is considered in these cases using a sensitivity (S_t) of 5.0. The weak layer is not considered in these cases, and the failure is initiated by gravitational force. The shear wetting is not considered in Case-2. Figure 4.22 shows the progressive formation of failure planes with time. The failure of soil blocks is initiated by a rotational failure, and the failed soil mass then breaks into pieces with downslope displacements. This type of failure pattern is generally classified as "flowslide." Compared to Case-1 simulation results, distinct failure planes form in this case through accumulation of localized large plastic shear strains around the failure plane, because of the strain-softening behaviour. As the soil becomes weaker due to strain-softening, the velocity of soil elements (e.g., frontal velocity) is higher in this case than in Case-1 (compare Figs. 4.17 and 4.23). Flowslides are commonly

observed in sensitive clays, and the remoulded shear strength is considered to be one of the primary factors related to flowslides (Tavenas 1984; Strand et al. 2017). In the present simulation (Case-2), the shear strength reduction occurs due to strain-softening, which causes flowslides. The mobilized shear strength at different stages is presented in Fig. 4.24, which shows that significantly large shear strength reduction occurs along the failure planes.

The Case-3 simulation is the same as Case-2, except for the consideration of shear wetting. In Case-3, the shear strength degrades to a very small value of $0.1s_{up}$ (= 0.4 kPa) at a large strain. Therefore, the failed soil mass travels at a larger velocity than in Cases-1 and -2 (compare Figs. 4.17, 4.23 and 4.26). The propensity of flowslide is higher in this case because of the low large-strain shear strength. Moreover, the run-out distance is higher in Case-3 than in Cases-1 and -2 (Figs. 4.17, 4.22 and 4.25).

The Case-4 simulation is performed to examine the effect of seabed slope angle on failure. A smaller slope angle of 4° is used in this case. The other conditions are the same as in Case-3. Figures 4.28–4.30 show that the failure pattern is again similar to flowslide; however, the velocity of soil elements and run-out distance are small compared to those found in the Case-3 simulation.

Case-2

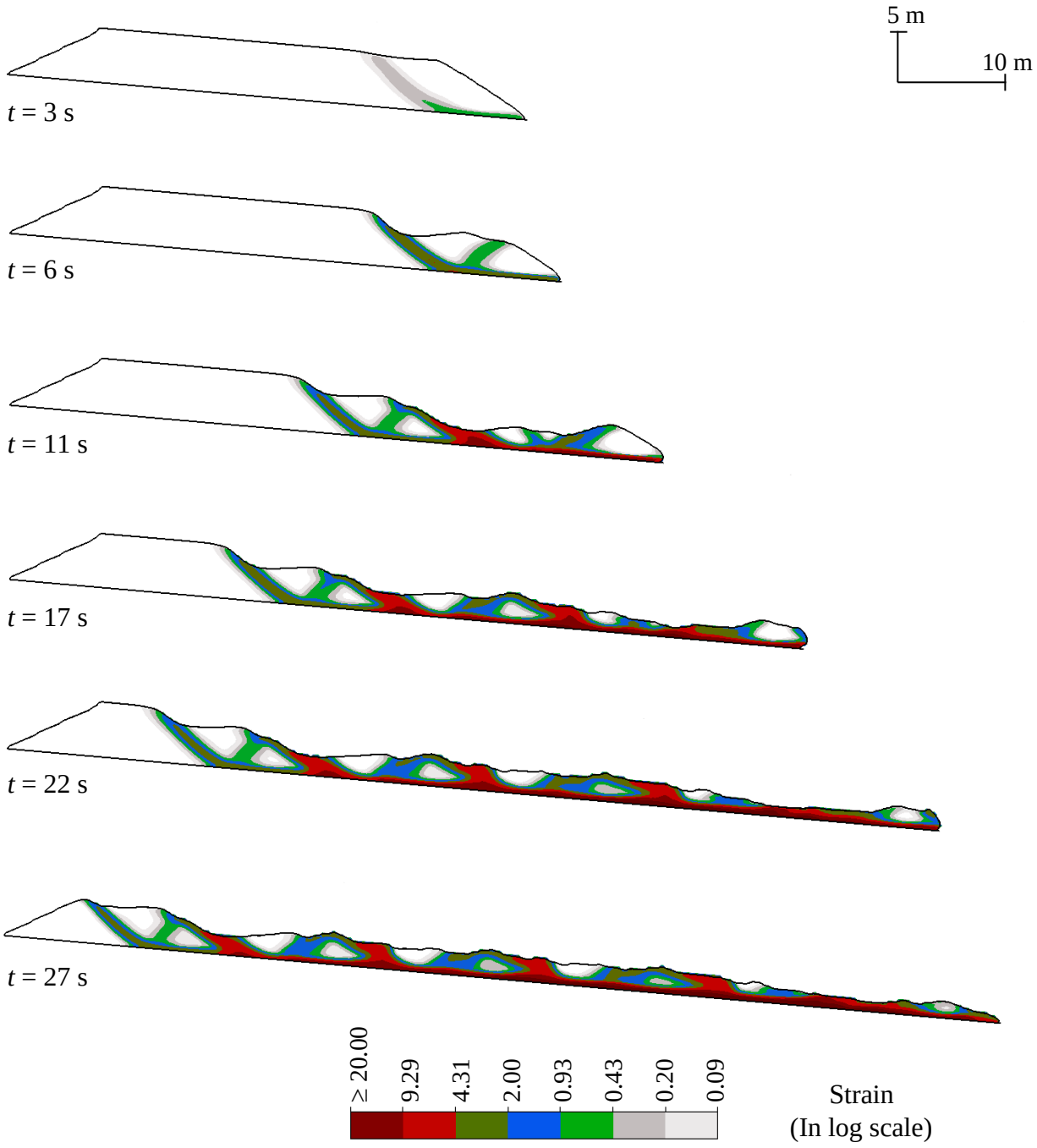

Fig. 4.22 Formation of failure planes in Case-2

Case-2

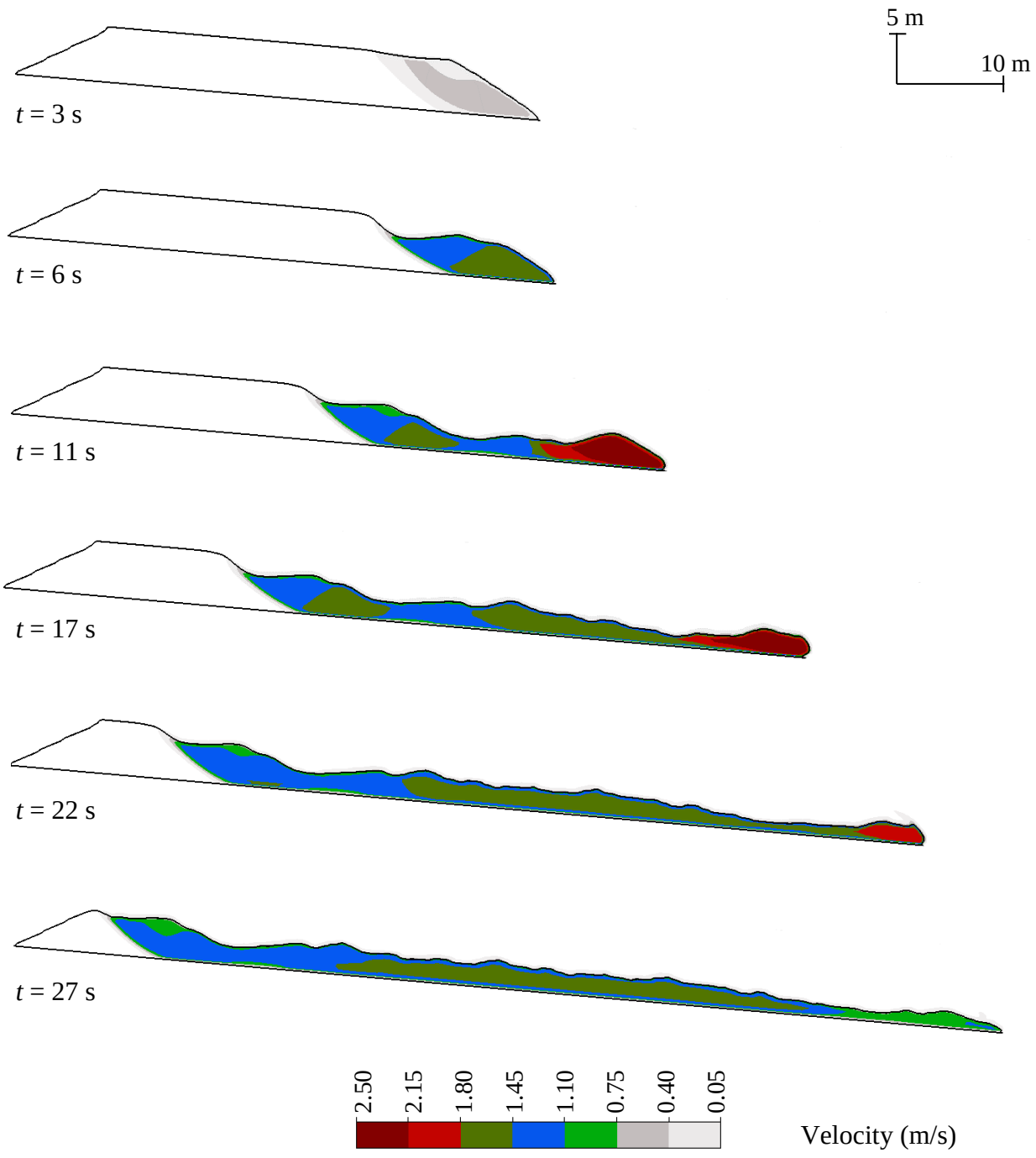

Fig. 4.23 Instantaneous velocity of soil elements in Case-2

Case–2

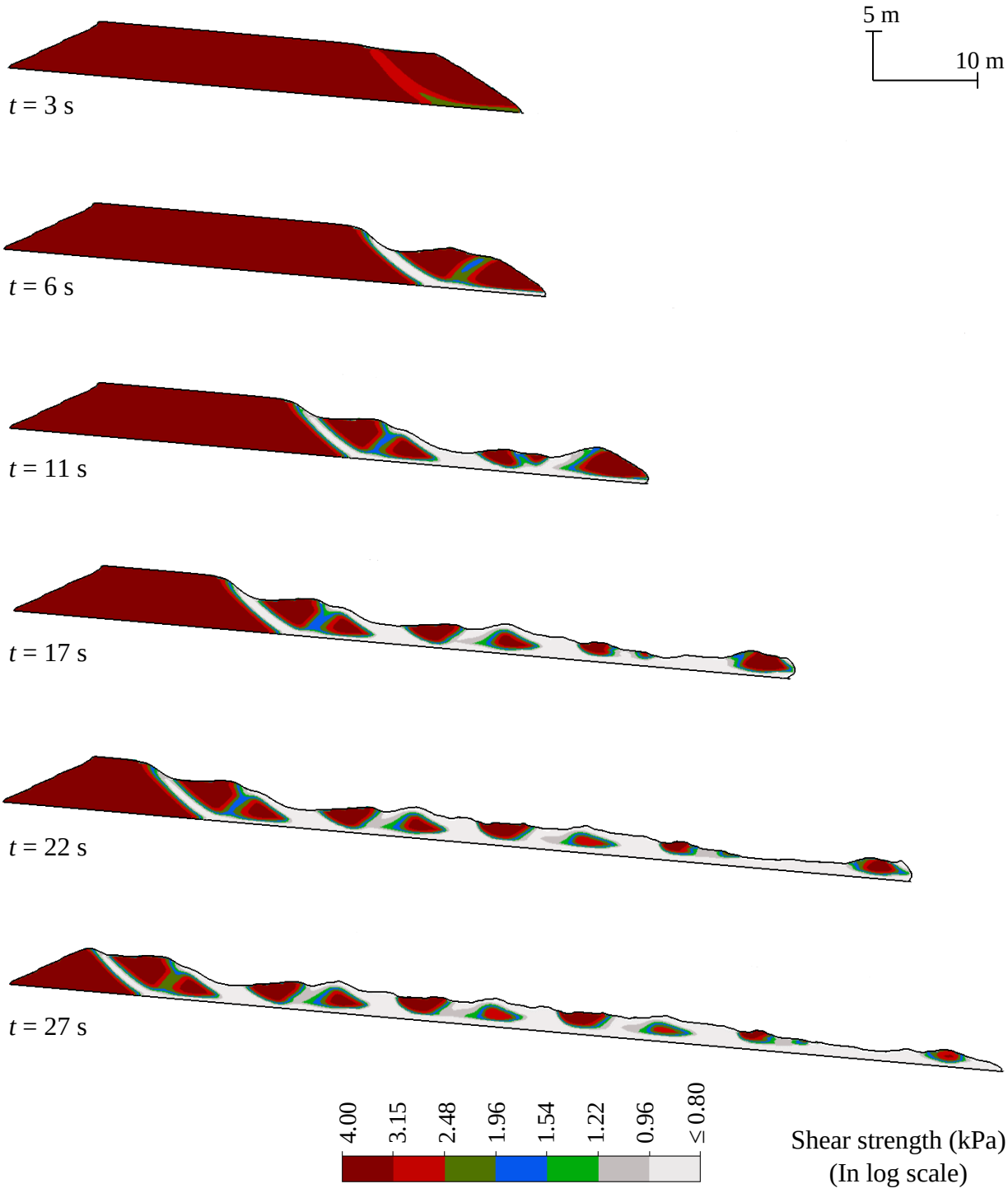

Fig. 4.24 Mobilized shear strength in Case-2

Case-3

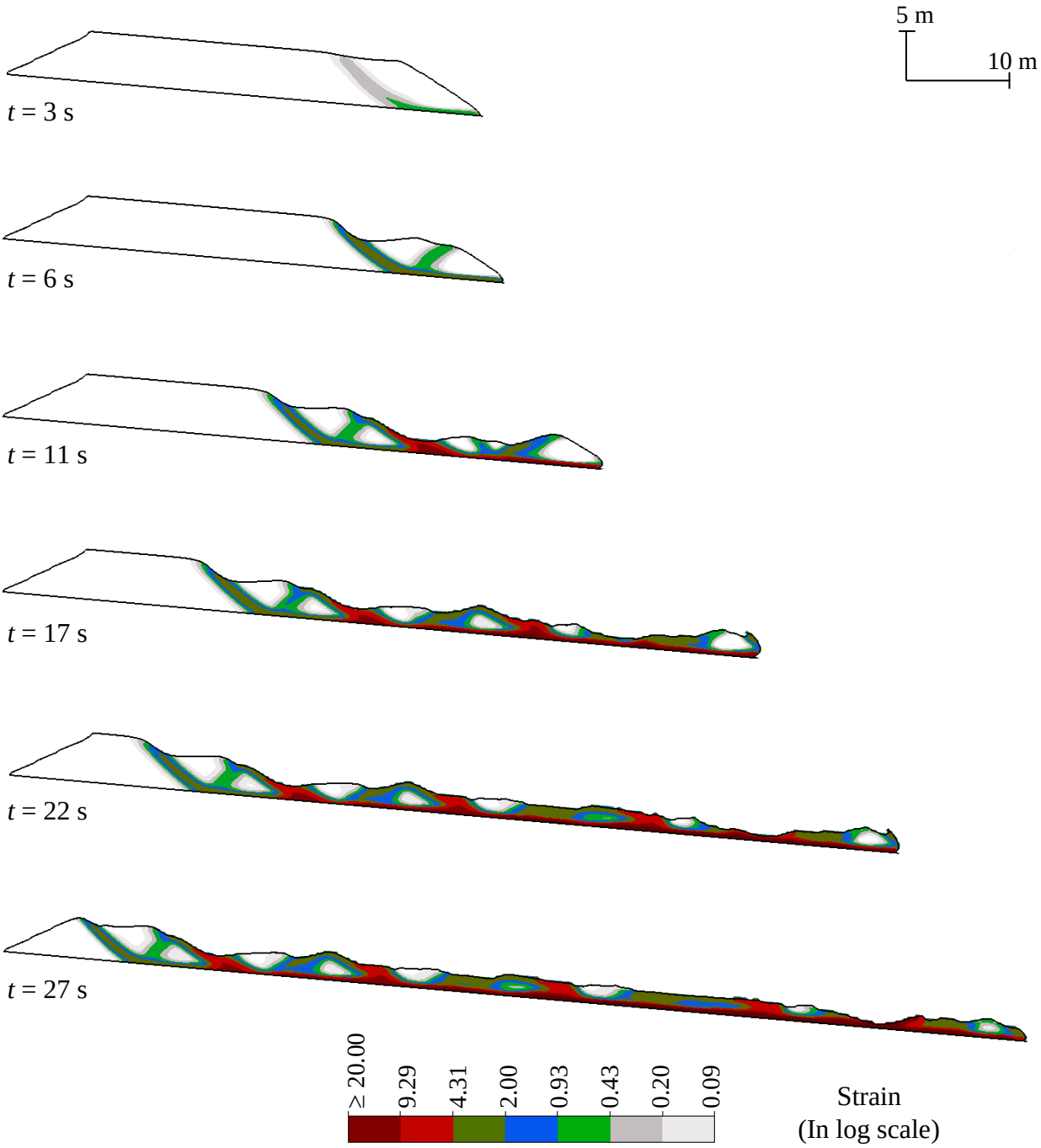

Fig. 4.25 Formation of failure planes in Case-3

Case - 3

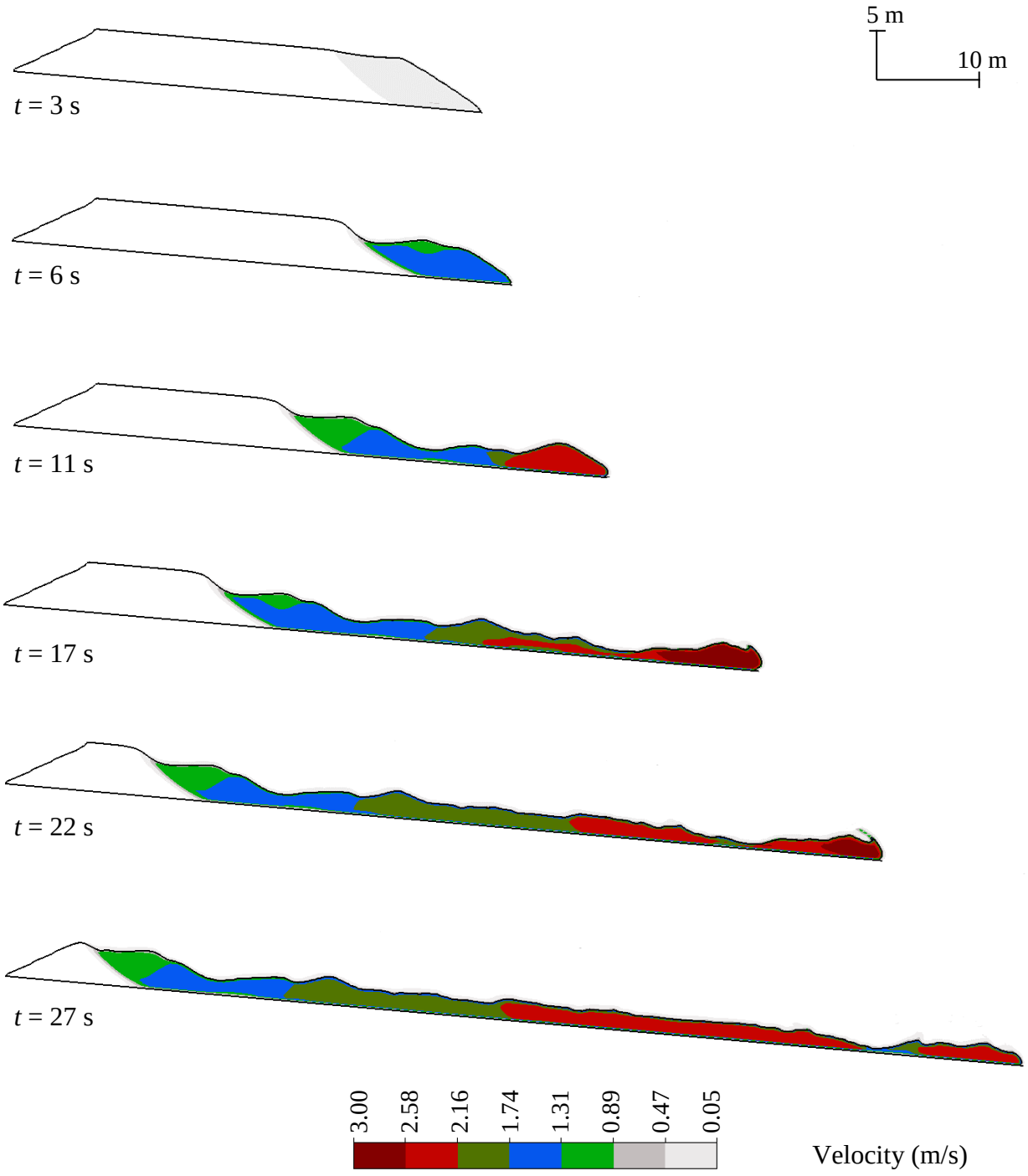

Fig. 4.26 Instantaneous velocity of soil elements in Case-3

Case - 3

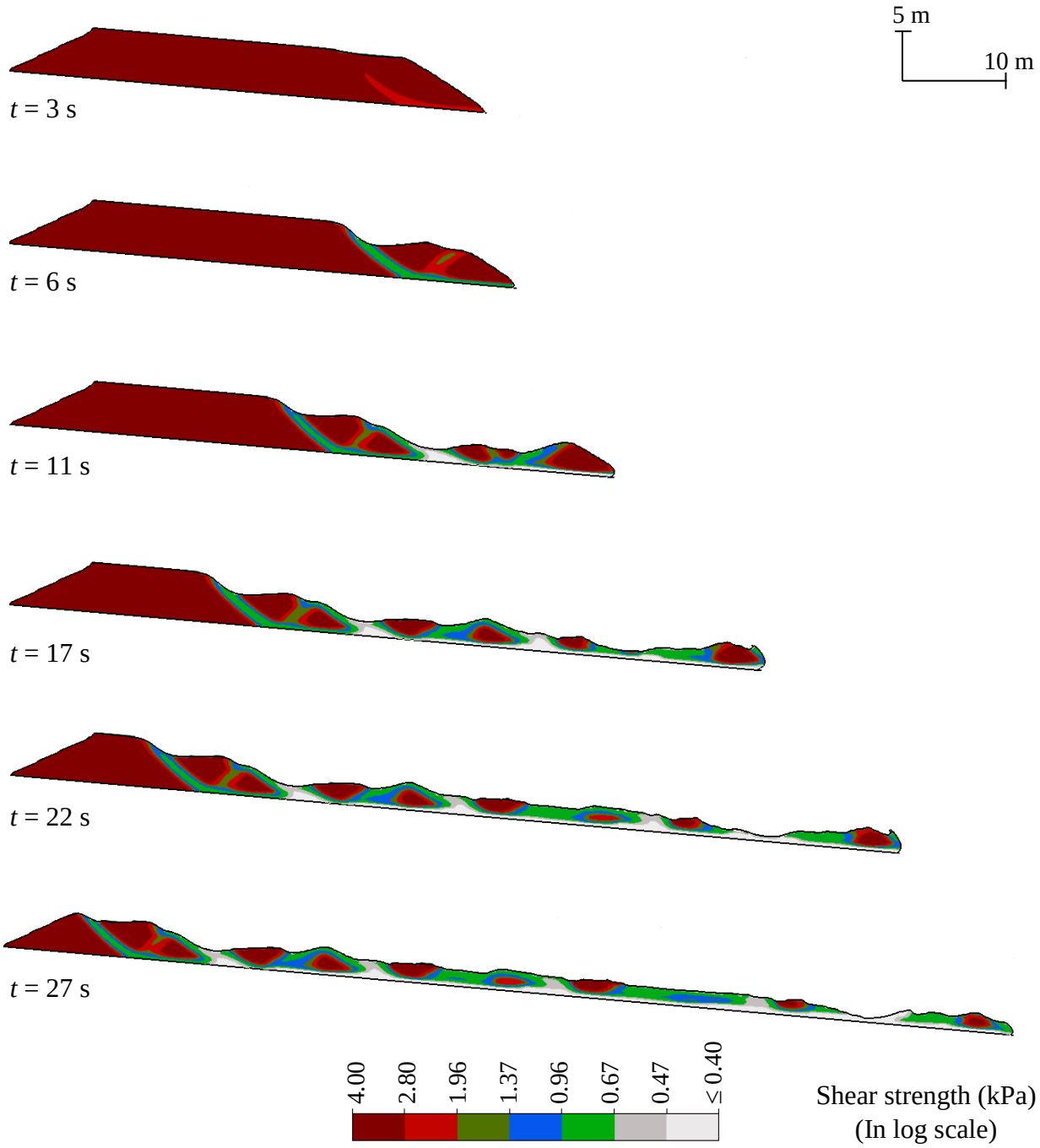

Fig. 4.27 Mobilized shear strength in Case-3

Case - 4

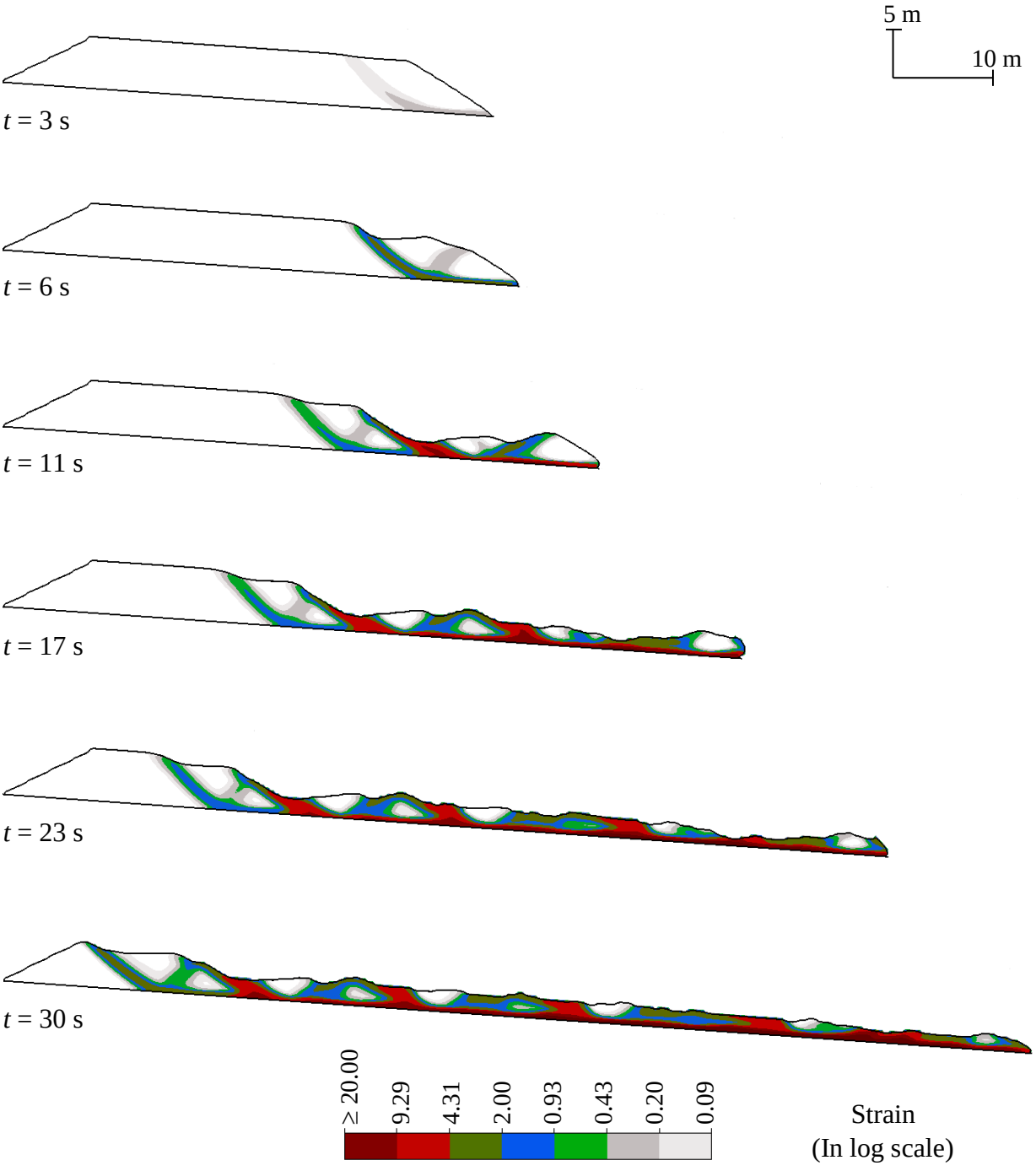

Fig. 4.28 Formation of failure planes in Case-4

Case - 4

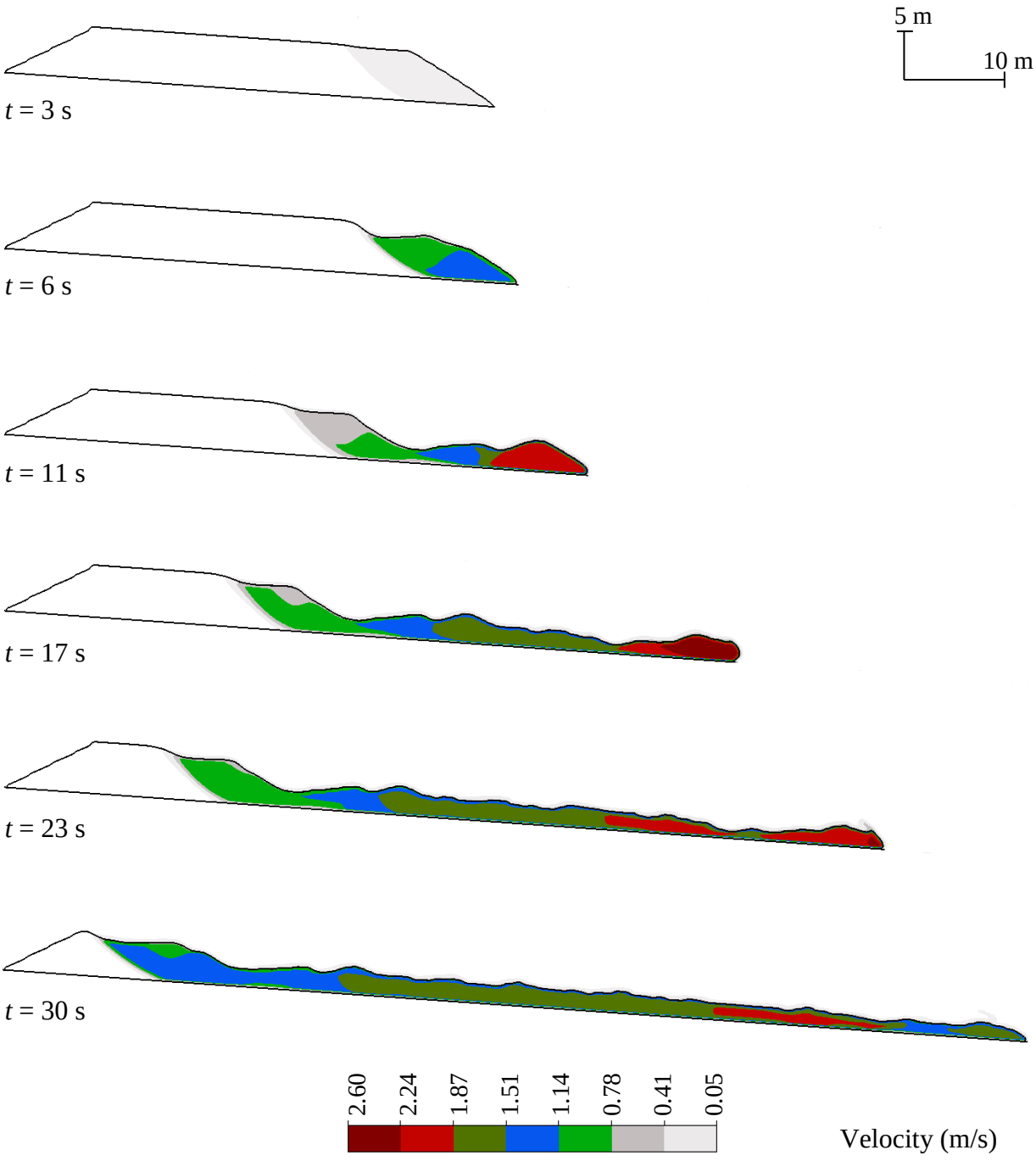

Fig. 4.29 Instantaneous velocity of soil elements in Case-4

Case - 4

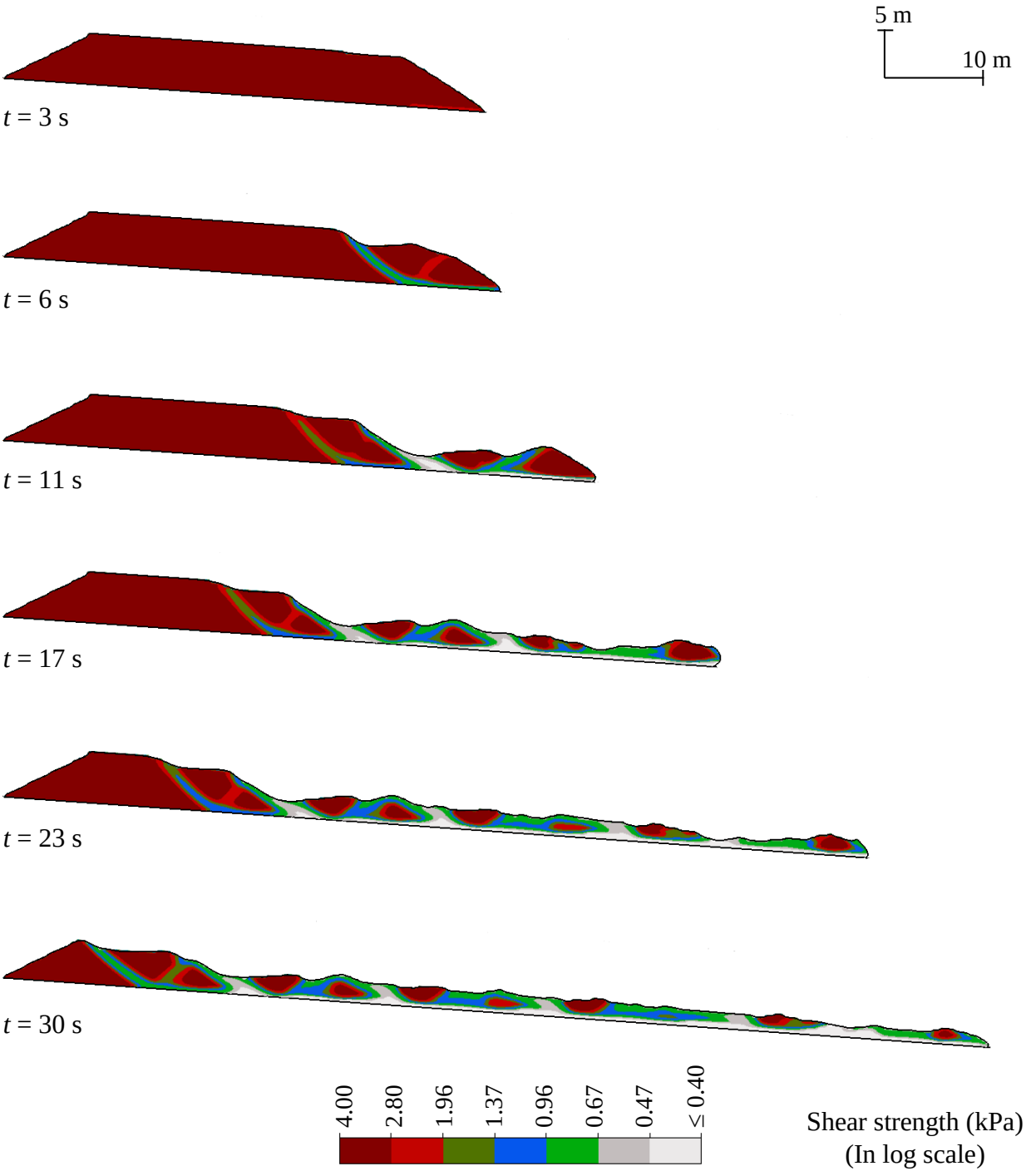

Fig. 4.30 Mobilized shear strength in Case-4

Figure 4.31 shows the run-out of the failed soil for Cases-2 to 4 (i.e., the lateral displacement of the front of the failed soil mass from its initial position). For Case-2, the run-out is completed at t ~ 70 s with a maximum run-out distance of ~ 88 m. At this time, the instantaneous velocity of the soil elements is negligible. For Case-3 and Case-4, the run-out is not completed during the analysis period of 75 s, even though a large run-out of 181 m in Case-3 and 133 m in Case-4 occurs. The final run-out distance can be obtained using a larger domain than that used in the present study; however, it will be computationally expensive, as is typical of large deformation modelling.

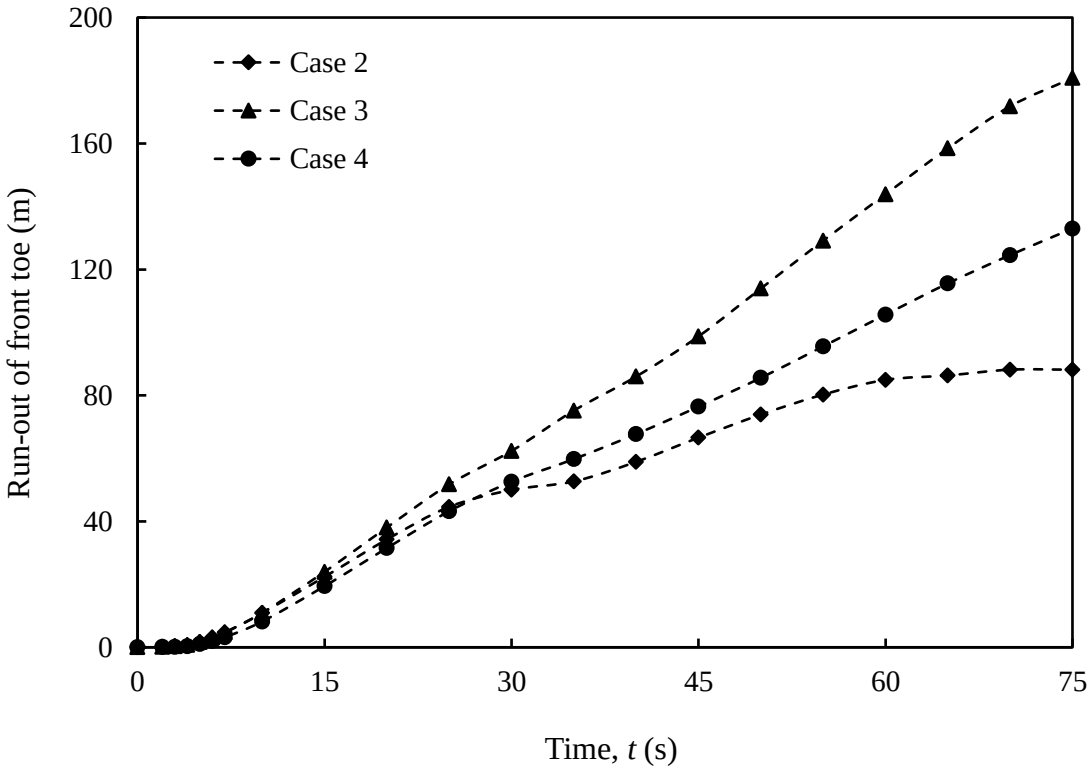

Fig. 4.31 Front toe run-out for Case-2 to Case-4

4.8.3.3 Simulation results for Cases-5 and -6

Case-5 and Case-6 simulations are performed for a smaller seabed slope angle (β = 4° and 2°) together with a weak layer above the seabed. Moreover, in the shear strength degradation model, both the undrained remoulding and shear wetting are considered.

Figures 4.32–4.34 show the simulation results for Case-5. Unlike Case-1 to Case-5, the shear failure in this case occurs in both the upslope and downslope sides of the sliding block. Moreover, the sliding block slides over the weak layer. With time, a number of shear bands form, inclined approximately at 45°, which create Λ-shaped horsts and V-shaped grabens. The grabens subside between the horsts at large displacements. The failure pattern in this case is similar to the "spread" as commonly observed in onshore sensitive clay slope failures, which is different from simulated flowslides in Cases-2 to -4.

Although the global failure of a soil block occurs initially in the upslope area (see the top figure of Fig. 4.32), Figure 4.33 shows that the displacement of the failed soil mainly occurs on the downslope side, with a higher instantaneous velocity of soil elements near the front toe. Figure 4.34 shows that a significant shear strength degradation occurs locally in the shear bands.

A spread-type failure also occurs in Case-6 (Figs. 4.35–4.37). As the seabed slope angle is very small (β = 2°), the movement of soil in the upslope area is higher in this case than in Case-5. Moreover, the shear strength degradation occurs quickly in this case, because of higher sensitivity used in this analysis.

Case-5

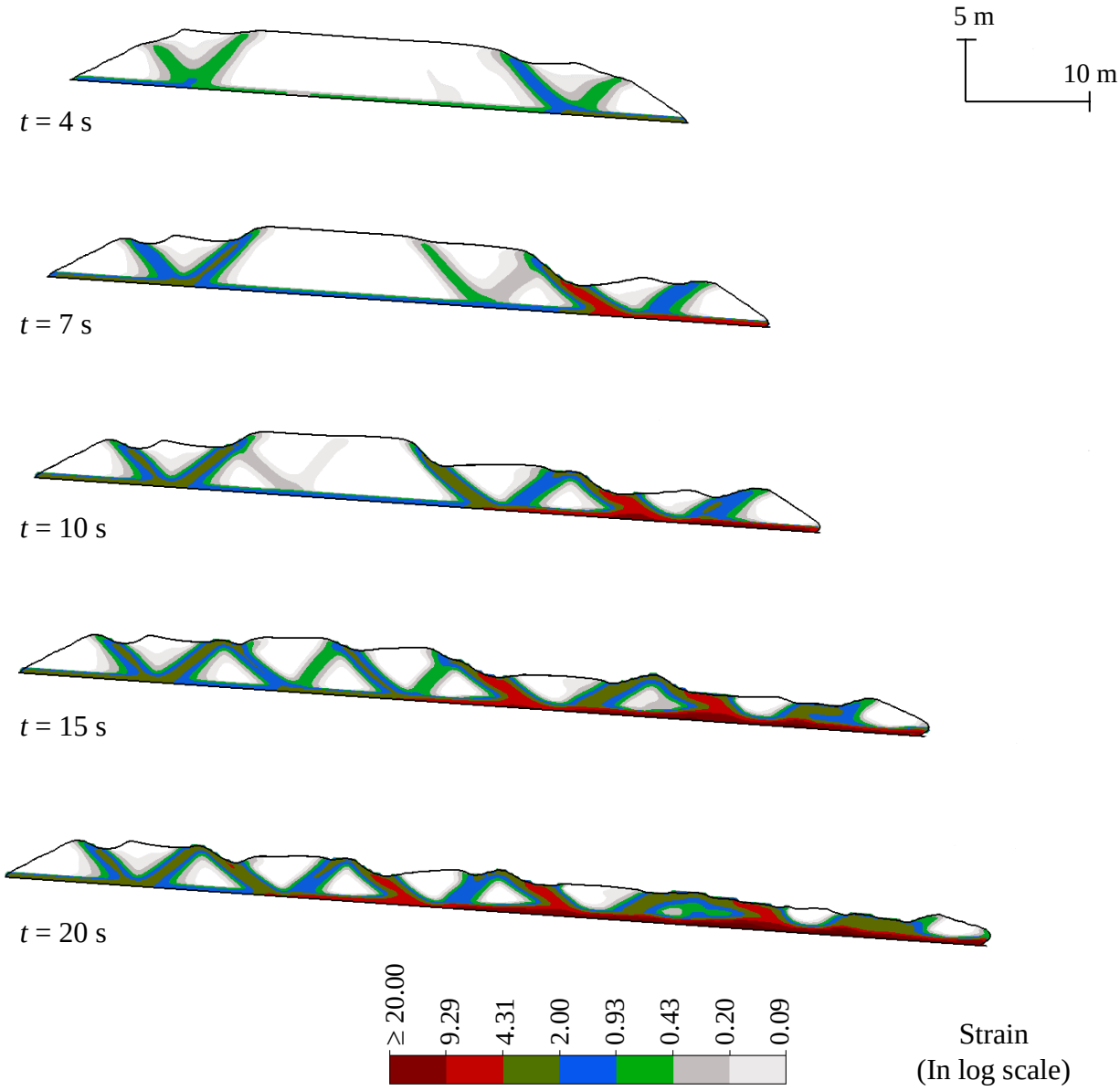

Fig. 4.32 Formation of failure planes in Case-5

Case-5

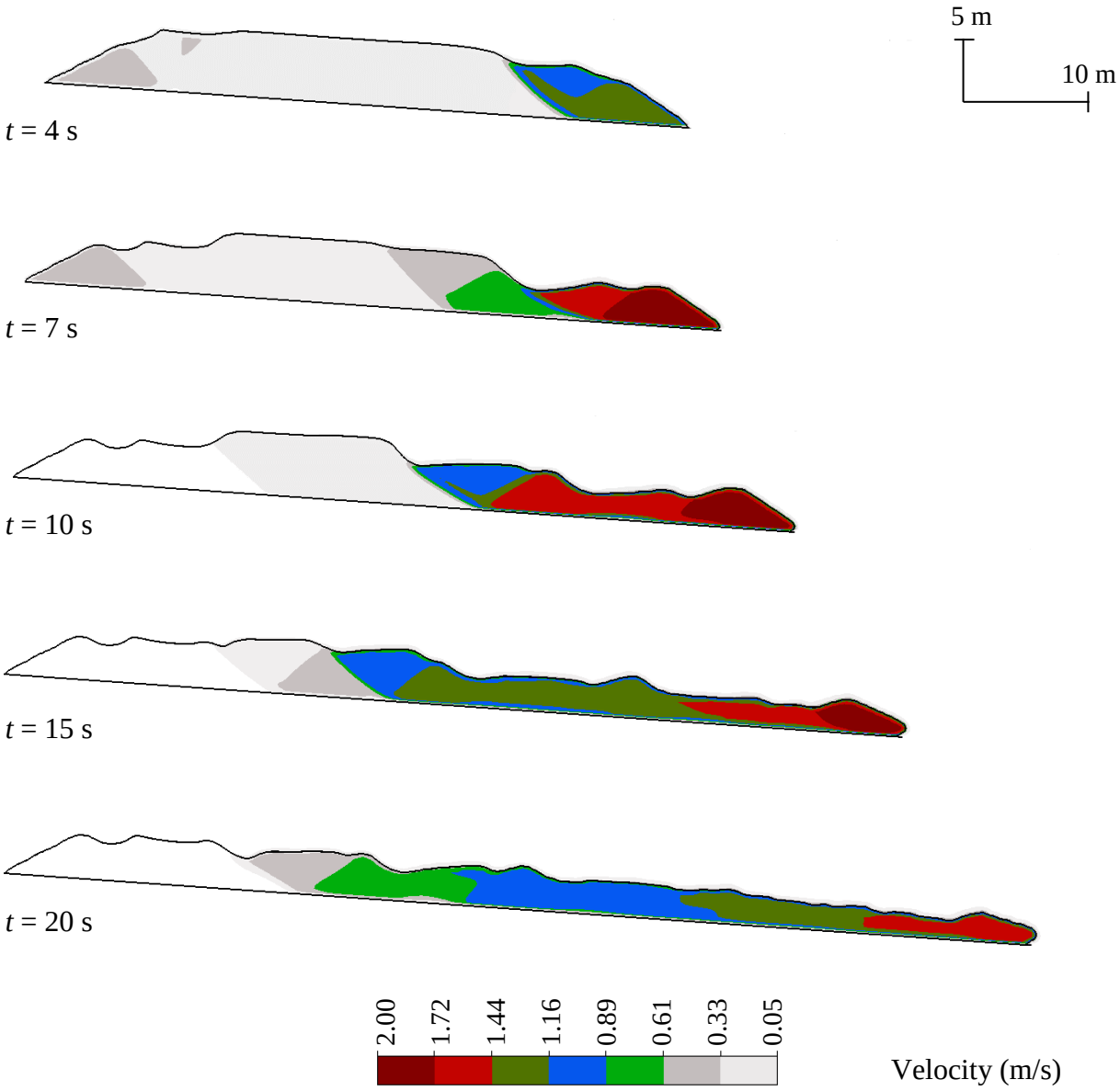

Fig. 4.33 Instantaneous velocity of soil elements in Case-5

Case-5

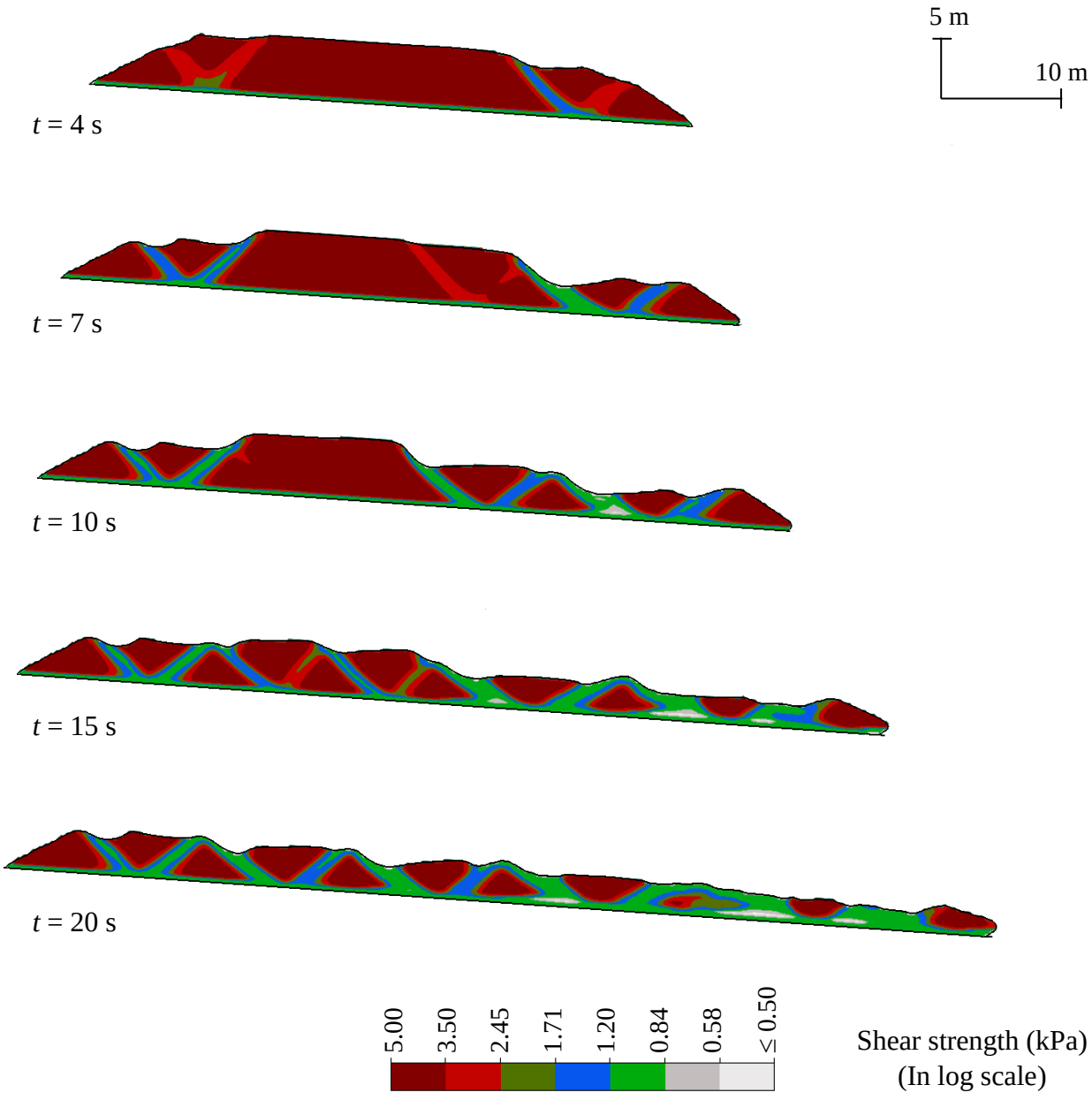

Fig. 4.34 Mobilized shear strength in Case-5

Case-6

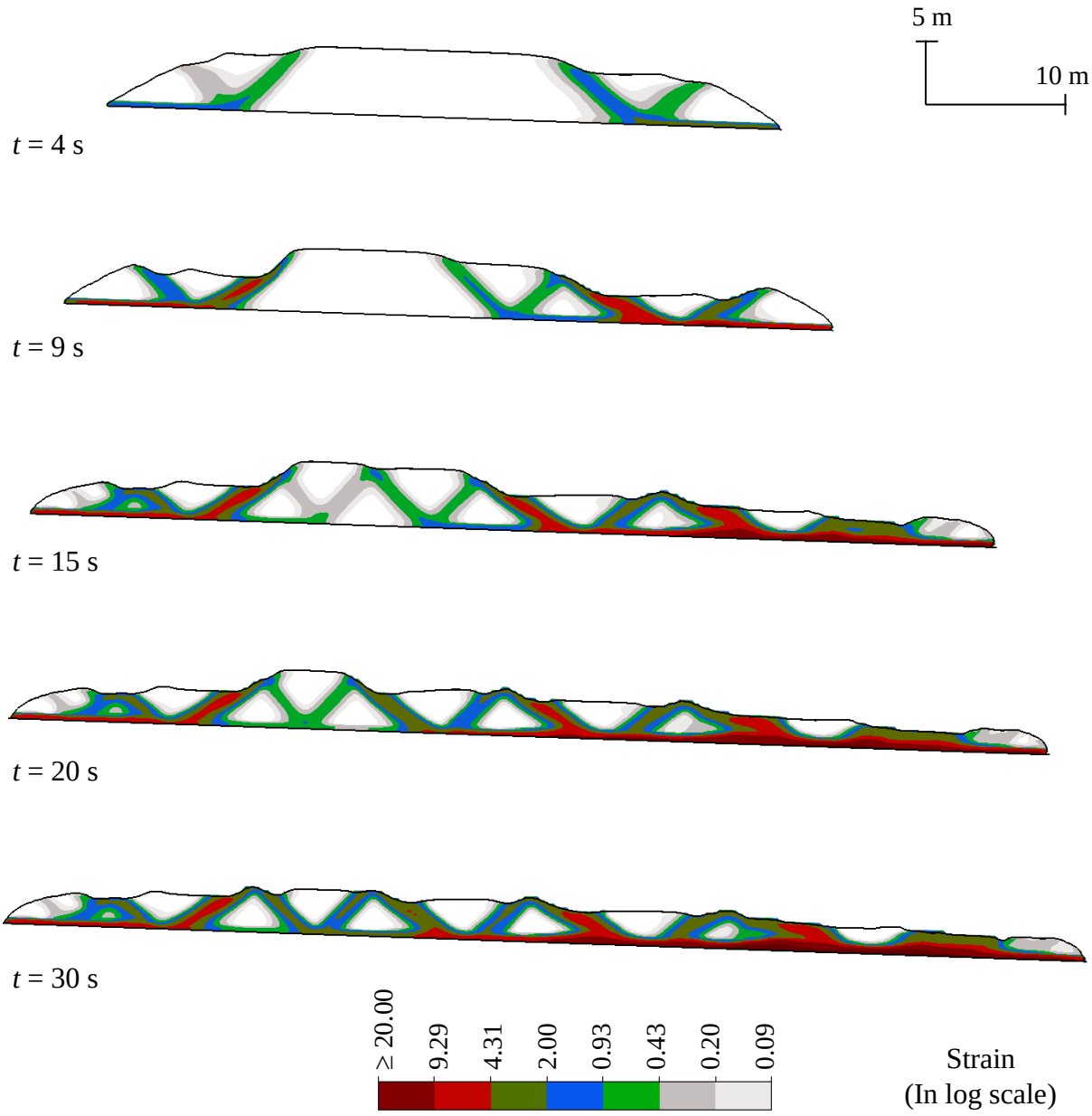

Fig. 4.35 Formation of failure planes in Case-6

Case-6

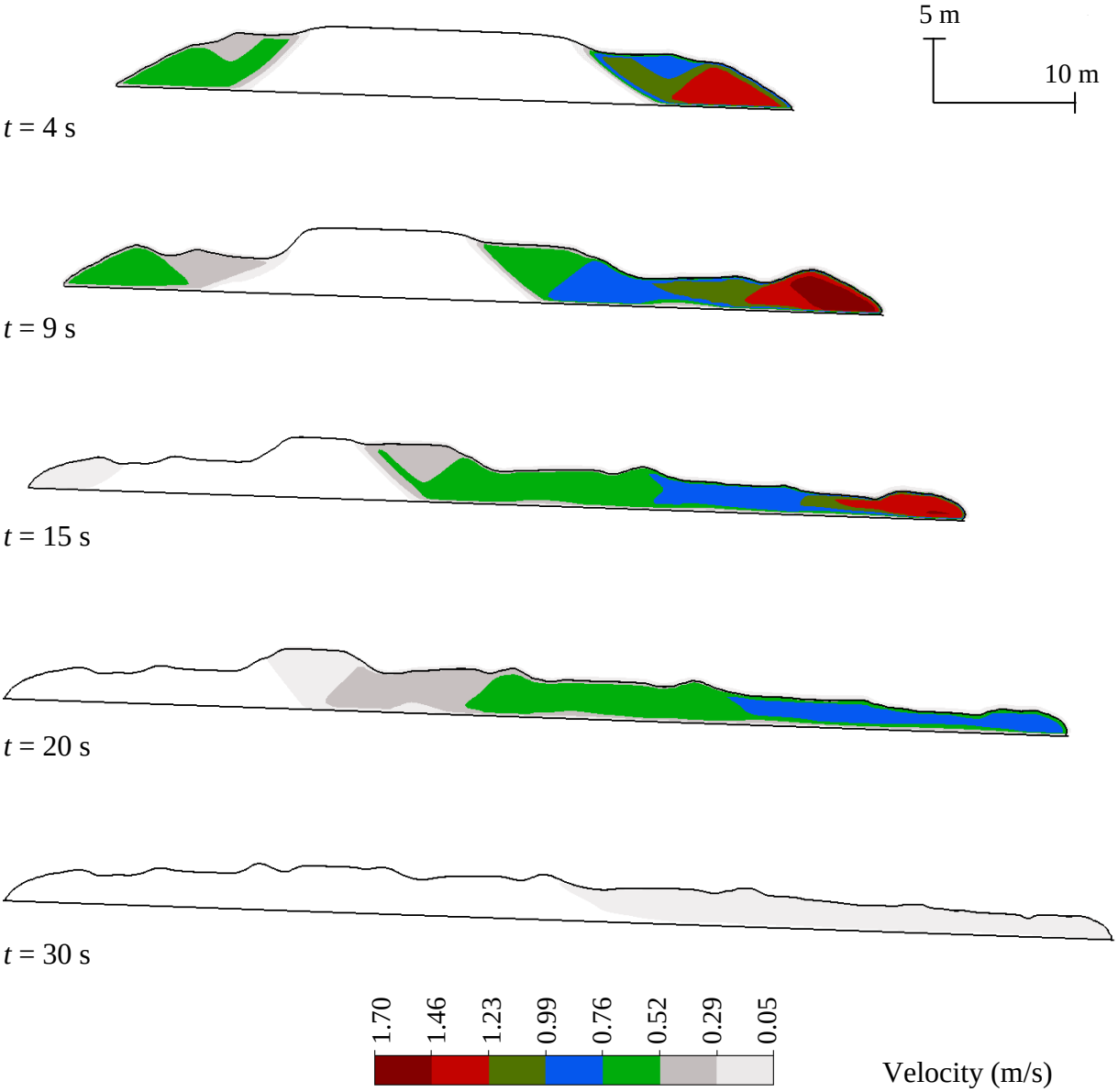

Fig. 4.36 Instantaneous velocity of soil elements in Case-6

Case-6

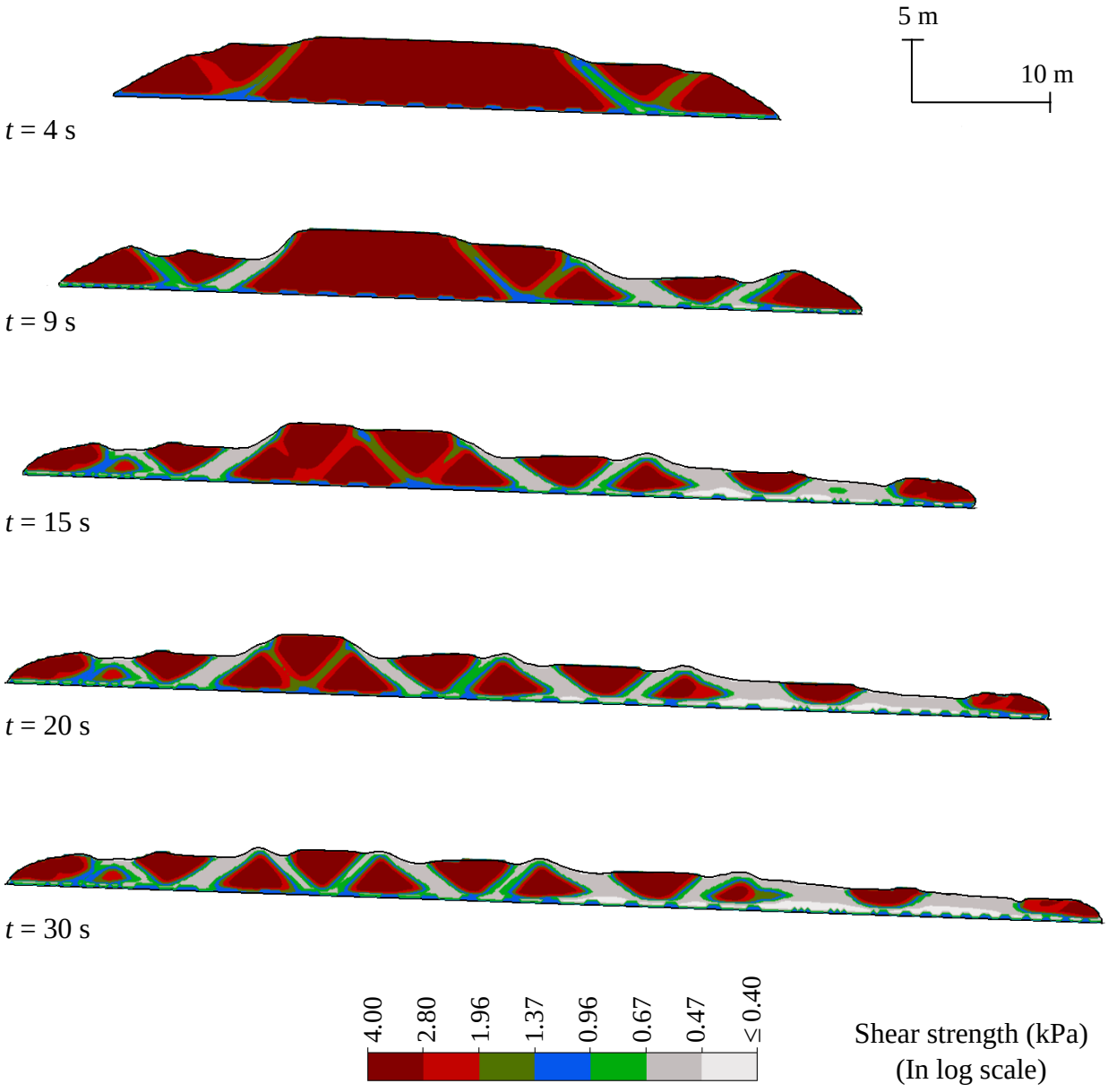

Fig. 4.37 Mobilized shear strength in Case-6

The lateral displacements of the front toe, for Case-5 and Case-6, are shown in Fig. 4.38. The run-out is completed at t ~ 38 s and t ~ 30 s, with the maximum run-out distance of ~ 45 m and ~ 28 m for Case-5 and Case-6, respectively.

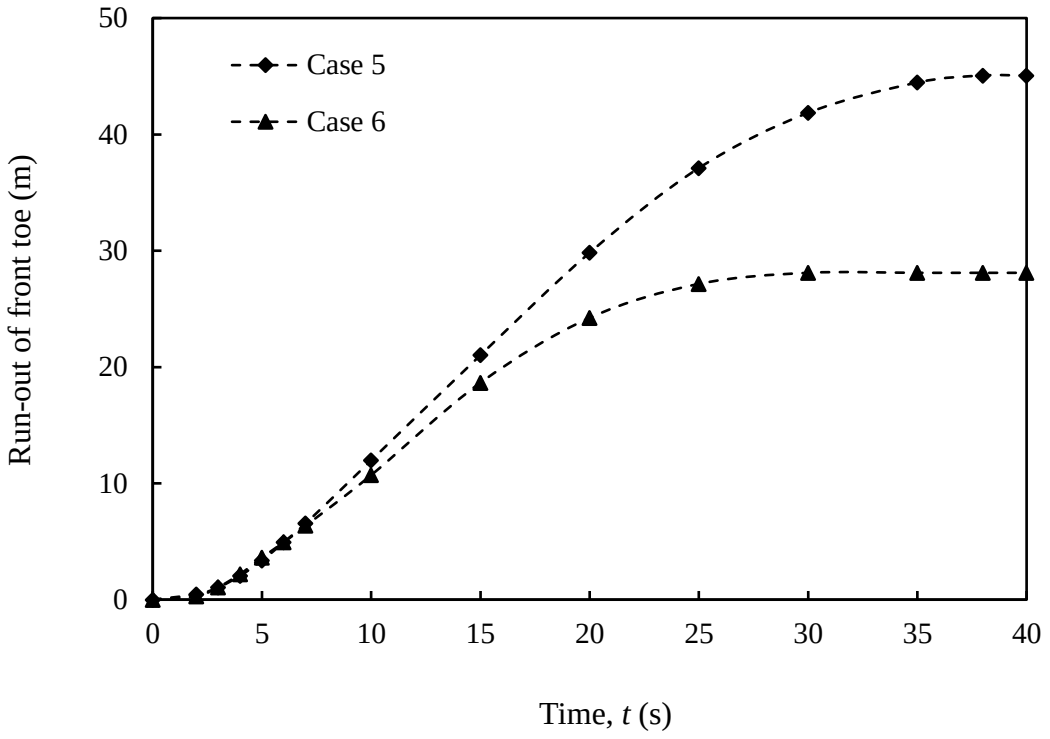

Fig. 4.38 Front toe run-out for Case-5 and Case-6

4.9 Summary

The run-out of idealized soil blocks, which could be originated from submarine landslides, is simulated in this chapter. The simulations are performed for three shapes of soil blocks: parabolic, rectangular and trapezoidal. The soil block displaces in the downslope direction through the water medium. The first set of simulations is performed for a parabolic-shaped debris block of very soft clay. Comparing the results with previous numerical simulations using the BING computer program, it is shown that the present numerical technique using the ANSYS CFX can successfully simulate the run-out. The second set of analyses is performed for downslope displacement of a relatively strong rectangular block through the water. The comparison between simulation results for the water and air as the ambient fluid shows that the water drag significantly influences the downslope velocity and run-out distance. The developed water pressure in front of the sliding block is the main source of the drag force. The final set of simulations is performed considering shear strength degradation effects. Two sources of shear strength degradation are considered, the undrained remoulding and the shear wetting due to water entrainment. An empirical model of shear strength degradation, as a function of accumulated plastic shear strain, is used to model both the undrained remoulding and shear wetting. Conducting simulations for varying seabed slope angles and strength degradation properties, it is shown that the soil block might fail into smaller pieces as a flowslide or as a spread, during the process of run-out, when strength degradation is considered.

CHAPTER 5

Conclusions and Future Recommendations

5.1 Conclusions

A submarine landslide can pose a significant threat to offshore structures such as deep water as-laid pipelines. Not only the movement of the soil in the area of landslide but also the downslope displacement of the failed soil blocks (run-out) that originate from a submarine landslide can exert a force on offshore structures. For the design of offshore structures in a landslide-prone area, two aspects need to be considered: (i) run-out distance and (ii) velocity of the sliding soil mass. The former one will indicate whether a failed soil block will strike the structure. If it strikes, the latter one will be useful to estimate drag force because the drag force increases with an increase in impact velocity of the soil block.

The run-out and velocity of the failed soil mass can be evaluated using two numerical approaches: (i) large-deformation finite element (FE) modelling and (ii) computational fluid dynamics approach (CFD). In the present study, numerical simulations are performed using the computer programs that have been developed based on these approaches. The large deformation FE analyses are performed using the coupled Eulerian-Lagrangian approach in Abaqus FE software (Abaqus CEL). The ANSYS CFX is used for CFD simulations. In both cases, the soil is modelled as Eulerian material; therefore, the numerical issues related to mesh distortion are avoided.

The comparison of the performance of FE and CFX simulations is presented in Chapter 3. All the simulations in this chapter have been performed with air as the ambient fluid. The effects of water

on the ambient fluid and strain-softening behaviour of the debris are presented in Chapter 4. The following conclusions can be drawn from the present study.

i. ANSYS CFX and Abaqus CEL can successfully model the run-out of a failed debris block that is displaced through an air domain. The calculated velocity, run-out distance, and soil failure patterns with these numerical modelling approaches are comparable. Similar to other large deformation finite element analyses, the computational cost is high.

ii. Water plays a significant role in the simulation results. The calculated maximum velocity for the in-air condition is almost double the maximum velocity when the debris is displaced through the water medium. However, the debris moves over a longer period for the in-water cases. Therefore, the final run-out distance is less sensitive to the ambient fluid than the maximum velocity.

iii. When the debris slides through water at high speed, the hydrodynamic pressure in front of the debris mainly increases the drag force.

iv. The shear failure of the debris occurs during run-out when it has a low undrained shear strength. The formation of a number of failure planes due to strain localization is obtained when the shear strength degradation of the debris is considered. Depending on geometry (seabed slope angle and existence of a weak layer) and the shear strength degradation, spread and flowslide type failures are obtained.

5.2 Recommendations for future work

A number of important features of debris flow and run-out are simulated in this study using the CFD approach in ANSYS CFX. However, this study has some limitations, which could be addressed in future studies.

- As expected, especially for shear strength degradation of materials, the solution could be mesh size dependent. Further studies on mesh dependency are required; an advanced numerical modelling technique or mesh size scaling rule could be implemented.
- The shear strength degradation due to water entrainment is modelled using an empirical model as a function of accumulated plastic shear strain. Water entrainment is a complex process. Laboratory tests and development of better models for this process are required.
- The effects of strain rate on shear strength are not considered in the present study and could be incorporated in future studies.
- An improved modelling of seabed–clay and clay–water interface is required.
- The simulation results can be compared with field evidence and large-scale test results, if available.

References

Abadie, S., Morichon, D., Grilli, S., and Glockner, S. 2010. Numerical simulation of waves generated by landslides using a multiple-fluid Navier–Stokes model. Coastal Engineering, **57**(9): 779–794. doi:10.1016/j.coastaleng.2010.03.003.

Benson, D.J., and Okazawa, S. 2004. Contact in a multi-material Eulerian finite element formulation. Computer Methods in Applied Mechanics and Engineering, **193**(39–41): 4277–4298. doi:10.1016/j.cma.2003.12.061.

Bohannon, R.G., and Gardner, J. V. 2004. Submarine landslides of San Pedro Escarpment, southwest of Long Beach, California. Marine Geology, **203**(3–4): 261–268. doi:10.1016/S0025-3227(03)00309-8.

Boukpeti, N., White, D., Randolph, M., and Low, H.E. 2009. Characterization of the solid-fluid transition of fine-grained sediments. *In* Proceedings of the ASME 2009 28th International Conference on Ocean, Offshore and Arctic Engineering, 31 May–5 June 2009, Honolulu, Hawaii, USA. OMAE2009-79738.

Boukpeti, N., White, D.J., Randolph, M.F., and Low, H.E. 2012. Strength of fine-grained soils at the solid–fluid transition. Géotechnique, **62**(3): 213–226. doi:10.1680/geot.9.P.069.

Cannon, S.H., and Savage, W.Z. 1988. A mass-change model for the estimation of debris-flow runout. The Journal of Geology, **96**(2): 221–227.

De Blasio, F.V, Issler, D., Elverhøi, A., Harbitz, C.B., Ilstad, T., Bryn, P., Lien, R., and Løvholt, F. 2003. Dynamics, velocity and run-out of the giant Storegga slide. *In* Proceedings: Submarine Mass Movements and Their Consequences, *Edited by* J. Locat and J. Mienert. pp.

223–230.

De Blasio, F.V., Engvik, L., Harbitz, C.B., and Elverhøi, A. 2004a. Hydroplaning and submarine debris flows. Journal of Geophysical Research: Oceans, **109**(C1). doi:10.1029/2002JC001714.

De Blasio, F.V., Elverhøi, A., Issler, D., Harbitz, C.B., Bryn, P., and Lien, R. 2004b. Flow models of natural debris flows originating from overconsolidated clay materials. Marine Geology, **213**(1–4): 439–455. doi:10.1016/j.margeo.2004.10.018.

De Blasio, F.V., Elverhøi, A., Issler, D., Harbitz, C.B., Bryn, P., and Lien, R. 2005. On the dynamics of subaqueous clay rich gravity mass flows—the giant Storegga slide, Norway. Marine and Petroleum Geology, **22**(1–2): 179–186. doi:10.1016/j.marpetgeo.2004.10.014.

De Blasio, F.V., Engvik, L.E., and Elverhøi, A. 2006. Sliding of outrunner blocks from submarine landslides. Geophysical Research Letters, **33**(6): 8–11. doi:10.1029/2005GL025165.

Dey, R., Hawlader, B., Phillips, R., and Soga, K. 2015. Large deformation finite-element modeling of progressive failure leading to spread in sensitive clay slopes. Géotechnique, **65**(8): 657–668.

Dey, R., Hawlader, B., Phillips, R., and Soga, K. 2016a. Modeling of large-deformation behaviour of marine sensitive clays and its application to submarine slope stability analysis. Canadian Geotechnical Journal, **53**(7): 1138–1155. doi:10.1139/cgj-2015-0176.

Dey, R., Hawlader, B.C., Phillips, R., and Soga, K. 2016b. Numerical modelling of submarine landslides with sensitive clay layers. Géotechnique, **66**(6): 454–468. doi:10.1680/jgeot.15.P.111.

Dong, Y. 2017. Runout of submarine landslides and their impact on subsea infrastructure using material point method. PhD thesis, The University of Western Australia, Perth, WA.

Dong, Y., Wang, D., and Randolph, M.F. 2017. Runout of submarine landslide simulated with material point method. Procedia Engineering, **175**: 357–364. doi:10.1016/j.proeng.2017.01.045.

Dutta, S., Hawlader, B., and Phillips, R. 2015. Vertical penetration of offshore pipelines: A comparative study between finite element and finite volume methods. *In* Proceedings of the ASME 2015 34th International Conference on Ocean, Offshore and Arctic Engineering, 31 May–5 June 2015, St. John's, Newfoundland, Canada. OMAE2015-42076.

Dutta, S., and Hawlader, B. 2016. A comparative study of advanced numerical methods for large deformation problems using cylindrical object penetration into seabed. 69th Canadian Geotechnical Conference, GeoVancouver 2016, 2–5 October, Vancouver, British Columbia, Canada.

Dutta, S., and Hawlader, B. 2018. Pipeline–soil–water interaction modeling for submarine landslide impact on suspended offshore pipelines. Géotechnique (accepted).

Dutta, S., Hawlader, B., and Phillips, R. 2018. Numerical modelling of a steel catenary riser section in the touchdown zone under cyclic loading. Ocean Engineering (accepted).

Einav, I., and Randolph, M.F. 2005. Combining upper bound and strain path methods for evaluating penetration resistance. International Journal for Numerical Methods in Engineering, **63**(14): 1991–2016. doi:10.1002/nme.1350.

Elverhøi, A., Breien, H., De Blasio, F.V., Harbitz, C.B., and Pagliardi, M. 2010. Submarine

landslides and the importance of the initial sediment composition for run-out length and final deposit. Ocean Dynamics, **60**(4): 1027–1046. doi:10.1007/s10236-010-0317-z.

Fine, I.V., Rabinovich, A.B., Bornhold, B.D., Thomson, R.E., and Kulikov, E.A. 2005. The Grand Banks landslide-generated tsunami of November 18, 1929: preliminary analysis and numerical modeling. Marine Geology, **215**(1–2): 45–57.

Gauer, P., Kvalstad, T.J., Forsberg, C.F., Bryn, P., and Berg, K. 2005. The last phase of the Storegga Slide: Simulation of retrogressive slide dynamics and comparison with slide-scar morphology. Marine and Petroleum Geology, **22**(1): 171–178. doi:10.1016/j.marpetgeo.2004.10.004.

Gauer, P., Elverhøi, A., Issler, D., and De Blasio, F.V. 2006. On numerical simulations of subaqueous slides: Back-calculations of laboratory experiments of clay-rich slides. Norsk Geologisk Tidsskrift, **86**(3): 295–300.

Hampton, M.A. 1972. The role of subaqueous debris flow in generating turbidity currents. Journal of Sedimentary Petrology, **42**(4): 775–793.

Hampton, M.A., Lee, H.J., and Locat, J. 1996. Submarine landslides. Reviews of Geophysics, **34**(1): 33–59. doi:10.1029/95rg03287.

Harbitz, C.B., Parker, G., Elverhøi, A., Marr, J.G., Mohrig, D., and Harff, P.A. 2003. Hydroplaning of subaqueous debris flows and glide blocks: Analytical solutions and discussion. Journal of Geophysical Research: Solid Earth, **108**(B7). doi:10.1029/2001JB001454.

Hoerner, S.F. 1965. Fluid-dynamic drag: practical information on aerodynamic drag and hydrodynamic resistance. Hoerner Fluid Dynamics, Bakersfield, CA, USA.

Hu, P., Wang, D., Cassidy, M.J., and Stanier, S.A. 2014. Predicting the resistance profile of a spudcan penetrating sand overlying clay. Canadian Geotechnical Journal, **51**(10): 1151–1164.

Huang, X., and Garcia, M.H. 1997. A perturbation solution for Bingham-plastic mudflows. Journal of hydraulic Engineering, **123**(11): 986–994.

Ilstad, T., De Blasio, F.V., Elverhøi, A., Harbitz, C.B., Engvik, L., Longva, O., and Marr, J.G. 2004a. On the frontal dynamics and morphology of submarine debris flows. Marine Geology, **213**(1–4): 481–497. doi:10.1016/j.margeo.2004.10.020.

Ilstad, T., Elverhøi, A., Issler, D., and Marr, J.G. 2004b. Subaqueous debris flow behaviour and its dependence on the sand/clay ratio: a laboratory study using particle tracking. Marine Geology, **213**(1–4): 415–438. doi:10.1016/j.margeo.2004.10.017.

Ilstad, T., Marr, J.G., Elverhøi, A., and Harbitz, C.B. 2004c. Laboratory studies of subaqueous debris flows by measurements of pore-fluid pressure and total stress. Marine Geology, **213**(1–4): 403–414. doi:10.1016/j.margeo.2004.10.016.

Imran, J., Parker, G., Locat, J., and Lee, H. 2001. 1D numerical model of muddy subaqueous and subaerial debris flows. Journal of Hydraulic Engineering, **127**(11): 959–968.

Jiang, L., and Le Blond, P.H. 1993. Numerical modeling of an underwater Bingham plastic mudslide and the waves which it generates. Journal of Geophysical Research: Oceans, **98**(C6): 10303–10317.

Kvalstad, T.J., Nadim, F., and Harbitz, C.B. 2001. Deepwater geohazards : geotechnical concerns and solutions. *In* Proceedings of the Offshore Technology Conference, 30 April–3 May 2001,

Houston, Texas, USA. OTC 12958.

Kvalstad, T.J., Nadim, F., Kaynia, A.M., Mokkelbost, K.H., and Bryn, P. 2005. Soil conditions and slope stability in the Ormen Lange area. Marine and Petroleum Geology, **22(1–2)**: 299–310.

Legros, F. 2002. The mobility of long-runout landslides. Engineering Geology, **63(3–4)**: 301–331. doi:http://dx.doi.org/10.1016/S0013-7952(01)00090-4.

Liu, J., Yu, L., Kong, X., and Hu, Y. 2011. Large displacement finite element analysis of submarine slide due to gas hydrate dissociation. International Conference on Ocean, Offshore and Arctic Engineering, ASME, June 19–24, Rotterdam, Netharlands, pp. 861–865.

Locat, J., Lee, H.J., Nelson, H.C., Schwab, W.C., and Twichell, D.C. 1996. Analysis of the mobility of far reaching debris flows on the Mississippi Fan, Gulf of Mexico. *In* Seventh International Symposium on Landslides. pp. 555–560.

Locat, J., and Lee, H.J. 2000. Submarine landslides: advances and challenges. *In* Proceedings of the 8th International Symposium on Landslides, June 2000, Cardiff, U.K.

Locat, J., and Lee, H.J. 2002. Submarine landslides: advances and challenges. Canadian Geotechnical Journal, **39**(1): 193–212. doi:10.1139/t01-089.

Locat, J., Lee, H.J., Locat, P., and Imran, J. 2004. Numerical analysis of the mobility of the Palos Verdes debris avalanche, California, and its implication for the generation of tsunamis. Marine Geology, **203**(3–4): 269–280. doi:10.1016/S0025-3227(03)00310-4.

Locat, J., and Lee, H.J. 2005. Subaqueous debris flows. *In* Proceedings: Debris-flow Hazards and Related Phenomena, *Edited by* M. Jakob and O. Hungr. pp. 203–245.

Ma, J. 2015. Numerical modelling of submarine landslides and their impact to underwater infrastructure using the material point method. PhD thesis, The University of Western Australia, Perth, WA.

Marr, J.G., Shanmugam, G., and Parker, G. 2001. Experiments on subaqueous sandy gravity flows: The role of clay and water content in flow dynamics and depositional structures. Bulletin of the Geological Society of America, **113**(11): 1377–1386.

Marr, J.G., Elverhøi, A., Harbitz, C.B., Imran, J., and Harff, P. 2002. Numerical simulation of mud-rich subaqueous debris flows on the glacially active margins of the Svalbard–Barents Sea. Marine Geology, **188**(3–4): 351–364. doi:10.1016/S0025-3227(02)00310-9.

Mohrig, D., Whipple, K.X., Hondzo, M., Ellis, C., and Parker, G. 1998. Hydroplaning of subaqueous debris flows. Bulletin of the Geological Society of America, **110**(3): 387–394. doi:10.1130/0016-7606(1998)110<0387:HOSDF>2.3.CO.

Mohrig, D., Elverhøi, A., and Parker, G. 1999. Experiments on the relative mobility of muddy subaqueous and subaerial debris flows, and their capacity to remobilize antecedent deposits. Marine Geology, **154**(1–4): 117–129. doi:10.1016/S0025-3227(98)00107-8.

Mohrig, D., and Marr, J.G. 2003. Constraining the efficiency of turbidity current generation from submarine debris flows and slides using laboratory experiments. Marine and Petroleum Geology, **20**(6–8): 883–899. doi:10.1016/j.marpetgeo.2003.03.002.

Newman, J.N. 1977. Marine Hydrodynamics. MIT Press, Cambridge, MA, England.

Norem, H., Locat, J., and Schieldrop, B. 1990. An approach to the physics and the modeling of submarine flowslides. Marine Geotechnology, **9**(2): 93–111.

Pelinovsky, E., and Poplavsky, A. 1996. Simplified model of tsunami generation by submarine landslides. Physics and Chemistry of the Earth, **21**(1–2): 13–17.

Piper, D.J.W., and Aksu, A.E. 1987. The source and origin of the 1929 Grand Banks turbidity current inferred from sediment budgets. Geo-Marine Letters, **7**(4): 177–182.

Piper, D.J.W., Cochonat, P., and Morrison, M.L. 1999. The sequence of events around the epicentre of the 1929 Grand Banks earthquake: initiation of debris flows and turbidity current inferred from sidescan sonar. Sedimentology, **46**(1): 79–97.

Prior, D.B., Bornhold, B.D., Coleman, J.M., and Bryant, W.R. 1982. Morphology of a submarine slide, Kitimat Arm, British Columbia. Geology, **10**(11): 588–592.

Pudasaini, S.P. 2012. A general two-phase debris flow model. Journal of Geophysical Research: Earth Surface, **117**(F3). doi:10.1029/2011JF002186.

Pudasaini, S.P. 2014. Dynamics of submarine debris flow and tsunami. Acta Mechanica, **225**(8): 2423–2434. doi:10.1007/s00707-014-1126-0.

Qiu, G., and Henke, S. 2011. Controlled installation of spudcan foundations on loose sand overlying weak clay. Marine Structures, **24**(4): 528–550.

Randolph, M.F., Gaudin, C., Gourvenec, S.M., White, D.J., Boylan, N., and Cassidy, M.J. 2011. Recent advances in offshore geotechnics for deep water oil and gas developments. Ocean Engineering, **38**(7): 818–834. doi:10.1016/j.oceaneng.2010.10.021.

Sahdi, F., Gaudin, C., White, D.J., Boylan, N., and Randolph, M.F. 2014. Centrifuge modelling of active slide–pipeline loading in soft clay. Géotechnique, **64**(1): 16–27. doi:10.1680/geot.12.P.191.

Shanmugam, G., and Wang, Y. 2015. The landslide problem. Journal of Palaeogeography, **4**(2): 109–166. doi:10.3724/SP.J.1261.2015.00071.

Strand, S.A., Thakur, V., L'Heureux, J.S., Lacasse, S., Karlsrud, K., Nyheim, T., Aunaas, K., Ottesen, H.B., Gjelsvik, V., Fauskerud, O.A., and Sandven, R. 2017. Runout of Landslides in Sensitive Clays. *In* Proceedings: Landslides in Sensitive Clays, *Edited by* Vikas Thakur, J.-S. L'Heureux, and A. Locat. pp. 289–300.

Tavenas, F. 1984. Landslides in Canadian sensitive clays–a state-of-the-art. *In* Proceedings of the 4th International Symposium on Landslides, Toronto, Ontario, pp. 16–21.

Taylor, O.D.S., Bradshaw, A.S., Baxter, C.D.P., and Grilli, S.T. 2008. The effects of basal resistance and hydroplaning on the initial kinematics of seismically induced tsunamigenic landslides. *In* Proceedings of GeoCongress 2008: Geosustainability and Geohazard Mitigation, pp. 522–529.

Tho, K.K., Leung, C.F., Chow, Y.K., and Swaddiwudhipong, S. 2010. Eulerian finite-element technique for analysis of jack-up spudcan penetration. International Journal of Geomechanics, **12**(1): 64–73.

Trapper, P.A., Puzrin, A.M., and Germanovich, L.N. 2015. Effects of shear band propagation on early waves generated by initial breakoff of tsunamigenic landslides. Marine Geology, **370**: 99–112. doi:10.1016/j.margeo.2015.10.014.

Van Weering, T.C.E., Nielsen, T., Kenyon, N.H., Akentieva, K., and Kuijpers, A.H. 1998. Large submarine slides on the NE Faeroe continental margin. Geological Society, London, Special Publications, **129**(1): 5–17. doi:https://doi.org/10.1144/GSL.SP.1998.129.01.02.

Vorren, T.O., Laberg, J.S., Blaume, F., Dowdeswell, J.A., Kenyon, N.H., Mienert, J., Rumohr, J.A.N., and Werner, F. 1998. The Norwegian–Greenland Sea continental margins: morphology and late Quaternary sedimentary processes and environment. Quaternary Science Reviews, **17**(1–3): 273–302.

Wang, D., Randolph, M.F., and White, D.J. 2013. A dynamic large deformation finite element method based on mesh regeneration. Computers and Geotechnics, **54**: 192–201. doi:10.1016/j.compgeo.2013.07.005.

White, D.J., Randolph, M.F., Gaudin, C., Boylan, N.P., Wang, D., Boukpeti, N., Zhu, H., and Sahdi, F. 2016. The Impact of Submarine Slides on Pipelines: Outcomes from the COFS-MERIWA JIP. *In* Proceedings of the Offshore Technology Conference, 2–5 May 2016, Houston, Texas, USA. OTC-27034-MS.

Wright, V.G., and Krone, R.B. 1987. Laboratory and numerical study of mud and debris flow. Report 1 and 2, Department of Civil Engineering, University of California, Davis, California.

Xiu, Z., Liu, L., Xie, Q., Li, J., Hu, G., and Yang, J. 2015. Runout prediction and dynamic characteristic analysis of a potential submarine landslide in Liwan 3-1 gas field. Acta Oceanologica Sinica, **34**(7): 116–122. doi:10.1007/s13131-015-0697-2.

Yang, W., Yang, T., Ying, C., De-ying, L., and Wei, W. 2014. Study on the velocity of partially submerged landslide. Journal of Engineering Science and Technology Review, **7**(3): 62–67.

Yoon, D.H., Yang, K.S., and Choi, C.B. 2010. Flow past a square cylinder with an angle of incidence. Physics of fluids, **22**(4).

Zakeri, A., Høeg, K., and Nadim, F. 2009. Submarine debris flow impact on pipelines — Part II:

Numerical analysis. Coastal Engineering, **56**(1): 1–10. doi:10.1016/j.coastaleng.2008.06.005.

Zakeri, A., and Hawlader, B. 2013. Drag forces caused by submarine glide block or out-runner block impact on suspended (free-span) pipelines—Numerical analysis. Ocean Engineering, **67**: 89–99. doi:10.1016/j.oceaneng.2013.03.007.

Zhang, W., Wang, D., Randolph, M.F., and Puzrin, A.M. 2015. Catastrophic failure in planar landslides with a fully softened weak zone. Géotechnique, **65**(9): 755–769.

Zhu, H., and Randolph, M.F. 2010. Large deformation finite element analyses of submarine landslide interaction with embedded pipelines. International Journal of Geomechanics, **10**(4): 145–152. doi:10.1061/(ASCE)GM.1943-5622.0000054.